Characterization and Delivery of DNA Aptamers Selected for the Prevention of Alpha-Synuclein Aggregation in Parkinson's Disease

by

Vernon Hunt

A thesis submitted to the Faculty of Graduate and Postdoctoral Affairs in partial fulfillment of the requirements for a degree of

Master of Science

In

Chemistry

Carleton University

Ottawa, Ontario

Abstract

Aptamers are functional nucleic acids that function in a wide variety of applications, from biosensing to catalysis to therapeutics. Considered functionally analogous to antibodies, aptamers are single-stranded oligonucleotides capable of binding to target molecules with great affinity and specificity. In the field of medicine, the potential biological application of aptamers as a therapeutic or diagnostic is ever growing. Aptamers designed to target α-synuclein, a protein implicated in the pathogenesis of Parkinson's disease due to its propensity to aggregate, were investigated to probe their affinity for the protein as well as their ability to hinder the aggregation of the protein *in vitro*. Aggregation assays have proven that the presence of the aptamer candidates targeting monomeric α-synuclein stunt the formation of protein fibrils. One promising aptamer from the research, a-syn-1, was successfully packaged into a liposome vesicle modified to cross the blood-brain barrier and used in *in vivo* applications. The a-syn-1 aptamer has been delivered to the brains of transgenic mice, expressing human α-synuclein, where it has been co-localized with α-synuclein, and ongoing pharmacokinetic studies are being pursued to investigate the lifetime and distribution of the aptamer in a mouse model through extraction and PCR amplification of the aptamer. Analysis of the liposomes used for the packaging and delivery of the aptamer has provided insight into the loading efficiency and production efficiency of liposome batches.

Acknowledgements

I have, without a doubt, too many people to thank for the wonderful experience I have had, for the knowledge I have gained, and the friendships I have forged.

The biggest thanks go to Dr. Maria DeRosa for accepting me into her lab. She has been a fantastic leader and teacher whose passion for science and discovery knows no bounds. It has been such a positive experience to work in this lab with her encouragement and inspiration, her kindness and understanding, and all-around down-to-earth nature. And I still cannot understand how she balances each day, it's truly quite a talent.

I must next thank Dr. Erin McConnell for all of her assistance and teaching in the lab. Having her help with experimental procedures, using equipment around the lab, and enduring all my questions has been instrumental to my learning. A big thanks for also helping me to overcome my innate discomfort of working with mouse tissues; after so many brain and liver samples, it finally normalized for me.

A major thanks to Josh Callahan who worked alongside me to ensure a smooth transition of the project. He made the late-night experiments all the more entertaining and enjoyable. It's been a pleasure working as a team and, even though the payload aptamer has been delivered, more objectives remain. Spencer, without a doubt, you will do amazing work on this project. I can already see your dedication and perseverance shining through in your work and eagerness to learn.

To all my new friends and lab mates, I thank you for the constant support throughout my degree. I appreciate the assistance and efforts everyone has put forth, whether it is during times of high or low stress, to be kind and awesome. To my friends of old and former co-workers, I am ever-thankful for their support too. Often lending an ear or an evening to help with my stresses,

bringing me food and good company, and sharing wonderful experiences throughout my program, I cannot have done this without their unconditional love and care. To my family in Ottawa and my grandfather, I am thankful for the support I received throughout my degree. They always had an open door and open arms.

Thank you everyone.

Table of Contents

List of Abbreviations

α-Syn: Alpha-synuclein

AD: Alzheimer's Disease

APS: Ammonium persulfate

Aβ: Amyloid beta

BBB: Blood brain barrier

BCA: Bicinchoninic acid

BSA: Bovine serum albumin

CMT: Carrier mediated transport

COMT: Catechol-O-methyltransferase

CPG: Controlled pore glass

Ct: Cycle threshold

Cy 3.5: Cyanine 3.5

DBA: Dopamine binding aptamer

DBS: Deep brain stimulation

DDAB: Dimethyldioctadecylammonium (bromide salt)

DLB: Dementia with Lewy bodies

DMT: 4,4'-dimethoxytrityl

DNA: Deoxyribonucleic acid

DPBS: Dulbecco's phosphate buffered saline

DSPE-PEG 2000: 1,2-distearoyl-sn-glycerol-3-phosphoethanolamine-N-[amino(polyethylene glycol)-2000] (ammonium salt)

DSPE-PEG 2000 Maleimide: 1,2-distearoyl-sn-glycerol-3-phosphoethanolamine-N-[maleimide(polyethylene glycol)-2000] (ammonium salt)

DTT: Dithiothreitol

EDX: Energy-dispersive X-ray spectroscopy

EIS: Electrochemical impedance spectroscopy

EMSA: Electrophoretic mobility shift assay

ER: Endoplasmic reticulum

ESI-MS: Electrospray ionization mass spectrometry

i.p.: Intraperitoneal

K_d: Dissociation equilibrium constant

L-DOPA: Levodopa

LRPE: 1,2-dipalmitoyl-sn-glycero-3-phosphoethanolamine-N-(lissamine rhodamine B sulfonyl) (ammonium salt)

MAOB: Monoamine oxidase B

MPS: Mononuclear phagocyte system

MSA: Multiple system atrophy

MST: Microscale thermophoresis

NAC: Non-amyloid-beta component

NACP: Non-amyloid-beta component precursor

PAGE: Polyacrylamide gel electrophoresis

PBS: Phosphate buffered saline

PD: Parkinson's disease

PDI: Protein disulfide isomerases

PEC: Polyethylene glycol

PES: polyethersulfone

PFF: Pre-formed fibrils

POPC: 1-palmitoyl-2-oleoyl-sn-glycerol-3-phosphocholine (16:0-18:1 PC)

PP2A: Protein phosphatase 2A

PrP: Prion protein

PrP^{C}: Cellular prion protein

PrP^{Sc}: Scrapie prion protein

PTPIP51: protein tyrosine phosphatase-interacting protein 51

qPCR: Quantitative polymerase chain reaction

RMT: Receptor-mediated transcytosis

RNA: Ribonucleic acid

SELEX: Systematic evolution of ligands by exponential enrichment

SNARE: Soluble N-ethylmaleimide-sensitive factor attachment protein receptor

SNCA: Synuclein alpha

SPE: Solid-phase extraction

SPR: Surface plasmon resonance

TBE: tris(hydroxymethyl)aminomethane, boric acid, ethylenediaminetetraacetic acid

TEAA: Triethylamine acetate

TEM: transmission electron microscopy

TEMED: tetramethylethylenediamine

TFA: Trifluoroacetic acid

ThT: Thioflavin-T

TR: Transferrin receptor

TRA: Transferrin receptor aptamer

UPP: Ubiquitin Proteasome Pathway

VAMP2: Vesicle-associated membrane protein 2

VAPB: Vesicle-associated membrane protein-associated protein B

List of Figures

Figure 2.5: The gel and binding isotherm of the DNase trial on the a-syn-1 aptamer. A) The laddering of the fluorescence as a result of the DNase interacting with and cleaving portions of the aptamer into fragments. Lane 2 is the undigested aptamer, lane 5 is the aptamer digestion without α-Syn present, and lanes 6 through 11 correspond to aptamer mixed with 15μM, 1.5μM, 0.3μM, 0.06μM, 0.012μM, and 0.0024μM α-Syn, respectively. B) The SpotDenso analysis of the gel where each lane is analyzed for total fluorescence and the fluorescence of each band in each lane is analyzed. C) The binding isotherm developed by the relative fluorescence of bands 37-42 plotted with a four-parameter regression analysis to provide the dissociation constant. From this analysis, the $K_d = 0.015\mu M \pm 0.07\mu M$.

Figure 2.6: Binding isotherms provided from 2bind for the A) a-syn-1, B) a-syn-2, C) a-syn-3, D) a-syn-4, E) a-syn-5, and F) M5-15 were all performed in duplicate. The dissociation constant of a-syn-2, a-syn-3, and M5-15 were calculated to be 285.5nM ± 37.9nM, 94.2nM ± 2.8nM, and 1009nM ± 192nM, respectively. Dissociation constants for a-syn-1, a-syn-4, and a-syn-5 were not able to be determined due to aggregation effects of the α-Syn.

Figure 2.7: TEM image of α-Syn aggregation following shipment to 2bind for MST analysis. Large aggregates of α-Syn observed under TEM are likely reason for the unsuccessful MST analysis. Images taken at the 2μm scale.

Figure 2.8: Binding of the Cu+ ion to bicinchoninic acid in the BCA creating a purple chromophore to quantify the amount of protein present in stock solutions. The complex of cuprous ions with bicinchoninic acid is also believed to exist in competition with Cu+ binding to the peptide backbone of the protein.

Figure 2.9: Quantification of the α-Syn stock using the BCA assay. The standard curve (blue) was created using known concentrations of BSA and absorbance of the resultant solutions at 562nm. The α-Syn (orange) stock concentration was determined using the absorbance at 562nm. Each standard and α-Syn sample was measured in triplicate.

Figure 2.10: TEM images of the α-Syn before incubation with a-syn-1 and M5-15 aptamers to observe the initial α-Syn morphology. After no incubation, the α-Syn stock was deemed to contain some aggregate in solution. Images were taken at 1μm scale and 120kV. EDX analysis was performed on the smaller aggregates imaged in the TEM and α-Syn was confirmed from the sulphur peaks on the EDX spectrum.

Figure 2.11: Aggregation of α-Syn after 25 days of incubation monitored using TEM to image the morphology of α-Syn in the A) α-Syn control, B) α-Syn incubated with M5-15 aptamer, and C) α-Syn incubated with a-syn-1 aptamer. Images were taken at 1μm scale at 120kV.

Figure 2.12: Quantification of the α-Syn for PFF stock using the BCA assay. The standard curve (blue) was created using known concentrations of BSA and the concentration of the stock α-Syn (orange) was determined using the absorbance at 562nm. Each standard and α-Syn sample was measured in triplicate.

Figure 2.13: Aggregation of α-Syn for PFF monitored using thioflavin T at day 0 (blue) and day 7 (orange) of incubation of α-Syn control (α-Syn) and α-Syn mixed with each a-syn aptamer and with the M5-15 aptamer, labelled with the name of the aptamer combined with α-Syn. Each sample represents the average of triplicate fluorescence measurements and the error is one standard deviation of the fluorescence.

List of Tables

1 Introduction

1.1 Parkinson's Disease

Parkinson's disease (PD) is a progressive neurodegenerative disease that affects around 1-2% of the population over the age of 60 and is the second most prevalent neurodegenerative disorder across the world[1,2,3,4,5,6]. The onset of PD develops as the formation of intracellular aggregates, such as Lewy bodies and Lewy neurites, form and are believed to cause dopaminergic neurons in the substantia nigra to degenerate[1]. The characteristic motor symptoms of PD, first compiled by James Parkinson in 1817, are tremors and shaking, bradykinesia, and difficulty walking or maintaining gait[1,3]. Non-motor symptoms are also present in PD, including cognitive impairment, sleep disorders, hyposmia, and depression[7]. The non-motor symptoms may arise due to neurodegeneration in other regions of the brain, such as the hypothalamus, sympathetic ganglia, and in peripheral parasympathetic neurons, in people with PD[2].

PD can develop in two ways: idiopathic PD is the spontaneous onset of the disease and familial PD is the hereditary variant that leads to early onset and is often developed due to autosomal dominant inheritance. Genetic mutations in the synuclein alpha (SNCA) gene, coding for the alpha-synuclein (α-Syn) protein, have been isolated in Greek and American-Italian kindreds that displayed early onset and hereditary PD[3,8].

1.2 Alpha-Synuclein

Previously known as Non-amyloid-beta component precursor (NACP)[9], α-Syn is a 14.46 kDa protein, consisting of 140 amino acids, which has the capability of aggregating and forming amyloids, large protein aggregates, through a fibrillization process. α-Syn is part of the synuclein

family of proteins, which includes the ß- and γ-synuclein proteins and synphilin-1 protein, all bearing some sequence homology to α-Syn without the ability of aggregating[10]. The sequence and structure of wild type α-Syn is shown in Figure 1.1.

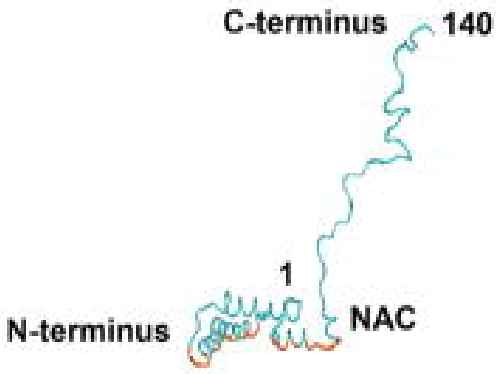

Figure 1.1: Monomeric α-Syn structure using a computer-generated model[11]. The structure displays the α-helical moiety of the N-terminus, the unstructured C-terminus, and the NAC region shown in orange. The 140-residue sequence of α-Syn is MDVFMKGLSKAKEGVVAAAEKTKQGVAEAAGKTKEGVLYVGSKTKEGVVHGVATV AEKTKEQVTNVGGAVVTGVTAVAQKTVEGAGSIAAATGFKKKDQLGKNEEGAPQEGI LEDMPVDPDNEAYEMPSEEGYQDYEPEA[12]. A portion of the sequence, residues 71-82 (VTGVTAVAQKTV) were discovered to be critical for the protein to aggregate.

The structure of α-Syn is split into two main regions: residues 1-95 comprise the N-terminus region, where residues 61-95 make up the non-amyloid-beta component (NAC) region, and residues 96-140 comprise the C-terminus region[2]. The N-terminus contains four imperfectly repeating sequences of 11 residues, each repeat containing a highly conserved KTKEGV sequence. When in the presence of a lipid membrane, this region forms an amphipathic α-helix structure that mediates binding to the protein to the membrane[10,13]. The NAC region is hydrophobic and is determined to be the amyloidogenic region of α-Syn. The NAC region contains three KTKEGV sequence repeats which can also form an amphiphilic α-helix structure in the presence of lipid membranes[9,13]. The C-terminus is highly charged, unstructured, and contains many acidic residues[10,13]. Many post-translational modifications are found on the C-terminus, including serine phosphorylation, tyrosine nitration, ubiquitination, and C-terminus

truncation[13]. This region of the protein is believed to have several possible roles: protein interaction; binding to ions, polycations and polyamines; modulating the association of α-Syn with membranes; and potentially protecting α-Syn from aggregation[9,13]. The C-terminus has also shown the ability to act as a protein chaperone and protect enzymatic activity of alcohol dehydrogenase, during heat stress, and protect aldolase from aggregating[14].

The native structure of monomeric α-Syn is believed to be unfolded and exist in multiple conformers with little to no secondary structure[9]. The mixture of monomeric forms is energetically minimized in the disordered and unfolded forms, despite the density of hydrophobic amino acids in the NAC[9]. The monomeric form is highly soluble and exists predominantly in the cytosol of neurons; when introduced to a lipid membrane, the monomer adopts an amphiphilic α-helical structure which allows it to interact with the lipid membrane[15].

The synuclein proteins are abundant in the brain with α-Syn representing up to 1% of the total protein isolated from the brain[10]. In the neuron, α-Syn is located around the synapse; the physiological function of the protein is not yet fully understood. The ability for α-Syn to interact with the presynaptic vesicles is of particular interest. A-Syn has been shown to exhibit soluble N-ethylmaleimide-sensitive factor attachment protein receptor (SNARE) chaperone activity when bound to the plasma membrane and was localized on vesicles at the presynaptic membrane. Upon binding to the membrane, α-Syn was shown to assemble into multimeric complexes which cluster synaptobrevin-2/vesicle-associated membrane protein 2 (VAMP2) proteins, effectively increasing the local concentration, and enhance the formation of a SNARE complex[16]. It is possible that the C-terminus of α-Syn is responsible for the interactions with synaptobrevin-2/VAMP2 since this region is capable of anchoring bound proteins to liposomes and vesicles[2].

Evidence suggests that α-Syn influences the size of the recycling pool in the bouton of the neuron and, thus, affects neurotransmitter release[17].

1.3 Alpha-Synuclein Aggregation in Parkinson's Disease and Synucleinopathies

α-Syn has been shown to play a critical role in the pathogenesis of PD, and other Lewy body diseases, due to the formation of stable oligomers and fibrils in pre-synaptic neurons[11,18,19]. Immunohistochemical staining of substantia nigra tissues from patients with non-familial PD, and patients with Dementia with Lewy Bodies (DLB), has proven that α-Syn is present in the Lewy bodies and neurites in affected neurons. The formation of Lewy bodies and other aggregations predominantly formed from α-Syn is linked to other neurodegenerative diseases known as synucleinopathies, including DLB, Lewy body variant of Alzheimer's disease, and Muscle System Atrophy (MSA)[2]. In MSA, the formation of cytosolic aggregations of α-Syn are found in glial cells, while Lewy Body diseases exhibit α-Syn aggregation in nerve cells[12].

Monomeric α-Syn is soluble in *in vitro* and *in vivo* systems, but the aggregation and structural change of α-Syn into ß-sheet filaments results in greatly decreased solubility of the protein. The decreased solubility of α-Syn filaments has been demonstrated in glial cytoplasmic inclusions[20] and Lewy bodies in PD and DLB[19]. The observed α-Syn aggregates in these inclusions contain a mixture of both full-length and truncated α-Syn integrated into the filaments[19,20,21]. The truncated α-Syn results from the loss of a portion of the C-terminus, which was observed from immunohistochemical staining of the α-Syn in both synthetic filaments[21] and aggregations isolated from brain tissue from humans who had MSA[22] and in PD and DLB[19].

As α-Syn aggregates and undergoes fibrillization, the aggregation process will incorporate other proteins as well as amyloid beta (Aß) peptides. Notably, synphilin-1 is found to be highly associated with α-Syn inclusions[23,24]. The ability for synphilin-1 to incorporate into α-Syn aggregations is influenced by the ubiquitylation of synphilin-1. Increasing evidence of the interactions of synphilin-1 with other proteins, such as E3 ligases and protein kinases, implies the formation of multi-protein complexes may underlie synucleinopathy pathology[24]. Immunohistochemical staining of brain tissues also proved that ubiquitin can also be present in Lewy bodies and neurites. Normally, the ubiquitylation of proteins results in proteasomal metabolism of proteins in the cytosol, a process termed the Ubiquitin Proteasome Pathway (UPP), wherein chains of ubiquitin are covalently bound to proteins and recognized by the proteasome for degradation. However, despite the high degree of ubiquitylation of α-Syn in oligomeric and fibrillized systems, Lewy bodies and aggregates tend not to undergo proteasomal degradation *in vivo* in several neurodegenerative diseases. Additional pathways for protein degradation involves the lysosome, an intracellular vesicle containing an array of enzymes for digesting biomolecules, for the process of autophagy[11]. Synphilin-1 overexpression has been correlated with decreased proteasomal function and, as such, increased formation of protein aggregates[24]. In cases if sporadic PD and other synucleinopathies, the inability for the protein aggregates to be degraded contributes to the formation of intracellular plaques and the onset of PD[11].

Aß-peptides are another group of biomolecules capable of aggregation, and these aggregates are strongly associated with the pathology of other neurodegenerative diseases, such as Alzheimer's disease (AD), Creutzfeldt-Jakob disease, and Huntington's disease[23]. The

presence of Aß-peptides in synucleinopathies is not unexpected; Aß-peptides have been detected in aggregations in patients with DLB and AD[25].

Two independent point mutations on the SNCA gene have been identified in conjunction with familial PD onset: the A53T mutant of α-Syn was discovered in the Contursi kindred and the A30P mutant isolated from a German family with a notably aggressive form of early-onset PD[2]. Mutations in the SNCA gene are rare, but the increased prevalence of PD from the mutations implies that α-Syn can display a gain-in-toxic functionality, increased neurotoxicity, resulting from alterations of the α-Syn facilitating more rapid aggregation[2].

1.4 Mechanism of Alpha-Synuclein Aggregation and Neurotoxicity

There are known mutant forms of the protein which result in a variation in the propensity to aggregate into amyloids. These mutant variants arise from singular point mutations in the N-terminus or NAC region of α-Syn; the mutant forms are A30P, E46K, H50Q, G51D, A53E, and A53T[13]. The A30P mutation was located in a family where members displayed characteristics of parkinsonism and it is postulated that the mutation influences the structure of α-Syn[8]. The A53E mutation was discovered in a case of atypical Parkinson's Disease where the substitution to the hydrophilic glutamate is believed to disrupt the amphiphilic α-helix structure and encourage fibrillization, and the aggregates were found to form a crescent shape[26].

A 12-residue portion of the hydrophobic region of the α-Syn, spanning residues 71-82, was found to be necessary for filament formation. ß-Synuclein lacks this group of residues and shows no aggregation in *in vitro* experiments. Deletion of the aforementioned residues from α-Syn resulted in greatly reduced aggregation. In addition, replacing the A76 residue with a

charged species resulted in a reduced rate of aggregation; the A76R mutation stunted the aggregation of α-Syn, compared to wild type α-Syn, and the A76E mutation showed even further reduction of aggregation for up to nine days. Furthermore, synthetic peptides of the 71-82 residue portion have been shown to fibrillize with each other and incorporate into the fibrillization of wild type α-Syn as well[27].

Aggregation of α-Syn was found to occur spontaneously under various conditions in *in vitro* investigations; fibrillization occurred closer to neutral pH, increased temperature, increased α-Syn concentration, or longer incubation times resulting in greater aggregation[28]. From *in vitro* studies, the aggregation of α-Syn is determined to occur in three phases: a lag phase, exponential phase, and plateau phase. The lag phase for the wild type α-Syn was shown to be two to three days, whereas the lag phase for the A53T, A30P, and E46K mutant variants of α-Syn were determined to be one to two days. Fibril formation has been observed at the end of the lag phase, for both the wild type and mutant α-Syn variants, with multiple morphologies. Further fibrillization leads to a more homogenous morphology of α-Syn in the plateau phase with the exception of the A53T mutant, which displays two different morphologies. After several months of fibril maturation, wild type α-Syn fibrils display decreased homogeneity suggesting that the fibrils present in the plateau phase are in a quasi-equilibrium state. Furthermore, the ß-sheet content of fibrils at the plateau phase and matured fibrils is similar, implying that any change in the morphology of fibrils over time is due to change in the tertiary or quaternary structure[29].

There are several characteristics which can influence the fibrillization of α-Syn *in vivo*, such as oxidation, C-terminal truncation, phosphorylation, nitration, and proteins which can bind to α-Syn. Oxidation of α-Syn was shown to induce self-polymerization of α-Syn to produce oligomeric forms of the protein in the presence of copper(II) and hydrogen peroxide as oxidizing

agents. The oxidation of α-Syn also shows potential pathological significance since the oligomers may present nucleation sites for fibrillization. Notably, the copper(II) induced oligomerization required the C-terminal of α-Syn to be present, whereas other metal-induced pathways of oligomerization, such as iron(III) and iron(II)/H_2O_2, function independently of the presence of the C-terminus[30]. Additionally, aggregation of α-Syn has been observed due to copper(I) species binding methionine in the N-terminus region[31]. Post-translational phosphorylation of the Ser 129 residue of α-Syn has been shown to dramatically increase the rate of fibrillization of α-Syn compared to α-Syn without phosphorylation. Lewy bodies isolated from human brain tissues, from patients with DLB, display higher amounts of phosphorylated α-Syn than brain samples that did not have Lewy bodies under normal physiological conditions. Since the phosphorylation of Ser 129 is not observed under normal physiological conditions, the modification of this residue is strongly linked to the pathology of synucleinopathies[32]. Nitration of tyrosine residues in the C-terminus of α-Syn has resulted in cross-linking of the protein which could lead to aggregation[33]. Furthermore, nitration of the Tyr 39 residue has resulted in a decreased ability for α-Syn to bind to lipid membranes and accelerated aggregation[34,35]. Interaction of α-Syn with lipid membranes influences fibrillization as well; high effective concentrations of α-Syn monomer in the membrane will encourage amyloid formation. Monomeric α-Syn bound to a membrane, and thus exhibiting α-helical structure, will be resistant to fibrillization. However, aggregate forms of α-Syn have been shown to penetrate lipid bilayers and disrupt vesicles to a greater extent than monomeric α-Syn[15].

Misfolding of the α-Syn protein can lead to multiple pathways of aggregation. Oligomers are noted to either be rich in ß-sheet formations whereas others remain comparatively disordered. Ring-like oligomeric structures have been identified and were initially regarded to be off-

pathway aggregations for the formation of fibrils[11]. However, evidence also suggests that the ring-like oligomers can disrupt the cellular membrane and nucleate fibril formation[10]. Off-pathway aggregation of α-Syn can also be observed where circular oligomers form stable structures which do not nucleate fibril formation[36]. Importantly, the monomer and aggregate forms of α-Syn have been observed in equilibrium, where oligomers can undergo slow alterations in the presence of monomer to become larger aggregates and eventually fibrils. The various ways aggregation have been observed are shown in Figure 1.2[11].

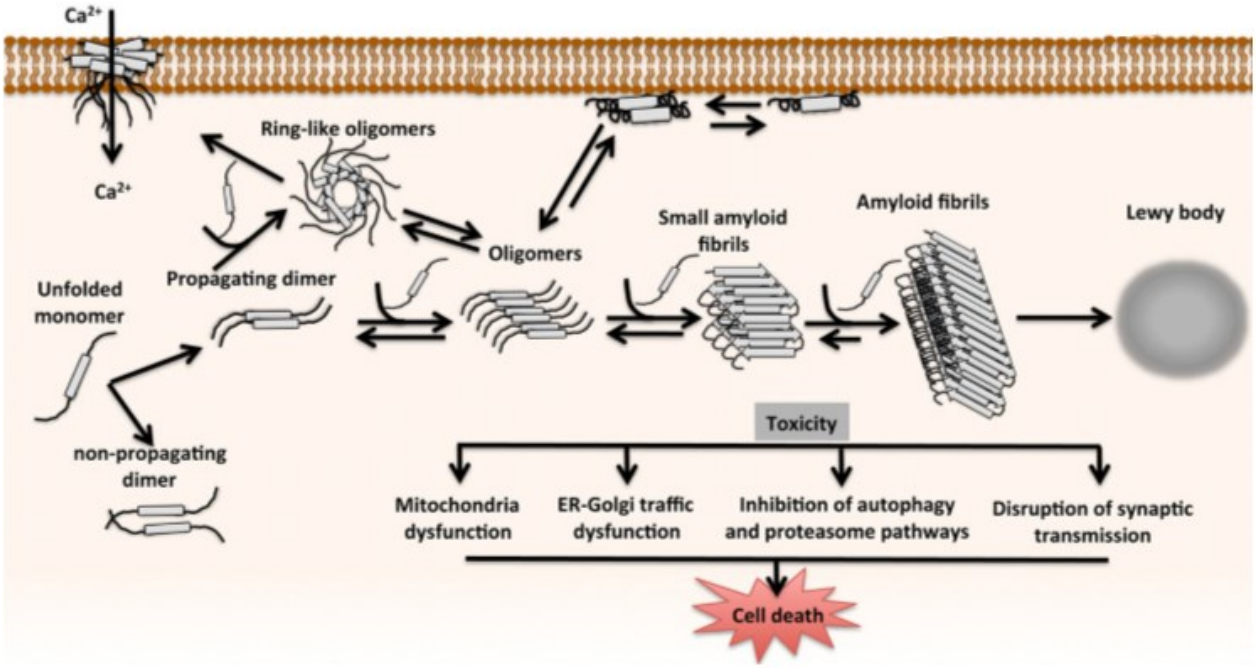

Figure 1.2: Proposed aggregation mechanism of α-Syn and the effects of aggregation on the cell. The fate of the α-Syn aggregation is not always neurotoxic and is, in many cases, reversible. The monomer initially can dimerize into non-propagating and propagating dimers, whereby only the propagating dimers can elicit negative effects on the cell through further aggregation into stable neurotoxic oligomers and amyloids. Aggregation of α-Syn to non-propagating structures are termed "off-pathway aggregation", though only some of those off-pathway aggregations may be neurotoxic[11].

The fibrillization of α-Syn and other Aß-peptides is not only a biomarker for neurodegenerative diseases but a causative factor for the process of apoptosis[23]. The

neurotoxicity of Lewy bodies and α-Syn aggregations has been investigated from several approaches.

The nitrosylation of cysteine residues of protein disulfide isomerases (PDI), an oxidoreductase chaperone associated with the ER, contributes to the onset of PD. Under normal physiological conditions, PDI has been shown to inhibit the fibrillization of α-Syn by binding late in the lag-phase. However, S-nitrosylation of PDI results in a decreased capability to prevent aggregation of α-Syn and synphilin-1[37]. Disruption to a signaling pathway between the endoplasmic reticulum (ER) and mitochondria has been demonstrated due to overexpression of α-Syn. The interaction of vesicle-associated membrane protein-associated protein B (VAPB), on the ER, and protein tyrosine phosphatase-interacting protein 51 (PTPIP51), on the outer mitochondrial membrane, is important for the delivery of Ca^{2+} from the ER to the mitochondria in order for the mitochondria to synthesize ATP. However, α-Syn can bind directly to VAPB and overexpression of α-Syn has resulted in decreased ATP production[38]. Disruption to the Golgi apparatus has also been observed as a consequence of α-Syn overexpression and could be related to the stress of α-Syn aggregates on the ER[39].

α-Syn has been shown to interact with and regulate protein phosphatase 2A (PP2A); increasing expression of α-Syn in dopaminergic neurons increased the activity of PP2A which reduced phosphorylation of tyrosine hydroxylase, an essential enzyme in the biosynthesis of dopamine[40]. Reuptake of dopamine from the extracellular space is accomplished through the dopamine transporter. α-Syn has been shown to interact with and regulate the behaviour of this transporter and increase dopamine reuptake. Increased cytosolic dopamine is toxic, due to its oxidative characteristics, and may contribute to neurodegeneration[2]. Additional evidence for the

regulation of dopamine was observed in the mouse model where mice not expressing α-Syn had an increased amount of released dopamine in the striatum[12].

Cellular degradation of α-Syn fibrils has shown the truncation of the N- and C- terminus from the fibril formation resulting in mitochondrial dysfunction as well as recruiting monomeric α-Syn to continue fibril growth. This is hypothesized to affect the synapse as well due to recruitment of and misfolding of monomeric α-Syn in the cell[41].

Some research hypothesizes that α-Syn behaves as a prion, a misfolded protein that negatively impacts cell physiology and functionality. The ability for α-Syn to form amyloids with a variety of conformations when aggregating is similar to the cellular prion protein (PrP^{C}); a change in the α-helical conformation of PrP^{C} to an insoluble ß-sheet aggregate scrapie prion protein (PrP^{Sc}) is observed[29,42,43]. Neurodegeneration in patients due to PrP aggregation has been noted to affect the electrophysiology of neuronal cells and are generally neurotoxic. Interestingly, the neurotoxic aggregates are postulated to be smaller aggregates, pre-fibrillar species, and not mature fibrils[43]. Additionally, the transmission of α-Syn between cells has been observed in research examining the onset of sporadic MSA[44].

1.5 Current Treatments for Parkinson's Disease

One approach to treatment of PD is to increase the amount of dopamine in the brain to offset the deficit due to loss of dopaminergic neurons. L-3,4-dihydroxyphenylalanine, also known as levodopa (L-DOPA), has been used for the treatment of PD symptoms for over 50 years[45]. L-DOPA is an orally administered amino acid that can be rapidly converted to dopamine in the brain. It is capable of passing through the blood-brain barrier (BBB) but has a short half-

life in peripheral organs and in the brain[6,46]. L-DOPA was combined with carbidopa, a peripherally active decarboxylase inhibitor, to protect circulating L-DOPA and increase the amount reaching the brain[46,47]. However, due to the short half-life, L-DOPA often results in fluctuations of dopamine levels, or "on-off" periods, that often lead to motor and non-motor complications[6,48,49]. For examples, long-term treatment with L-DOPA has been associated to the onset of dyskinesia[50]. Increased effects of L-DOPA treatment have been observed with the use of dopamine agonists, such as ropinirole and pramipexole, by extending the half-life of the dopamine in the brain. Monotreatment of PD with ropinirole was shown to treat dyskinesia for up to five years, with L-DOPA if necessary[51]. But, dopamine agonists often display strong negative symptoms, including a slew of negative neuropsychiatric effects such as hallucination and psychosis. Monoamine oxidase B (MAOB) inhibitors, compounds such as rasagiline and selegiline, are often employed as a monotherapy for patients in early stages of PD or as an adjunct to L-DOPA to increase the efficacy of treatments. MAOB inhibitors effectively increase the longevity of dopamine, be it endogenous or exogenous, in the brain by inhibiting the metabolism of dopamine and, thus, increasing synaptic concentrations of dopamine. Additionally, the use of MAOB inhibitors have been shown to impart neuroprotective effects on dopaminergic neurons[50,52]. The use of catechol-O-methyltransferase (COMT) inhibitors, such as entacapone and tolcapone, is also an avenue of treatment. COMT inhibitors prevent the metabolism of dopamine and are currently used to treat the motor symptoms that arise during L-DOPA treatment[53].

Another approach to treating PD is through the use of deep brain stimulation (DBS). Deep brain stimulation involves the insertion of tiny electrodes into a specification region of the

brain, with minimal damage to the surrounding tissue, through which electrical impulses can be used to alleviate involuntary movement and motor symptoms[54].

Some small molecules have been approached for their ability to hinder the aggregation of α-Syn *in vitro*. Squalamine was found to reduce aggregation of α-Syn on membrane surfaces[55] as well as the molecule trodusquemine[56]. Baicalein, a compound extracted from the *Scutellaria baicalensis Georgi* plant displays neuroprotective affects in mouse models of PD[57]. These compounds are not established as treatment options for PD but are simply providing insight into potential means of stalling α-Syn aggregation.

Importantly, all of the current treatments are not a cure for PD, they only ameliorate the symptoms of PD and improve quality of life. Current approaches to PD research seek to produce therapeutics with few to no negative side-effects or, ultimately, to find a cure.

1.6 Aptamers

Aptamers are synthetic single-stranded RNA or DNA oligonucleotides capable of binding to targets with high affinity and selectivity. Aptamers are able to recognize and bind to a variety of target molecules, including metal ions, small molecules, proteins, eukaryotic and prokaryotic cells, and viruses[4]. The binding of an aptamer to its target is achieved through non-covalent interactions, such as van der Waals forces, dipole interactions, hydrogen bonding, and base and π-π stacking interactions, to name a few.

Due to the many ligand-target interactions, aptamers are seen as chemically analogous to antibodies. However, aptamers show greater potential than antibodies in many applications due to their longer shelf life and thermostability, ability to function outside of physiological

conditions, lack of toxicity and immunogenicity, ease to chemically modify, and their lower batch-to-batch variation and efficient synthetic production[4]. In addition, due to aptamers being considerably smaller than antibodies, they tend to bind to intracellular targets more easily, though the smaller size subjects aptamers to greater renal clearance from the bloodstream[4,58].

The process to find an aptamer or group of aptamer candidate(s) is called SELEX, the systematic evolution of ligands by exponential enrichment. The traditional SELEX process involves multiple cycles of two main steps: a partitioning step followed by an amplification step. During the partitioning step, a pool of randomized oligonucleotides are allowed to interact with a target of interest, and those which bind to the target are isolated. Then, the isolated oligonucleotides are amplified and the process is repeated with further separation and amplifications[4]. In 1990, the first *in vitro* selection of aptamers was performed by two individual groups, Tuerk and Ellington[59,60]. The selection process for aptamers has also become an area of further interest as more stringent *in* vitro environments and procedures have been used to find new aptamers, as well as the use of *in vivo* SELEX[61]. Such procedures have involved the use of targets on cell surfaces and in human plasma[62].

1.7 Aptamers as a Therapeutic

For several decades, traditional approaches to therapeutics have often looked towards the use of antibodies due to their ability to interact with particular target compounds and their array of applications. However, aptamers have been moving into the territory of molecular recognition, diagnostics, and therapeutics due to their marked advantages over antibodies.

The delivery of aptamers to tissues and organs is limited due to endogenous nucleases, which greatly reduce the half-life of aptamer therapeutics. Additionally, removal of circulating oligonucleotides by renal filtration is a major issue for aptamer delivery. The addition of a polyethylene glycol (PEG) group has been shown to increase circulation time of aptamer therapeutics[63]. The conjugation of aptamers to nanoparticles is proving to be an effective strategy for drug delivery. The materials employed for improved drug delivery have included peptides, quantum dots, viruses, and liposomes[4].

The exploration of aptamers as a treatment method of neurodegenerative diseases has been ongoing since 1997 when an RNA aptamer targeting prion protein (PrP) was investigated[64] and, more notably, in 2010, when the M5-15 aptamer was isolated targeting α-Syn oligomers[4,65]. The M5-15 aptamer was found to bind more effectively to oligomeric α-Syn than monomeric α-Syn[65]. This discovery has been a hallmark in the development of aptamers targeting PD, and potentially other neurodegenerative diseases, since the binding to the toxic oligomeric structures could inhibit further fibrillization. However, this has left room for the investigation of potential aptamer therapeutics which could target the monomeric α-Syn for the prevention of oligomerization in the first place. Only recently has an aptamer candidate been presented in the literature which is capable of binding to monomeric α-Syn and hindering the aggregation[66]. Aptamer candidates targeting monomeric α-Syn have also been selected in the DeRosa lab which show inhibition of α-Syn aggregation[67].

1.8 Drug Delivery Across the Blood-Brain Barrier

The BBB is comprised of specialized, tightly-linked endothelial cells, as shown in Figure 1.3, and presents a challenging interface for the delivery of drugs and therapeutics due to its

selectivity for the types of molecules which can pass through[68]. There are endogenous receptors and transporters in the BBB and in astrocyte membranes that can interact with certain compounds in the bloodstream. These transporters are classified as either carrier mediated transport (CMT), which apply to small molecule transport across the endothelium, and receptor mediated transport (RMT), which applies to large molecules[69]. Examples of such receptors are the transferrin receptor (TR) and insulin receptor, which exist in the BBB and brain cell membrane[68], and allow for the transcytosis of transferrin and insulin, respectively, from the bloodstream to the intracellular space of brain cells[70]. The function of transferrin, specifically, is to bind to iron and move it across the BBB for use in brain cells[71]. The proposed scheme for movement of TR across the BBB, shown in Figure 1.4 as receptor-mediated transcytosis, follows that transferrin binds to the TR, is endocytosed and moved through the endothelial cell, then exocytosed into the brain[69].

Various approaches have been examined for the endo- and transcytosis of large molecules, such as proteins and plasmid DNA, through the BBB. Monoclonal antibodies targeting peptide receptor transporters are capable of moving across the BBB, without interfering with the normal functioning of the transporter, and have been investigated as potential carriers to move conjugated therapeutics across the BBB. Another vector for drug delivery across the BBB is through the use drug-loaded liposomes; modifying the surface of the liposome to be recognized by a transporter in the BBB allows for endocytosis of the liposome into the brain[70,73]. An example of this system has been observed in rats induced with PD where a liposome containing DNA plasmids coding for tyrosine hydroxylase were successfully endocytosed, following intravenous liposome injections, and the plasmids transcribed. This resulted in a normalized tyrosine hydroxylase levels in the rats for approximately one week following the

injection[73]. Liposomes used as means to deliver DNA plasmids, drugs, and therapeutics that would otherwise be unable to cross the BBB has been termed “molecular Trojan horses”[74].

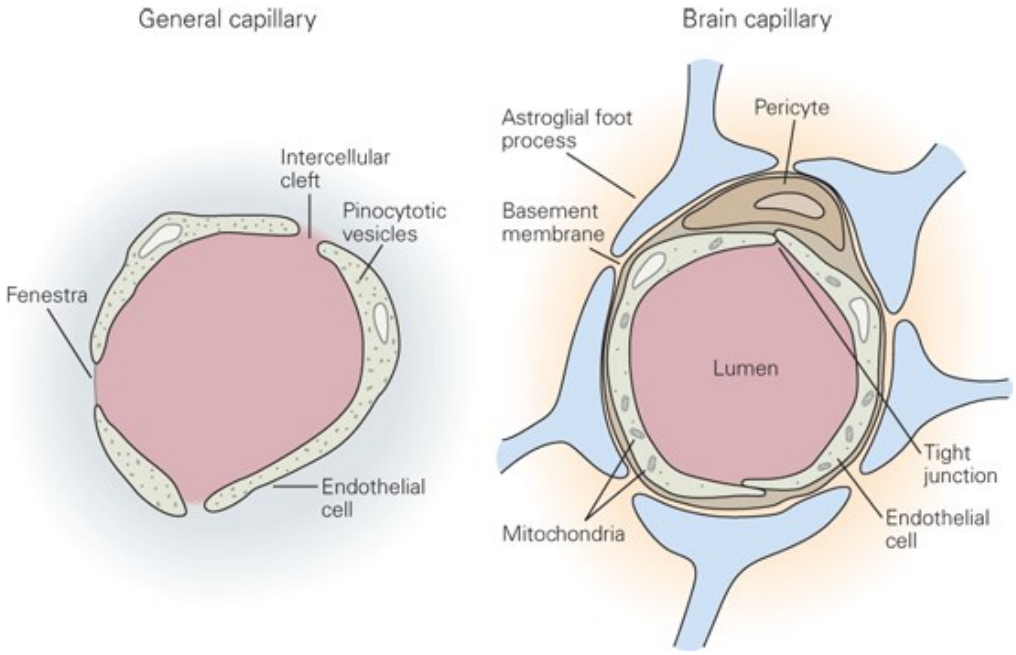

Figure 1.3: The physiology of capillaries throughout the body differs from those moving blood through the brain. General capillaries are comprised a single layer of endothelial cells allowing for the movement of water and dissolved ions out of the capillary. By contrast, capillaries in the BBB are tightly locked together and only permit the passive movement of water, gases, and small hydrophilic molecules between the endothelial cells[72].

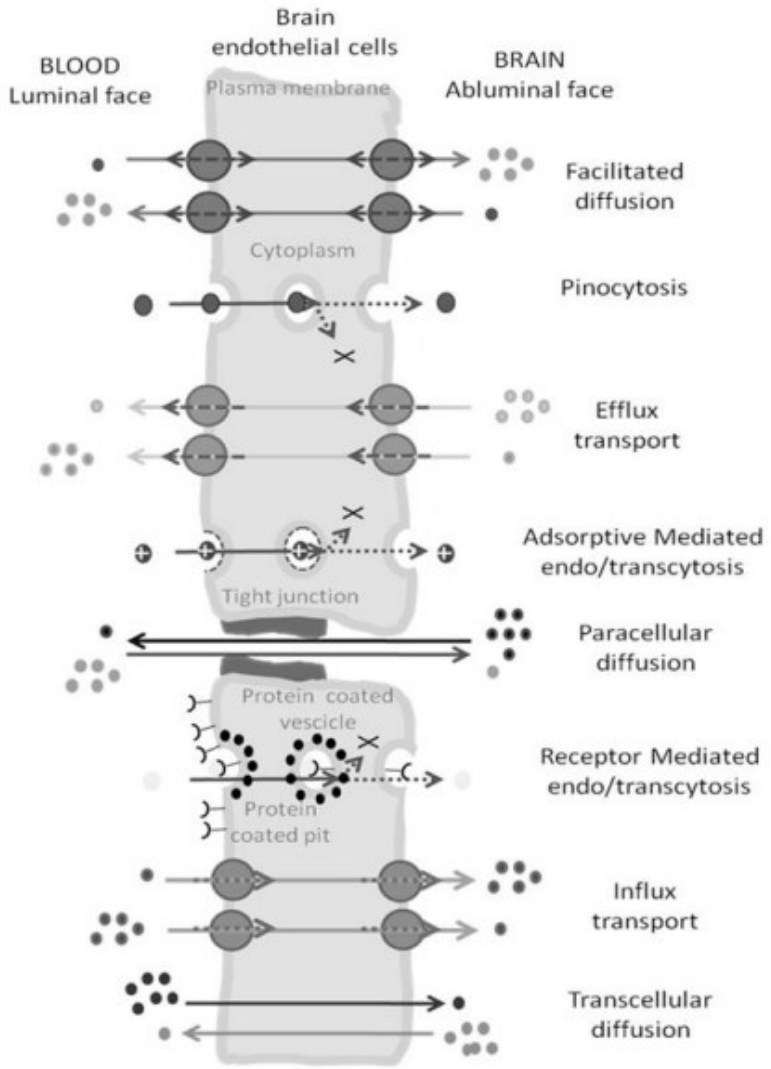

Figure 1.4: Movement of molecules through the endothelium of the BBB is highly regulated through influx and efflux transporters, absorptive-mediated and receptor-mediated endocytosis and transcytosis. The proposed scheme for the receptor mediated transcytosis by exploiting the transferrin receptor (TR) of the BBB to transcytose compounds from circulating blood and into the brain[75].

The ability for TR to recognize and carry transferrin through the BBB has also been exploited through the use of aptamers. In 2008, DNA and RNA aptamers were developed to target mouse TR for the purpose of carrying enzyme-loaded liposomes through the BBB. Both aptamers were found to bind non-competitively with TR as the interaction was not hindered in

the presence of transferrin-iron complexes[76]. In 2013, an *in vivo* SELEX procedure was identifying RNA aptamers that could pass the BBB which may present alternative entry options into the brain[61]. Liposomes with modifications to target multiple transport mechanisms have also been investigated for the ability to cross the blood brain barrier and endothelium of the choroid plexus for drug delivery to the central nervous system[77].

1.9 SELEX for Aptamers Targeting Monomeric Alpha-Synuclein

The SELEX process to determine the aptamer candidates, reported in Josh Callahan's thesis[67], involved multiple selective pressures in order to find potential aptamers targeting monomeric α-Syn, showing little to no binding to oligomeric α-Syn, and inhibition of the aggregation of the α-Syn. Two pools of randomized oligonucleotides were generated based off the M5-15 aptamer: a novel pool was generated using the primers of the M5-15 aptamer with 100% randomization between the primers, and a mutant pool was generated with 30% randomization between the primers. The pools were incubated with monomeric α-Syn and then subjected to fractional ultracentrifugation in order to separate out larger α-Syn morphologies from the monomer. The centrifugation fraction containing the monomeric α-Syn was placed onto nitrocellulose filter paper to immobilize the α-Syn and retain any aptamers from the pool that are bound to the protein. Aptamers bound to the monomeric α-Syn were extracted from the protein and amplified and sequenced. To determine that the aptamers were selected for monomeric α-Syn, the aptamer sequences in the centrifugation fraction containing monomeric α-Syn were compared to those sequences enriched from the fraction containing α-Syn aggregates. The five aptamers discovered from this SELEX process are collectively referred to as the a-syn aptamers, spanning a-syn-1 through 1-syn-5.

During the selection of the aptamers, the a-syn-1 aptamer had greater amplification in the fraction of monomer α-Syn and lower amplification in the fraction of oligomeric α-Syn than the other aptamer candidates resulting from the selection rounds. The a-syn-1 aptamer became a focus of the research for preventing α-Syn aggregation compared to the literature M5-15 aptamer.

1.10 Thesis Objectives

This research project was composed of multiple objectives: to investigate the *in vitro* affinity of the aptamers, previously selected in the DeRosa lab, for monomeric α-Syn and compare the affinity of these aptamers to the literature aptamer M5-15; to characterize the aptamers and their ability to prevent fibrillization of α-Syn, *in vitro*; and to synthesize and characterize dual-aptamer liposomes designed to carry a payload of a-syn-1 aptamer across the BBB using transferrin receptor aptamer modified to the liposome surface. This research has three primary hypotheses: firstly, that the aptamers selected to bind to and inhibit the aggregation of monomeric α-Syn will effectively stall α-Syn aggregation *in vitro* and outperform the M5-15 aptamer, known to bind to oligomeric forms of α-Syn; secondly, that the affinity of each aptamer for monomeric α-Syn could be determined and prove greater binding than the M5-15 aptamer; and lastly, that the a-syn-1 aptamer could be packaged into a liposomal delivery vector that would carry the aptamer payload in *in vivo* studies where it would penetrate the blood-brain barrier in transgenic mice.

2 Preparation, Characterization, and Efficacy of Aptamers Selected to Bind and Inhibit the Aggregation of Alpha-Synuclein

2.1 Statement of Contribution

Previous research in the DeRosa lab[67] examined the aggregation of α-Syn and designed the aptamer candidates for study as a therapeutic to hinder α-Syn aggregation. Aggregation assays were run by Dr. Erin McConnell and Josh Callahan. A novel pool and a mutant pool of aptamer candidates were prepared for selection against α-Syn through a rigorous SELEX procedure. SELEX was performed by Josh Callahan, Dr. Erin McConnell, and Dr. Emily Mastronardi[67]. TEM imaging throughout the SELEX process was performed by Josh Callahan, Dr. Erin McConnell, and Dr. Jianqun Wang.

TEM images for the aggregation of α-Syn was performed by Dr. Jianqun Wang. SEM images of the aggregation of α-Syn was performed by Yun Liu at the University of Ottawa. EMSA experiments were performed with assistance from Dr. Erin McConnell and Josh Callahan. Assistance and supervision for the synthesis and purification of oligonucleotides provided by Dr. Erin McConnell and Josh Callahan.

2.2 Introduction

2.2.1 Aptamer Characterization

Aptamers can form intramolecular hydrogen bonds, via to G-C and A-T base-pairing, between regions of sequence complementarity causing the aptamer to fold upon itself and create secondary and tertiary structures. Duplex formation within an aptamer commonly results in the

formation of a hairpin, a structure where DNA hybridization creates a single-stranded loop connecting the two complementary regions. The unhybridized loop portion of the DNA has been widely studied for stability[78] and target binding[79]. Aptamer sequences that are rich in guanine and contain four repeating stacks of two or more guanines can form the tertiary G-quadruplex structure through Hoogsteen base-pairing[80,81]. Melting temperatures (T_m) of aptamers are defined as the temperature at which half of the intramolecular bonds have dissociated, or, half the aptamer has denatured, and can be monitored by measuring the absorbance of the aptamer in solution at 260nm as temperature is increased or decreased.

Binding assays are used to find if two molecules can interact with each other and the affinity of the interaction; for the interest of this research, the binding interaction occurs between aptamers and protein. Binding affinity studies begin with the assumption that the binding between two molecules is reversible and occurs in a 1-to-1 stoichiometry. The equation for this model is $A + B \rightleftharpoons AB$. The affinity for one molecule to bind to another is often measured using the dissociation equilibrium constant, or K_d, defined as the rate of dissociation (K_{off}) divided by the rate of association (K_{on}) of the two molecules at equilibrium, described by the equation $K_d=[A_{eq}][B_{eq}]/[AB_{eq}]$. A smaller K_d means a greater formation of the AB complex from the individual reactants, A and B, has occurred at equilibrium[82].

Electrophoretic mobility shift assay (EMSA) is a method for observing interactions between DNA, or RNA, and proteins and can be used to determine the dissociation constant of aptamers for a protein target. The basis of the assay is that DNA bound to protein will migrate through a gel at a slower rate than unbound protein and unbound DNA thus resulting in a shift in the location of the DNA-protein complex on a non-denaturing gel[83,84]. By changing the concentration of the target protein while maintaining a concentration of a fluorescently-labelled

aptamer, change in the fluorescence intensity of the DNA-protein complex can be observed as a function of protein concentration. This generates a binding isotherm for determining the dissociation constant of the aptamer to the target protein.

DNase assay is one potential method for determining the affinity of aptamers for their targets. Originally, DNase footprinting were designed to find locations where proteins could bind to genomic DNA sequences. When the DNA sequence is exposed to DNase, a series of fragments are generated and can be separated by size using denaturing PAGE. When using DNA containing a radiolabel or fluorescent tag on one end of the sequence, fragments can be observed as a ladder of radiolabeled or fluorescent DNA. When protein is bound to a DNA sequence, the region where the protein is bound can offer protection from the DNase activity causing alterations in the DNA fragment laddering. To determine aptamer affinity for a target, a range of target concentrations while keeping the aptamer concentration constant; this results in a concentration-dependent ladder detectable on a denaturing PAGE. Comparing the relative radioactive or fluorescent signal of a fragment across each concentration of target can create a binding isotherm which can then be used to determine the target-binding affinity[85,86,87].

Other methods exist for the determination of the binding affinity of aptamers to their targets which do not include the use of gel-based assays, such as EMSA or DNase I, where a gel matrix is used to separate components of a system by size. Creation of biosensors by immobilization of aptamers to the surface of an electrode or optical fiber, termed aptasensors, generate label-free and real-time biosensing alternatives. Through electrochemical impedance spectroscopy (EIS), changes in the impedance of an aptasensor can be observed as a function of the concentration of target in solution and then used to determine target-binding affinity[88]. Similarly, square wave voltammetry can be used for the detection of the target binding to

aptasensors. Using an aptasensor where the aptamer is internally modified with methylene blue, increasing concentrations of target elicits changes in the current response of the aptasensor and the binding affinity of the aptamer can be determined using the peak current response at each concentration of target[89].

2.2.2 Chapter Objectives

The objectives of this chapter were to synthesize, characterize, and utilize the a-syn aptamer candidates to determine the binding affinity of the aptamers to monomeric α-Syn and to observe their efficacy in reducing α-Syn aggregation.

2.3 Materials and Methods

2.3.1 Automated Aptamer Synthesis

An automated MerMade 6 DNA Synthesizer (BioAutomation) was used to synthesize the aptamers a-syn-1, a-syn-2, a-syn-3, a-syn-4, a-syn-5 (collectively the a-syn aptamers), and M5-15 using phosphoramidite chemistry to achieve solid-phase oligonucleotide synthesis. Synthesis of the oligonucleotides occurs in a 3' to 5' direction through a repeating series of organic reactions. The sequences are shown in Table 2.1. Each of the a-syn aptamers used the same 3' and 5' primers as the literature M5-15 aptamer, shown in black text, and a randomized region, shown in blue text in Table 2.1.

The phosphoramidites, dA-CE, Ac-dC-CE, dmf-dG-CE, and dT-CE (GlenResearch), were dissolved in anhydrous acetonitrile (GlenResearch) to create 0.1µM solutions of each

amidite, respectively. Each a-syn aptamer and the M5-15 aptamer sequence was fluorescently labelled, on the 5' end of the aptamer, using either fluorescein phosphoramidite or 5'-fluorescein phosphoramidite (GlenResearch), which was dissolved in anhydrous acetonitrile, to 0.1μM concentration, and connected to the DNA synthesizer. The dissolved phosphoramidites were connected to the DNA synthesizer along with anhydrous acetonitrile (BDH VWR Analytical), activator solution, cap A solution, cap B solution, deblock solution, and oxidizer solution (GlenResearch). The synthesis columns for each aptamer containing an initial adenine, 1000Å 1.0μmole dA(Bz) controlled pore glass (CPG) columns (BioAutomation), were also connected to the DNA synthesizer. The appropriate script file was loaded on the MerMade software and synthesis performed overnight.

2.3.2 Purification of Synthetic Oligonucleotides

Following synthesis, the solid support was removed from the columns and the DNA cleaved from the supports in 1mL of 28% ammonium hydroxide overnight at 55°C in centrifuge tubes set in a dry bath incubator. Two different purification methods have been followed based on the fluorescein used to label the aptamer: aptamers modified with fluorescein phosphoramidite underwent reverse phase polymer affinity purification and those modified with 5'-fluorescein phosphoramidite underwent gel purification. In the event that reverse phase polymer affinity purification resulted in low purity, the gel purification method was followed.

Table 2.1: Sequences of the fluorescein-modified a-syn aptamers selected to bind to and inhibit the aggregation of α-Syn and the sequence of the M5-15 aptamer which is known to bind to monomeric and oligomeric forms of α-Syn. The primer regions are shown in black text and the regions that were randomized during selection are shown in blue. Theoretical extinction coefficients of each aptamer sequence calculated with OligoAnalyzer® Tool, version 3.1.

Sequence Name	Aptamer Sequence	Extinction Coefficient at 260nm (L mol^{-1} cm^{-1})
a-syn-1	5'-fluorescein-ATA GTC CCA TCA TTC ATT GTA AGG AAA CGC TAC GGG GTG GGT ACG GCA AGA TAT TAG CAA GTG TCA-3'	743000
a-syn-2	5'-fluorescein -ATA GTC CCA TCA TTC ATT GTA TGG TAC GGC GCG GTG GCG GGT GCG GGG AGA TAT TAG CAA GTG TCA-3'	716800
a-syn-3	5'-fluorescein -ATA GTC CCA TCA TTC ATT GTA TGA GAT GGG GTG GTG ACG TCA GCA TGG AGA TAT TAG CAA GTG TCA-3'	735000
a-syn-4	5'-fluorescein -ATA GTC CCA TCA TTC ATT GTA CGG AAT GGC GCG GTG ACC GGA TAG TGT AGA TAT TAG CAA GTG TCA-3'	736300
a-syn-5	5'-fluorescein -ATA GTC CCA TCA TTC ATT GTA TGA TAC AGT GAG GTG GCA GAT GCA TGC AGA TAT TAG CAA GTG TCA-3'	738700
M5-15	5'-fluorescein -ATA GTC CCA TCA TTC ATT GTA TGG TAC GGC GCG GTG GCG GGT GCG TGG AGA TAT TAG CAA GTG TCA-3'	714000

2.3.2.1 Reverse Phase Polymer Affinity Purification of Synthetic Oligonucleotides

The reverse phase polymer affinity purification method for fluorescein-labelled oligonucleotides started with pre-treating the 50mg Glen-Pak DNA Purification Cartridges (GlenResearch) on a vacuum manifold with 0.5mL of acetonitrile followed by 1.0mL of 2M TEAA (GlenResearch). The oligonucleotide and ammonium hydroxide mixture were centrifuged at 5000RPM for 5 minutes to pull the solid support to the bottom of the centrifuge tube, and the supernatant was pipetted onto the purification cartridges. 1.0mL of salt wash solution, containing 5% acetonitrile in 100mg/mL sodium chloride, was placed into the centrifuge tubes with the solid supports and centrifuged again. The supernatant was pipetted onto the purification cartridges. The cartridges were then washed with two 1.0mL aliquots of 2% trifluoroacetic acid (TFA) (GlenResearch) to remove the 4,4'-dimethoxytrityl (DMT) protecting group. The cartridge was rinsed with two 1.0mL aliquots of deionized water and the aptamers were eluted with 1.0mL of 50% acetonitrile in deionized water containing 0.5% ammonium hydroxide. The collected oligonucleotides were dried down in an Automatic Environmental SpeedVac® System AES2010 (Savant), herein called SpeedVac, overnight. The dried oligonucleotides were dissolved in 1x Dulbecco's phosphate buffered saline (DPBS) (ThermoFisher) and then quantified using UV-Vis spectroscopy. For each experiment, the 1x DPBS lacked calcium and magnesium ions.

2.3.2.2 PAGE Purification of Synthetic Oligonucleotides

Preceding the gel purification procedure, aptamers dissolved in ammonium hydroxide were first dried. The oligonucleotide and ammonium hydroxide mixture was centrifuged at

5000RPM for 5 minutes to pull the solid support to the bottom of the centrifuge tube, and the supernatant was pipetted into a separate centrifuge tube. The supernatant was dried in the SpeedVac overnight and dissolved in deionized water. The gel purification of oligonucleotides involves the separation of the full-length aptamer from any sequences which failed to fully synthesize through the use of a polyacrylamide matrix.

An 18% denaturing polyacrylamide gel was created for each column of oligonucleotide that was synthesized on the MerMade 6 DNA Synthesizer. Two gels were created by mixing 31.5g of urea with 23.5mL of 40% 19:1 acrylamide:bisacrylamide, 15mL of 5x TBE (0.445M Tris, 0.445M boric acid, and 0.010M EDTA; pH=8.3), and 14mL of deionized water. The solution was stirred until the urea fully dissolved and was then passed through filter paper (Whatman). 450µL of 10% ammonium persulfate (APS) in deionized water and 35µL of tetramethylethylenediamine (TEMED) were mixed into the acrylamide solution and briefly stirred to initiate polymerization. The acrylamide solution was poured into vertical casting plates (SE6102, Fisher Scientific) and allowed to set with a single well for sample loading. This procedure was repeated to create as many gels as there were columns on the synthesizer

An equal volume of formamide was added to the dissolved oligonucleotides to weigh down the oligonucleotides when pipetted into the gel well. If the sample was impure after the reverse phase polymer affinity purification, the oligonucleotide dissolved in 1x DPBS was weighed down with an equal volume of formamide. The oligonucleotide solution was pipetted onto the gels and the polyacrylamide gel electrophoresis (PAGE) was run at 300V for 2.5 hours using a FB1000 Electrophoresis Power Supply (Fisher Scientific). The gel was imaged using a MultiImage™ Light Cabinet (Alpha Innotech), herein called AlphaImager, and the band of full-length aptamer was cut from the gel and placed into a 50mL tube.

To extract the aptamer from the gel, the DNA band cut from the gel was shaken in water and placed into an Innova 40 incubator (New Brunswick Scientific) set to 37°C and 130RPM overnight to elute the oligonucleotide from the gel. After incubation, the gel slurry was poured into a syringe with a 0.22µm pore polyethersulfone (PES) filter (CELLTREAT) and the oligonucleotide solution was filtered into a new tube. The retained gel was disposed of. Following filtration, the oligonucleotide solution was desalted using Amicon® Ultra centrifugal filter units with a 3000 molecular weight cutoff (Millipore Sigma). The oligonucleotide solution was pipetted into the filter unit and centrifuged at 10000RPM for 20 minutes until the entire sample was desalted. Three washes with deionized water were also performed by centrifuging at 10000RPM for 20 minutes. After washing, the sample was collected in a new centrifuge tube and stored at -20°C until quantification.

2.3.3 Quantification of Aptamers using UV-Vis Spectroscopy

The amount of aptamer in solution from either purification method is determined using UV-Vis spectroscopy; a Cary 300 Bio UV Visible Spectrophotometer was utilized for all UV-Vis experiments. Aliquots of the oligonucleotide stock solutions were diluted with deionized water so that the absorbance at 260nm was measured between 0.4 and 0.8. Using the Beer-Lambert law, the absorbance of the aptamer at 260 nm and the theoretical extinction coefficient, provided through the use of OligoAnalyzer® Tool, version 3.1, on the Integrated DNA Technologies, IDT, website (PrimerQuest® program, IDT, Coralville, Iowa, USA), for each sequence were used to determine the concentration of the purified oligonucleotide in solution.

To determine the purity of the aptamer, mass spectrometry was used. Samples of 1nmol of the aptamer solution were dried using the SpeedVac and sent to Novatia for ESI-MS analysis.

2.3.4 Secondary Structure Prediction of Aptamers using RNAstructure

The secondary structures of the aptamers were predicted using RNAstructure[90], version 6.0.1, from the Mathews lab, to determine the minimum free energy structure of the aptamer sequences. The online tool was set to DNA and all other options were left at the default settings.

2.3.5 Aptamer Melting Temperature Studies

Each of the fluorescently labelled aptamer candidates was diluted to 3µM in 1x DPBS and 3mL of each aptamer solution was placed in a multi-cell UV-Vis with a temperature control unit. The absorbance of the aptamer candidates was scanned at 295nm, using 1x DPBS as a blank, and the temperature was ramped from 25°C to 85°C with a ramp rate of 2°C/min. Two complete cycles, ascending and descending, of temperature ramping were performed. Absorbance values were recorded at every 1°C interval on both ascending and descending temperature ramps. This experiment was repeated at 260nm using a sample of the aptamers further diluted in 1x DPBS so that the absorbance of the sample was between 0.2 and 0.8.

2.3.6 Electrophoretic Mobility Shift Assays of Alpha-Synuclein Monomer with Aptamer Candidates

For each of the following studies, the wild type α-Syn and A30P mutant α-Syn was purchased from rPeptide. The 1x PBS formulation was 137mM NaCl, 2.7mM KCl, 8.1mM Na_2HPO_4, and 1.8mM KH_2PO_4 combined in deionized water and balanced to pH=7.4.

2.3.6.1 EMSA of Varying Alpha-Synuclein Concentrations

Six 8% multi-welled non-denaturing polyacrylamide gels were prepared using three batches of the following recipe: 18mL of 40% acrylamide, 18mL of 5x TBE, and 53mL of deionized water, followed by 900µL of 10% APS and 70µL of TEMED. The gel was poured into a vertical casting unit and a multi-well comb was used to form the wells. 20µL of 1µM of fluorescently-labelled aptamer candidate was combined with 20µL of α-Syn at a range of concentrations, from 40µM to 4nM. A DNA control lane for each aptamer was prepared by mixing 20µL of the aptamer with 20µL of 1x PBS and an α-Syn control lane was prepared by mixing 20µL of 40µM α-Syn with 20µL of 1x PBS. The samples were incubated at 37°C for 1.5 hours at 137RPM. Following incubation, 40µL of 50% glycerol in water was added to each sample and the samples were loaded onto the gels. The gels were run at 200V for 2.5 hours in 1x TBE. The gels were imaged using the AlphaImager to identify the migration of the aptamer in the gel with and without α-Syn present, and then stained in Coomassie G-250 overnight. Pictures of the stained gels were taken to locate the protein bands on the gel.

2.3.6.2 EMSA of Alpha-Synuclein using Reduced Aptamer Concentration

Six 8% multi-welled non-denaturing polyacrylamide gels were prepared following the procedure above. Each aptamer candidate was diluted to 0.5µM in 1x PBS, heated to 90°C for five minutes in a dry-bath incubator and allowed to cool to room temperature. Each aptamer candidate was diluted to 0.5µM solutions in 1x PBS, heated to 90°C for five minutes, and allowed to cool to room temperature. 30µL of the 0.5µM aptamer candidate was combined with 30µL of 40µM α-Syn, in triplicate. An α-Syn control lane was prepared by mixing 30µL of 40µM α-Syn with 30µL of 1x PBS. Similarly, control lanes for each aptamer were prepared by mixing 30µL of 0.5µM aptamer solution with 30µL of 1x PBS. All solutions were incubated at 37°C for 1.5 hours at 120RPM. Following incubation, the samples were mixed with 60µL of 50% glycerol in water and loaded onto the gels. A Precision Plus Protein ™ Standards protein ladder was loaded onto the gel as well. The gel was run at 250V for 2.5 hours in 1x TBE and then were imaged and stained in Coomassie G-250 overnight. After staining, the gels were rinsed and pictures were taken to observe any changes in the protein migration through the gel with and without the presence of aptamer.

A variation of the above protocol was performed wherein 20µL of 0.5µM aptamer solutions were mixed with 20µL of 40µM α-Syn, in triplicate, and an aptamer control lane made from 20µL of 0.5µM aptamer solution and 20µL of 1x PBS. The samples were incubated at 37°C for 1.5 hours and 130RPM. The samples were mixed with 40µL of 50% glycerol in water and 70µL of the sample was loaded onto the gel. The gel was run at 300V for three hours and then imaged.

2.3.6.3 EMSA of Alpha-Synuclein Mimicking SELEX Conditions

To emulate the same conditions of the SELEX, 30μM solutions of the aptamer candidates were prepared in 1x PBS. 20μL of 30μM aptamer solution was mixed with 20μL of 30μM α-Syn. A-Syn control was made by mixing 20μL of 30μM α-Syn with 20μL of 1x PBS. All samples were incubated for 2 hours at 37°C for 2 hours at 130RPM. Each sample was mixed with 40μL of 50% glycerol in water. Six 8% multi-welled non-denaturing polyacrylamide gels were prepared following the method above. 70μL of each sample was loaded onto the gel. The gel was run at 250V for three hours and then imaged.

2.3.6.4 EMSA of A30P Mutant Alpha-Synuclein

The A30P mutant form of α-Syn was also studied using EMSA. 20μL of 0.5μM aptamer solution was mixed with 20μL of 30μM mutant α-Syn. The mutant α-Syn control was made by mixing 20μL of 30μM mutant α-Syn with 20μL of 1x PBS. Aptamer controls were prepared by mixing 20μL of 0.5μM aptamer solutions with 20μL of 1x PBS. All samples were incubated at 37°C for two hours at 130RPM. Two 8% multi-welled non-denaturing polyacrylamide gels were prepared following the method above. Each sample was mixed with 40μL of 50% glycerol in water and loaded onto the gel. The gel was run at 250V for three hours and then imaged.

2.3.6.5 EMSA of Alpha-Synuclein after Long-Term Storage in Freezer

A stock solution of α-Syn, which had been frozen at -20°C for several months, was investigated to observe differences in migration through the gel and the interaction between the protein and aptamer candidates compared to freshly dissolved α-Syn. 30μL of 40μM α-Syn was

mixed with 30µL of 0.2µM aptamer candidates m5-15 or a-syn-1, in triplicate for each aptamer. A-Syn control lanes were made by combining 30µL of 40µM α-Syn with 30µL 1x PBS. Similarly, aptamer control lanes were made by combining 30µL of 0.2µM aptamer solution with 30µL of 1x PBS. All solutions were incubated at 37°C for one hour at 130RPM. After incubation, the samples were mixed with 60µL of 50% glycerol in water. Two 8% multi-welled non-denaturing polyacrylamide gels were prepared following the method above. 80µL of each sample was loaded onto the gels, along with a Precision Plus Protein™ Standards protein ladder, and run at 200V for 3.5 hours in 1x TBE. The gels were imaged and stained in Coomassie G-250 overnight. After staining, the gels were rinsed and images were taken.

2.3.6.6 EMSA of Alpha-Synuclein after Long-Term Incubation

A 40µM stock solution of α-Syn, which had been stored at 37°C and 130RPM for seven weeks, was removed from incubation. 20µL of the incubated α-Syn was mixed with 20µL of 1x PBS, making two sets of triplicates, and then heated to 95°C for ten minutes and allowed to cool. Two more triplicates of incubated α-Syn were prepared following the aforementioned procedure except that heating the samples to 95°C was omitted. A 12% denaturing gel was prepared by mixing 27mL of 40% acrylamide with 15mL of 5x TBE and 44mL of deionized water. The acrylamide solution was heated to 37°C on a hotplate with stirring to dissolve the urea. The acrylamide was filtered and mixed with about 1mL of 10% APS in water and 90µL of TEMED. The acrylamide solution was set in vertical casting units.

2.3.7 DNase I Assay

Serial dilutions of α-Syn were prepared, ranging from 15μM to 2.4nM, from a stock solution of α-Syn monomer using 1x DPBS. A 20μL aliquot of each α-Syn concentration in the dilution series was mixed with 20μL of 10μM aptamer in 1x DPBS. A blank sample was prepared using 20μL of 10μM aptamer combined with 20μL of 1x DPBS. The samples were incubated at 37°C while shaking at 130RPM for one hour. Each sample was then mixed with 4μL of DNase I in 10x reaction buffer for 15 minutes with intermittent gentle shaking followed by 2μL of stop buffer and heating the sample to 85°C for 5 minutes with a dry-bath incubator. Two 19% denaturing polyacrylamide gels were prepared by dissolving 31.5g of urea with 37.5mL of 40% acrylamide and 15mL of 5x TBE, pouring the solution through filter paper, and adding 60μL of TEMED and 600μL of 10% APS. The gels were poured into vertical casting units and a multi-well comb was used to form the wells. The gels were run at 300V for at least 30 minutes in 1x TBE before the samples were loaded. Each sample was combined with 40μL of formamide to denature the samples and weigh them down in the wells of the gel. 20μL of 10μM aptamer was combined with 20μL of 1x PBS and mixed with 40μL formamide without undergoing nuclease treatment. The total volume of each sample was loaded onto the gel and the gel was run at 300V for at least three hours in 1x TBE. The gel was removed and imaged under 302nm fluorescent light to observe the conserved regions of DNA at each concentration of α-Syn. The AlphaImager was used to run spot density (SpotDenso) analysis on each gel lane to find a ratiometric amount of fluorescence of each band, with the “auto background” setting on, of DNA compared to the overall fluorescence of the lane. The ratiometric values for each band were plotted on a logarithmic graph and fitted using a 4-parameter logarithmic curve. The

dissociation coefficient was determined from the inflection point of the fitted curve for each band.

2.3.8 Microscale Thermophoresis

Each aptamer was diluted in 1x PBS to 100µM and 5µL of each aptamer was frozen and mailed to 2bind for microscale thermophoresis (MST). A fresh vial of 1.0mg α-Syn was mailed to 2bind on dry ice with 1x PBS for dilutions.

2.3.9 Longitudinal Aggregation of Alpha-Synuclein Monitored by TEM

The ability for the aptamers to inhibit the aggregation of α-Syn monomer (rPeptide) was investigated using TEM. The α-Syn stock was first quantified using the bicinchoninic acid (BCA) assay. The Pierce™ BCA Protein Assay Kit (Thermofisher) was used for the quantification of the α-Syn. The 1x PBS formulation was 137mM NaCl, 2.7mM KCl, 8.1mM Na_2HPO_4, and 1.8mM KH_2PO_4 combined in deionized water and balanced to pH=7.4.

2.3.9.1 BCA Assay for Protein Quantification of Alpha-Synuclein Monomer

A standard series of albumin was created by diluting a 2mg/mL standard solution with 1x PBS, as per the instructions om the kit, to create a series of concentrations ranging from 25µg/mL to 2mg/mL. Working Reagent was prepared by mixing 50mL of BCA Reagent A with 1mL of BCA Reagent B. A vial of 1.0mg α-Syn was dissolved in 200µL of 1x PBS to create a 5mg/mL α-Syn stock solution. A 35µL aliquot of the α-Syn stock was diluted 1-in-10 in 1x PBS. Each standard and unknown solution was prepared in triplicate by pipetting 100µL of the sample

into a microcentrifuge tube and mixing with 2mL of Working Reagent. The samples were vortexed briefly and placed on the incubator at 37°C and shaken at 130RPM for 30 minutes. The samples were allowed to cool to room temperature and the absorbance of the samples was examined at 562nm.

2.3.9.2 TEM Preparation and Imaging of Alpha-Synuclein Aggregation

The α-Syn solution was diluted to 40μM in 1x PBS to be incubated either combined with a-syn-1 or M5-15, or without the presence of an aptamer. Aliquots of the a-syn-1 and M5-15 stock solutions were diluted to 40μM in 1x PBS. 20μL of α-Syn was combined with either 20μL of a-syn-1 aptamer, 20μL of M5-15 aptamer, or 20μL of 1x PBS as a control. The samples were briefly mixed and 8μL of the α-Syn control was plated on Carbon 200 mesh TEM grids for ten minutes. The excess solution was removed and placed back into the respective incubation sample, and the grids were left to dry. The samples were incubated at 37°C and shaken at 130RPM for 25 days. After 25 days of incubation, 8μL of the α-Syn control, α-Syn and a-syn-1 aptamer, and α-Syn and M5-15 aptamer were plated onto Carbon 200 mesh TEM grid for ten minutes. The excess solution was removed from the grid and placed back into the respective incubation sample, and the grids were left to dry. TEM grids were also plated after four, eight, and ten days of incubation to monitor potential fibril growth.

2.3.10 Longitudinal Assay of Alpha-Synuclein for Pre-Formed Fibrils by Thioflavin T and SEM

A solution of α-Syn for pre-formed fibrils (PFF) (Proteos), formulated to undergo more rapid fibrillization, was purchased. The α-Syn solution was quantified using the Pierce™ BCA Protein Assay Kit. The ability for the aptamers to inhibit the aggregation after one week of incubation was examined by SEM. The protocol supplied with the α-Syn provided the quantification of and aggregation conditions for the α-Syn.

2.3.10.1 BCA Assay for Protein Quantification of Alpha-Synuclein for Pre-Formed Fibrils

A formulation of α-Syn for PFF was firstly quantified using the Pierce™ BCA Protein Assay Kit. The standard series of albumin was created by diluting the 2mg/mL standard with 1x DPBS following the Standard Test Tube Protocol as per the instructions included with the kit. Working Reagent was prepared by mixing 50mL of BCA Reagent A with 1 mL of BCA Reagent B. The α-Syn for PFFs was dissolved in 200µL of 1x DPBS to create a 5mg/mL stock and a 35µL aliquot was diluted 1-in-10 in 1x DPBS. Each standard solution and the unknown solution was prepared in triplicate by pipetting 100µL of the sample into a microcentrifuge tube and mixing with 2mL of Working Reagent. The samples were vortexed briefly and placed on the incubator at 37°C and shaken at 130RPM for 30 minutes. The samples were allowed to cool to room temperature and the absorbance of the samples was examined at 562nm.

2.3.10.2 Thioflavin T Assay for Alpha-Synuclein Aggregation and SEM Sample Preparation and Imaging

Thioflavin T (ThT) stock solution was prepared by dissolving 0.0128g of ThT in 40mL of 1x DPBS. For each day the experiment was conducted, the working ThT solution was produced by diluting 25µL of the stock solution with 975µL of 1x DPBS. Each aptamer candidate was combined with α-Syn PFFs in a 1-to-1 ratio and diluted with 1x DPBS to bring the working solutions to 50µL. An α-Syn control was also prepared to the same final concentration in 50µL of 1x DPBS. 2.5µL of each sample was mixed with 95µL of the working ThT and allowed to stand for 2 minutes. The solutions were then diluted 1:10 with 1x DPBS in triplicate. Sample fluorescence was tested by exciting the sample at 440nm and detecting emission at 482nm. The samples were incubated at 37°C at 135RPM for seven days and the ThT protocol was followed for each sample again.

Samples of each solution were diluted 1:10 and 1:100 and plated for 20 minutes on Carbon 200 mesh TEM grids at the day 0 and day 7 time points, following the ThT assay. The samples for day 0 and day 7 were imaged using a JEOL JSM-7500F Field Emission SEM.

2.4 Results and Discussion

2.4.1 Synthesis and Purification of Aptamers

Each aptamer used for the *in vitro* experiments was synthesized with a fluorescein label on the 5' end of the aptamer. Following synthesis, the aptamers had to be purified to remove incomplete sequences from the synthesis. PAGE purification was performed to separate the sequences by size. Images of the gels were taken using the epi UV setting and 302nm fluorescent

setting to visualize the DNA and the fluorescein label, respectively. The band exhibiting the fluorescein corresponded with the full-length aptamer since the modification occurs on the 5'-tail of the oligonucleotide. An example of PAGE purification is shown in Appendix 6.1. The theoretical extinction coefficients of each aptamer were calculated using the OligoAnalyzer® Tool, version 3.1. The extinction coefficients of each aptamer are shown in Table 2.1. Results of the ESI-MS from Novatia confirm the mass of the aptamer. An example of the mass spectrometry results is shown in Appendix 6.2.

2.4.2 Secondary Structure Prediction of Aptamers using RNAstructure

The secondary structures of the aptamers were predicted using the online tool RNAstructure[90] to find the minimum free energy structure of the aptamer sequences, Figure 2.1. All of the aptamer sequences display stem-loop formations in their structures with regions that bulge in parts of the stem where there is no base complementarity. It is likely that binding of the aptamer to α-Syn is reliant on the loops present in the secondary structure of each aptamer. Unfortunately, due to the complexity of secondary and tertiary aptamer structures, predictions of G-Quadruplex formation and visualization with this software is not possible.

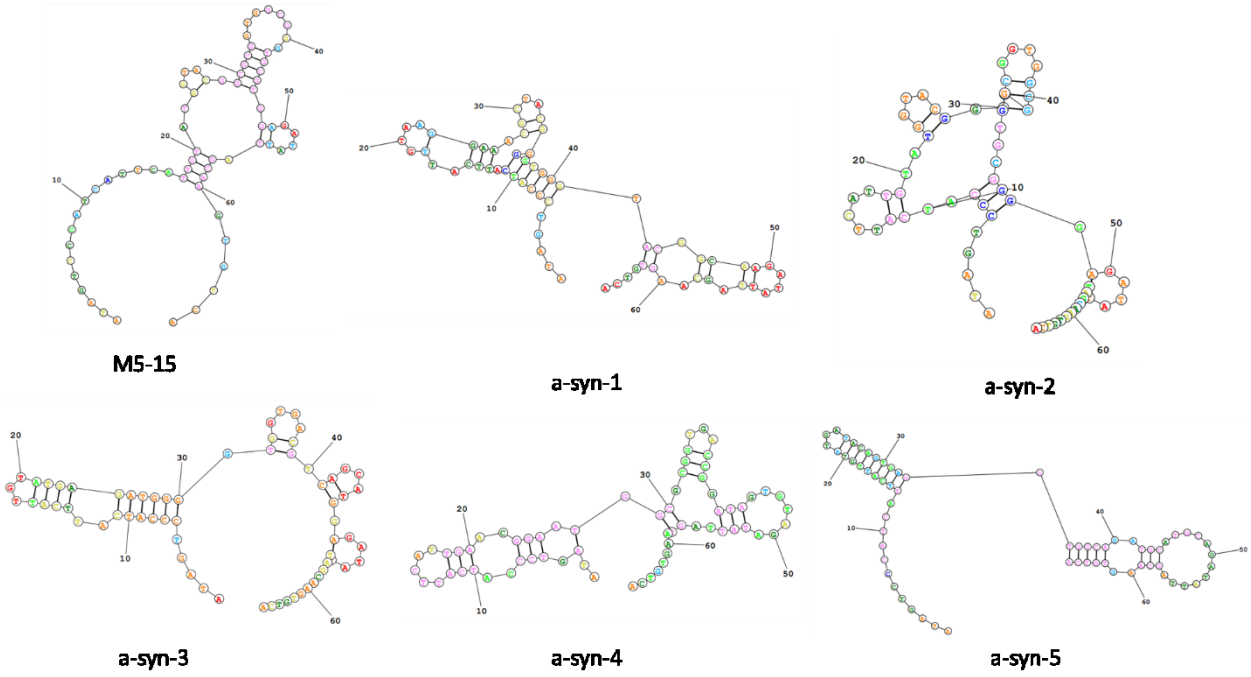

Figure 2.1: Predicted secondary structures of the M5-15 and a-syn aptamers to determine the minimum free energy conformations.

2.4.3 Melting Temperature Analysis for Aptamer Structure Determination

Melting temperature analysis was performed on all of the aptamers to better understand their structure and stability. The melting temperatures of each aptamer were determined in 1x PBS by measuring the absorbance of the DNA at 260 nm and 295 nm across a temperature gradient of 25°C to 85°C. As the temperature of an aptamer solution rises, hydrogen bonding between base pairs and base stacking is disrupted causing the aptamer to denature and unfold. This denaturing is observed as an increase in absorbance at both 260 nm and 295 nm. G-rich sequences can form a stable quadruplex; G-quadruplex conformations result in hyperchromicity of the aptamer at 295 nm. As the temperature is increased and the G-quadruplex melts, hypochromicity of the sample is observed resulting from the loss of the chromophore at 295nm.

The T_m, the point at which half of the aptamers in solution have denatured, for each aptamer was determined from the inflection point of the curve after fitting a four-parameter logistical curve to the average absorbance obtained at each temperature point. The error of the melting temperature was determined using the standard error from the four-parameter logistical regression.

The thermal denaturation of each aptamer at 260 nm is shown in Figure 2.2 and the resulting T_m of the aptamers, shown in Table 2.2, range between 36 and 49°C. The thermal denaturation of each aptamer at 295 nm, shown in Figure 2.3, shows that only the a-syn-2 sequence was capable of forming a G-quadruplex since hypochromicity is observed between 50°C-60°C. Initial hyperchromicity at 295nm, resulting from the denaturing of the aptamer, is offset by hyperchromicity of the G-quadruplex. Since only one of the aptamers displayed a G-quadruplex conformation, the G-quadruplex structure is not determined to be necessary for the aptamers to bind to α-Syn.

Table 2.2: Melting temperatures (Tm) of the a-syn aptamers and M5-15 aptamer determined using UV-Vis Spectroscopy at 260nm. Error of the melting temperature determined from the standard error of the four-parameter logistical curve. Conformation of a G-quadruplex was tested for each aptamer sequence by recording the absorbance at 295nm and observing whether or not the aptamer displayed hyperchromicity. Only the a-syn-2 aptamer displayed hyperchromicity at 295nm as temperature was ramped signifying the formation of a G-quadruplex.

Aptamer Name	T_m at 260nm (°C)	Hypochromicity at 295nm with increasing temperature
a-syn-1	36.3 ± 1.0	No
a-syn-2	37.6 ± 0.2	Yes
a-syn-3	49.5 ± 0.1	No
a-syn-4	37.9 ± 0.2	No
a-syn-5	40.8 ± 0.1	No

M5-15	38.2 ± 0.2	No

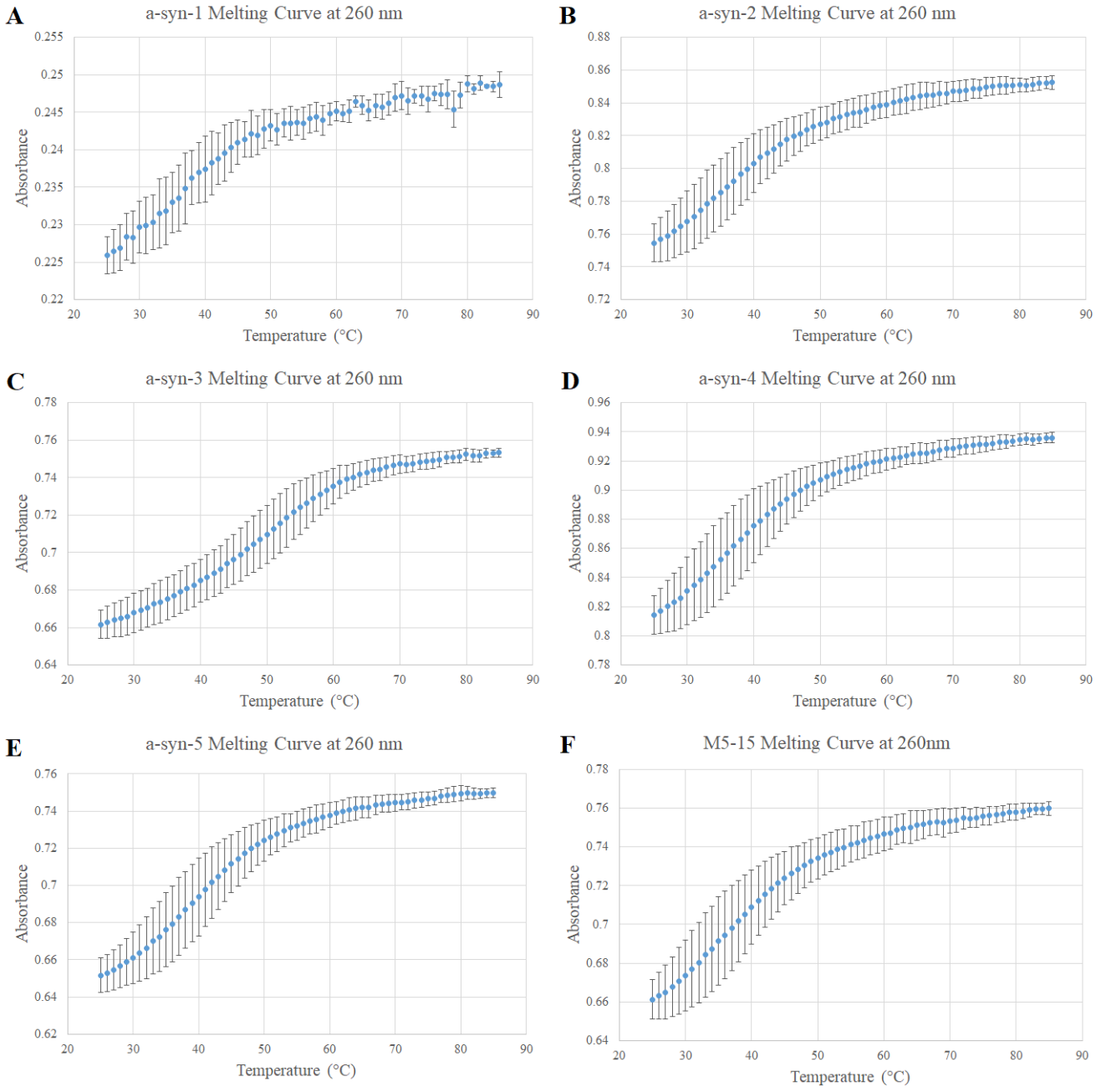

Figure 2.2: Melting temperature (Tm) analysis of A) a-syn-1, B) a-syn-2, C) a-syn-3, D) a-syn-4, E) a-syn-5, and F) M5-15 aptamer at 260nm. Each data point represents the average of two temperature ramps between 25°C and 85°C. The fit curves of the average values for each aptamer were predicted using SigmaPlot 10.

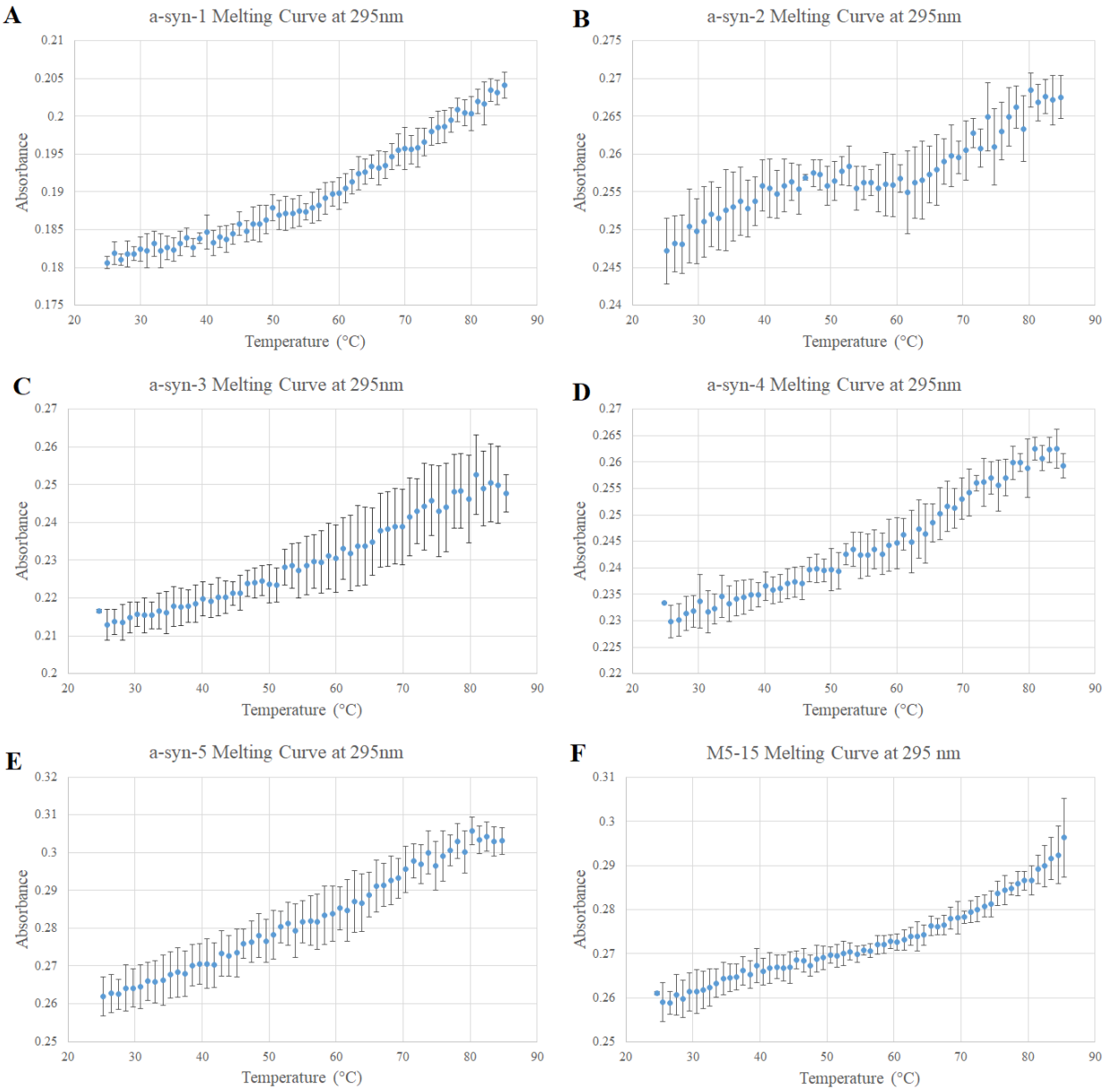

Figure 2.3: Melting temperature (Tm) analysis of A) a-syn-1, B) a-syn-2, C) a-syn-3, D) a-syn-4, E) a-syn-5, and F) M5-15 aptamer at 295nm to observe potential hypochromicity due to G-quadruplex formation. The plateau and hypochromicity of a-syn-2 melting is indicative of G-quadruplex melting as a response to increasing temperature. Each data point represents the average of two temperature ramps between 25°C and 85°C.

2.4.4 Determining the Dissociation Constant of the Aptamers to Monomeric Alpha-Synuclein

2.4.4.1 Electrophoretic Mobility Shift Assay

Gel shift experiments were used to determine the affinity of the aptamers to monomeric α-Syn. Results from the EMSA experiments to determine the dissociation constant of the aptamers to α-Syn can be summarized as non-conclusive across all of the experimental methods attempted. Normally, binding between protein and DNA results in a larger complex that moves through a gel matrix at a reduced rate compared to unbound protein or unbound DNA. Typically, one of the two components are either fluorescently-labelled or radiolabeled for simple visualization and quantification purposes. The result, when imaged, is a visual shift in the location of the protein-DNA complex compared to the migration of unbound DNA and unbound protein. By varying the concentration of one component and maintaining the concentration of the other, the magnitude of the shift will change as more protein-DNA complex is formed. Quantifying the intensity of the fluorescence of the shift across each concentration of α-Syn provides the relative amount of protein-DNA complex leading to the creation of a binding isotherm curve and finding the dissociation constant.

The initial EMSA studies focused on the use of a concentration gradient of α-Syn, from 4nM to 40μM, mixed with a constant concentration of each aptamer. However, no observable shift was produced from any of the a-syn aptamers under the conditions tested. The fluorescent and epi UV images of the gels used in the EMSA assay are shown in Figure 2.4a and b, respectively. To visualize the protein bands to try to observe a shift in the α-Syn migration, the gels were stained in Coomassie G-250, shown in Figure 2.4c. The EMSA utilizing a-syn-2 is displayed as an example. Two notable observations arise: only the lane containing the highest

concentration of α-Syn could be seen when stained and the α-Syn migration through the gel did not align with the protein ladder where the molecular weight of the monomeric α-Syn would be. The sensitivity of the Coomassie stain at the lower limit is 8-28ng of protein, which should be sufficient for the staining of the protein in the 4μM and 0.4μM bands, at least. However, no protein band could be observed. A more sensitive dye may be required for imaging the α-Syn after it is run through gels to detect lower concentrations of protein. The major issue, however, was the probability that the α-Syn used for the EMSA was not actually monomeric. The band of the α-Syn appears beside the protein ladder around 80kDa, instead of approximately 15kDa, in the gel, and there is a thick band at the top of the well where the α-Syn did not enter the gel for separation. While typical PAGE analysis of the α-Syn display proper migration through a gel matrix, the improper migration of the protein through the gel has also been observed[91]. More reasonably, the protein sample, to start, was already aggregating. The addition of α-Syn to the gel matrix may coax the protein to aggregate further, but this would require further investigation.

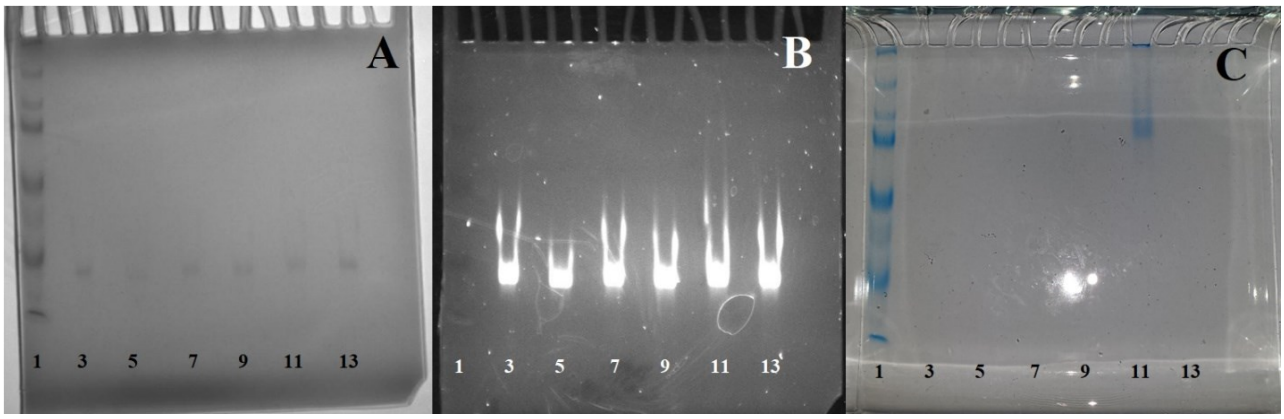

Figure 2.4: Gel shift assay using a concentration gradient of α-Syn incubated with 1μM a-syn-2 aptamer imaged under A) epi UV imaging, B) fluorescence imaging, and C) imaged after Coomassie staining. The lanes are: 1) protein ladder, 3) 0.004μM α-Syn, 5) 0.04μM α-Syn, 7) 0.4μM α-Syn, 9) 4μM α-Syn, 11) 40μM α-Syn, and 13) a-syn-2 control. A typical EMSA should display one band in the aptamer control lane and two bands in the samples with protein and aptamer where the second band is shifted upwards as the protein-DNA complex migrates more slowly through the gel.

The EMSA experiments were repeated using fresh α-Syn monomer, A30P mutant α-Syn, and mimicking the concentrations used during the selection of the aptamers. Unfortunately, under each of these conditions, the α-Syn did not migrate through the gel as expected; protein bands still appeared around 80kDa when compared to the protein ladder. Additionally, no shift in the fluorescent band of the aptamers was observed. For the samples of α-Syn which were incubated or frozen for a long period of time, EMSA was run to investigate potential binding of the a-syn aptamers to various oligomeric forms. No shift in the fluorescent band was observed for these studies either. The gels for each of these experiments are shown in Appendix 6.3.

2.4.4.2 DNase I Assay

The DNase assay was used for two purposes: to find the affinity of the aptamers for monomeric α-Syn and to probe for potential minimers, which may have a greater affinity for the α-Syn monomer than the full-length aptamer. Additionally, since the design of the EMSA requires the protein and aptamer migrate through the gel properly, the usefulness of the DNase approach is that only the DNA need be visualized since the laddering of the aptamer fragments is a result of binding in solution and ignores effects that the gel may impart on the binding between the α-Syn and aptamer.

Results from the DNase I assay also proved inconclusive for the determination of the dissociation constant of the a-syn aptamers to α-Syn. Each lane of a DNase gel contains varying concentrations of α-Syn and constant concentrations of the fluorescently-labelled a-syn aptamers, similar to the EMSA experiments. Following incubation and binding of the aptamers to the α-Syn, DNase degradation can digest the bound and unbound aptamer leading to cleaved oligonucleotide strands of various lengths depending on the portions of the aptamer that are

accessible to degradation. With more target present, more aptamer in solution will exist in a bound state leading to increased representation of certain oligonucleotide strands and thus increased fluorescence of those bands on a gel. The relative fluorescence of each band in a lane is compared to the fluorescence of the same bands in the other lanes using SpotDenso analysis, as shown in Figure 2.5. The values of the SpotDenso analysis are plotted and the trendline is determined using a four-parameter logistical curve regression. The resulting trendline develops the Hill equation where the inflection point of the analysis is the K_d of the aptamer to the α-Syn.

From the trial DNase assay, bands 37-42 provided a binding isotherm and the dissociation constant was determined as 0.015μM ± 0.07μM. Unfortunately, no trend was observed for the full-length aptamer across several gels, and the apparent dissociation constant of the aptamer is based solely on the isotherm generated by a fragment of the aptamer. The DNase assay was inconsistent in producing trends across multiple gels, and so binding affinities for each aptamer were not determined using this method. Another example of a DNase gel for a-syn-1 is shown in Appendix 6.4. DNase digestion would vary, despite strict digestion timing and intermittent agitation of the sample to ensure proper mixing while undergoing DNase treatment, leading to the formation of irregular or incomplete digestion of the aptamer in solution. Another potential limitation of this application is that the only digestion fragments that can be observed are ones where the 3' end has been truncated leaving the 5' fluorophore and varying lengths of digested aptamer. The method could be repeated using a 3'-fluorescently labelled aptamer to observe the truncation of the 5' end of the aptamer through DNase digestion.

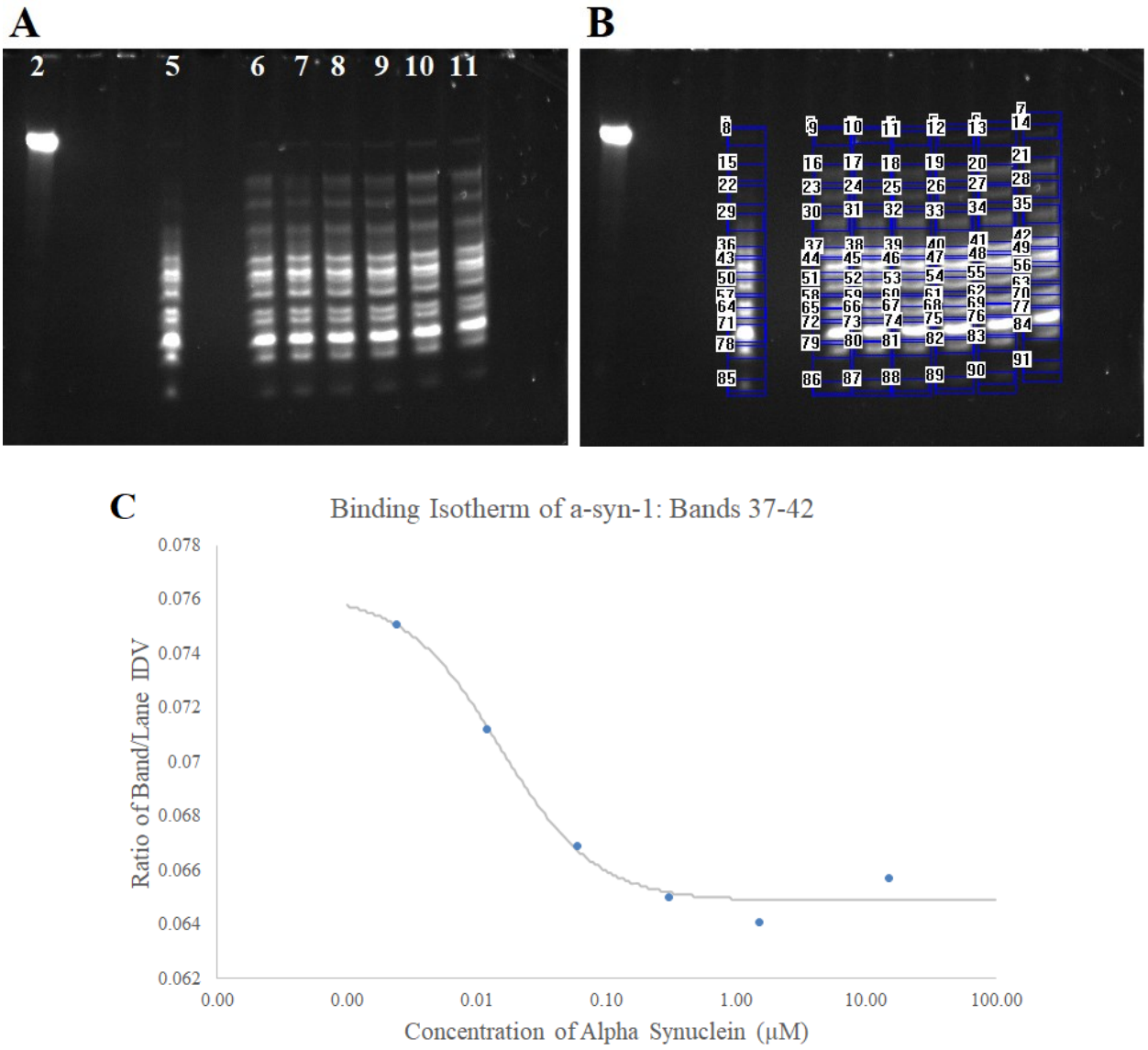

Figure 2.5: The gel and binding isotherm of the DNase trial on the a-syn-1 aptamer. A) The laddering of the fluorescence as a result of the DNase interacting with and cleaving portions of the aptamer into fragments. Lane 2 is the undigested aptamer, lane 5 is the aptamer digestion without α-Syn present, and lanes 6 through 11 correspond to aptamer mixed with 15µM, 1.5µM, 0.3µM, 0.06µM, 0.012µM, and 0.0024µM α-Syn, respectively. B) The SpotDenso analysis of the gel where each lane is analyzed for total fluorescence and the fluorescence of each band in each lane is analyzed. C) The binding isotherm developed by the relative fluorescence of bands 37-42 plotted with a four-parameter regression analysis to provide the dissociation constant. From this analysis, the K_d = 0.015µM ± 0.07µM.

2.4.4.3 Microscale Thermophoresis

Microscale thermophoresis is a highly sensitive method for measuring binding affinity between biomolecules in solution, a ligand and a target. An infrared laser is used to induce a temperature gradient in the solution and the thermophoretic movement of fluorescently-labelled solutes is measured and quantified. The movement of the molecules is dependent on the size, charge, hydration shell, and conformation of the fluorescently-labelled molecule. The ligand-target complex changes these properties and results in a different thermophoretic movement. By altering the concentration of one of the compounds, the observed movement can be plotted as a function of concentration. This results in a binding isotherm from which the dissociation constant of the ligand can be determined[92].

Results from the MST experiments were able to provide a dissociation constant for three of the aptamers, a-syn-2, a-syn-3, and M5-15. But, it was noted that aggregation events had occurred during testing which interfered with the acquisition of the binding isotherm. Figure 2.6 shows the isotherms generated for each of the aptamers. Unfortunately, the binding affinities calculated from this method are likely due to binding of the aptamers to aggregates of α-Syn, or combinations of aggregate and monomer, and not necessarily just monomer α-Syn. The α-Syn sample sent for MST was returned and imaged using TEM to observe the morphology of the protein, shown in Figure 2.7. As expected, large aggregates were observed under TEM.

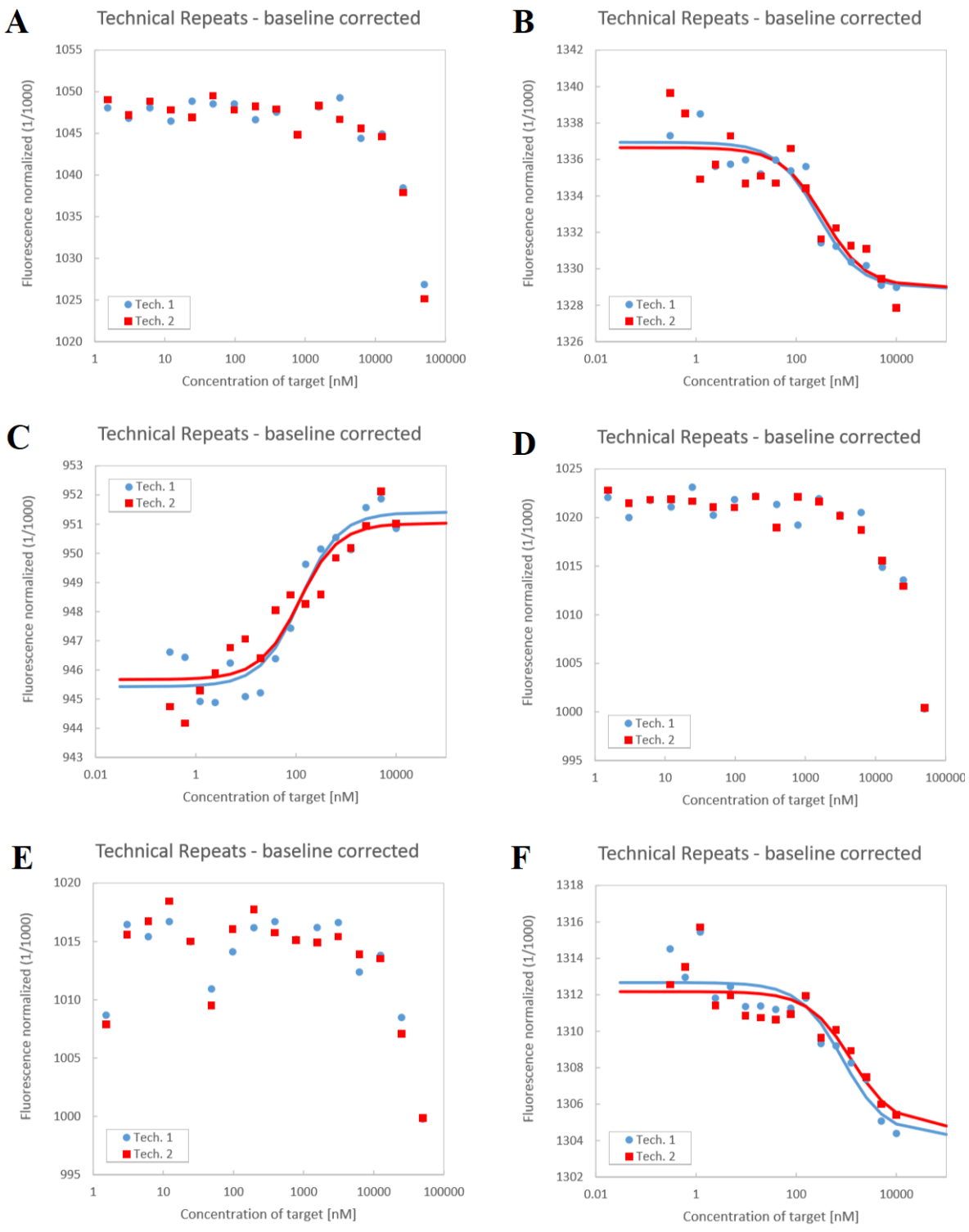

Figure 2.6: Binding isotherms provided from 2bind for the A) a-syn-1, B) a-syn-2, C) a-syn-3, D) a-syn-4, E) a-syn-5, and F) M5-15 were all performed in duplicate. The dissociation constant of a-syn-2, a-syn-3, and M5-15 were calculated to be 285.5nM ± 37.9nM, 94.2nM ± 2.8nM, and 1009nM ± 192nM, respectively. Dissociation constants for a-syn-1, a-syn-4, and a-syn-5 were not able to be determined due to aggregation effects of the α-Syn.

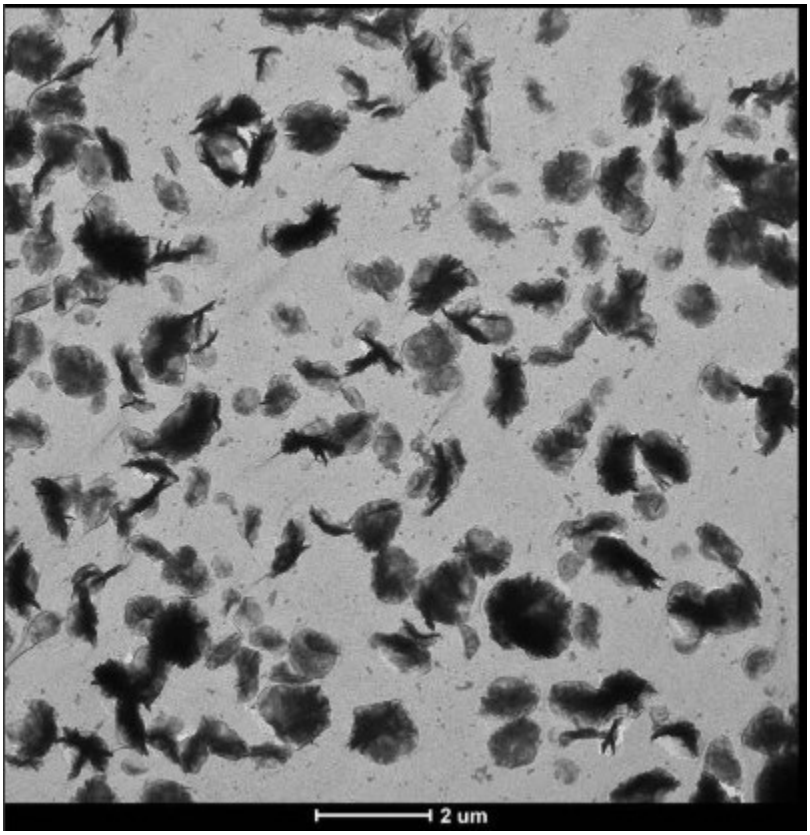

Figure 2.7: TEM image of α-Syn aggregation following shipment to 2bind for MST analysis. Large aggregates of α-Syn observed under TEM are likely reason for the unsuccessful MST analysis. Images taken at the 2µm scale.

2.4.5 Longitudinal Aggregation of Monomeric Alpha-Synuclein

2.4.5.1 BCA Assay of Monomeric Alpha-Synuclein

The stock solution of α-Syn was quantified for use in a long-term incubation mixed with equimolar amounts of aptamers. The BCA assay quantifies proteins based on their ability to convert aqueous Cu^{2+} to Cu^{+}, also known as the biuret reaction, in an alkaline solvent. Bicinchoninic acid is a water-soluble chromophore that complexes with a Cu^{+} ion, shown in Figure 2.8, and produces a purple solution. The intensity of the purple colour is proportional to the concentration of the protein in solution and can easily be measured through UV-Vis spectroscopy at 562nm[93].

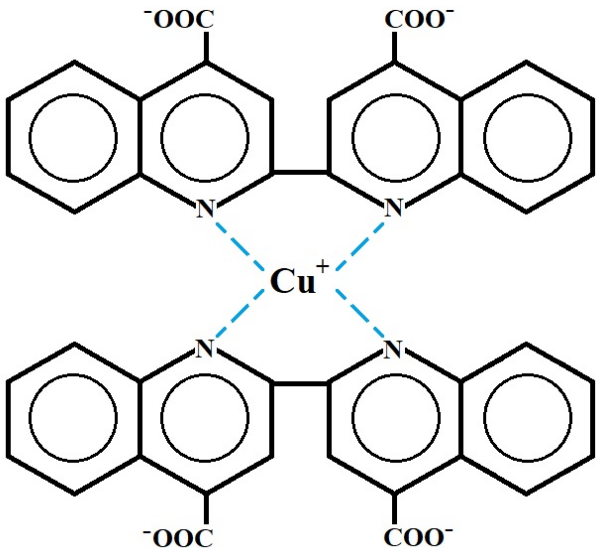

Figure 2.8: Binding of the Cu^{+} ion to bicinchoninic acid in the BCA creating a purple chromophore to quantify the amount of protein present in stock solutions. The complex of cuprous ions with bicinchoninic acid is also believed to exist in competition with Cu+ binding to the peptide backbone of the protein[94].

Prior to aggregation studies, the stock rPeptide α-Syn was quantified using the BCA assay. The standard curve, shown in Figure 2.9, of this assay is based off the formation of Cu^{+}

ions by bovine serum albumin (BSA). Based on the average absorbance of the diluted α-Syn triplicate, the amount of protein in the stock solution was 843µg ± 138µg. Since the protein was supplied at 1.0mg per vial, the BCA assay estimated that 84.3% of the stated protein content was present in the stock solution.

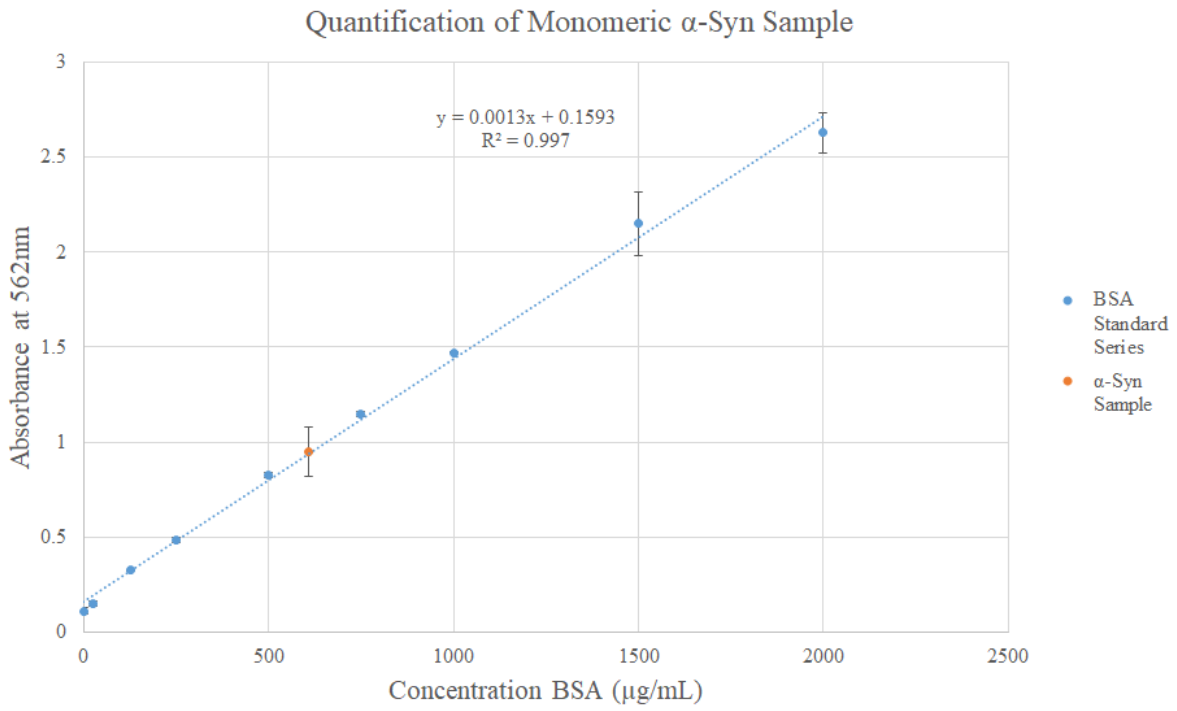

Figure 2.9: Quantification of the α-Syn stock using the BCA assay. The standard curve (blue) was created using known concentrations of BSA and absorbance of the resultant solutions at 562nm. The α-Syn (orange) stock concentration was determined using the absorbance at 562nm. Each standard and α-Syn sample was measured in triplicate.

While the BCA assay boasts higher sensitivity and lower variability in protein quantification than other techniques, namely the Lowry assay, the ability to accurately quantify some proteins based on the BSA standard can still vary. Reduction of Cu^{2+} has been shown to occur due to cysteine, tryptophan, and tyrosine residues as well as the peptide bond itself[95]. Of these amino acids, α-Syn contains only four tyrosine residues in its 140-residue sequence. By

contrast, BSA contains 601 residues of which 35 are cysteine, three are tryptophan, and 21 are tyrosine[96]. The potential for BSA to reduce Cu^{2+} simply by number of residues is much higher than α-Syn. However, the oxidation of the cysteine, tryptophan and tyrosine residues, and the peptide bond at the 37°C incubation temperature is not as great when compared to higher incubation temperatures, which may offset the resulting colour intensity of the BCA as a consequence of fewer Cu^{+} ions forming. The disparity between the supplied 1.0mg of α-Syn and the 843.2µg quantified from the BCA assay may be due to compatibility of the assay for α-Syn.

2.4.5.2 Monitoring Aggregation of Monomeric Alpha-Synuclein using TEM

Equimolar mixtures of the α-Syn stock with either a-syn-1 or M5-15 aptamer were incubated along with a control solution of α-Syn. The aggregation of monomeric α-Syn in the presence of the a-syn-1 and M5-15 aptamers was performed as a comparative study to visualize the efficacy of the aptamers to inhibit aggregation. The α-Syn, which was sourced from rPeptide at the time, showed some larger morphologies in the initial TEM imaging meaning that aggregation of the sample to larger, visible oligomers had already begun. Images of the initial state of the α-Syn solution are shown in Figure 2.10 where a combination of the protein morphologies was observed. Energy-dispersive X-ray spectroscopy (EDX) confirmed the α-Syn in the initial TEM images, as shown in Figure 2.10 by the sulphur peaks from the methionine residues in the α-Syn. The solutions of α-Syn with and without the aptamers was incubated to observe the change in the protein morphology over the course of 25 days.

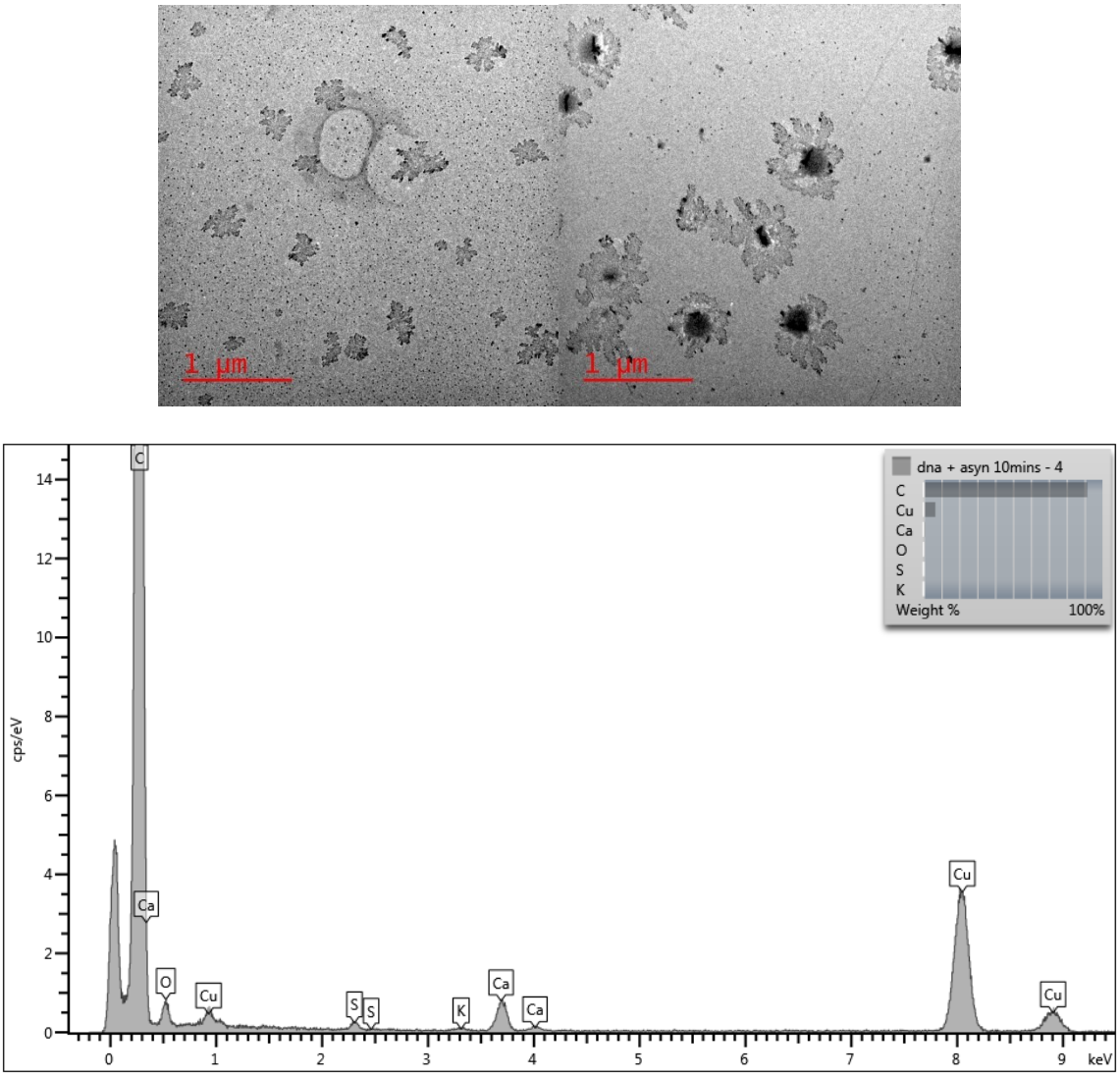

Figure 2.10: TEM images of the α-Syn before incubation with a-syn-1 and M5-15 aptamers to observe the initial α-Syn morphology. After no incubation, the α-Syn stock was deemed to contain some aggregate in solution. Images were taken at 1µm scale and 120kV. EDX analysis was performed on the smaller aggregates imaged in the TEM and α-Syn was confirmed from the sulphur peaks on the EDX spectrum.

After 25 days of incubation, the α-Syn control began to show the formation of larger aggregates but many of the oligomers remained morphologically similar as those observed in the TEMs of the protein at day 0. Figure 2.11a shows an overall view of the α-Syn size and morphology after 25 days of incubation. The larger aggregates do not appear to have undergone

fibrillization in this system. Likewise, the α-Syn which had been mixed with the M5-15 aptamer and incubated also showed some evidence of larger morphologies but remained primarily as smaller oligomers, as shown in Figure 2.11b.

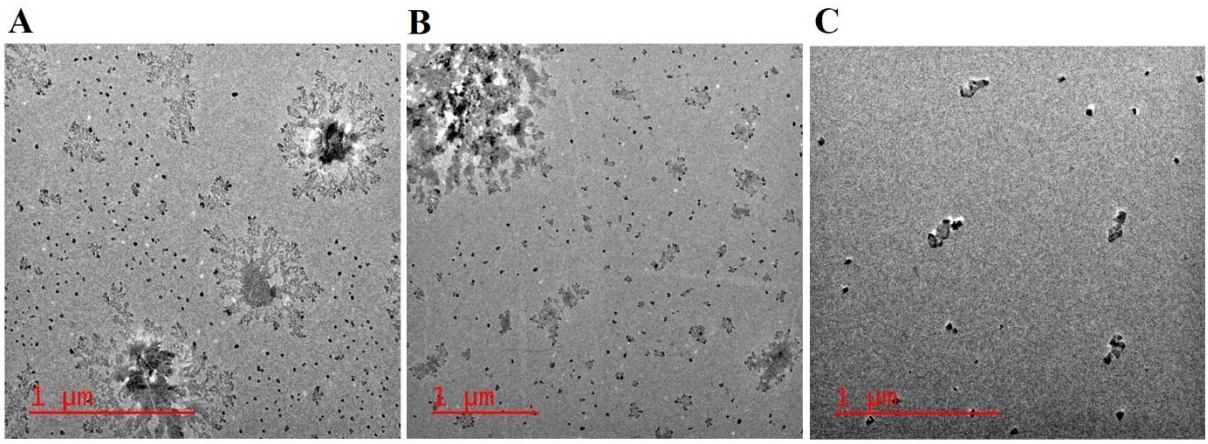

Figure 2.11: Aggregation of α-Syn after 25 days of incubation monitored using TEM to image the morphology of α-Syn in the A) α-Syn control, B) α-Syn incubated with M5-15 aptamer, and C) α-Syn incubated with a-syn-1 aptamer. Images were taken at 1µm scale at 120kV.

By comparison, the α-Syn which was combined with the a-syn-1 aptamer showed considerably smaller aggregates of α-Syn over the 25-day incubation period. Figure 2.11c displays the morphology of the α-Syn aggregates after incubation; no aggregations were found to be similar in size to those seen in the control and M5-15. Consequently, the ability for the a-syn-1 aptamer to inhibit the aggregation of α-Syn more effectively than the M5-15 aptamer became a primary focus. Since the a-syn-1 aptamer showed greatest amplification in the selection process, the initial focus was placed on the a-syn-1 aptamer for aggregation studies.

The shape of the observed aggregates and lack of fibrillization present in the α-Syn control after 25 days of incubation was, at first, unexpected. But, it is possible that the concentration of α-Syn was too low to facilitate the oligomerization and fibrillization of the

protein throughout the incubation. The existence of oligomeric structures of α-Syn at the initial timepoint may have also undermined further aggregation; despite incubation, stable oligomeric forms may not be as susceptible to further aggregation. Incubation of α-Syn oligomers at relatively low concentrations with incubation and shaking have not been shown to form fibrils in solution. But, increasing the concentration of the oligomers to an equivalent of 250μM monomeric α-Syn has resulted in the formation of fibrils after one week[97]. The need for a strictly monomeric α-Syn stock, particularly one that would undergo more rapid fibrillization, was necessary to carry out aggregation studies. Fortunately, a special formulation of monomeric α-Syn for the generation of pre-formed fibrils was available and purchased for further aggregation studies.

2.4.6 Longitudinal Assay of Alpha-Synuclein for Pre-Formed Fibrils by Thioflavin T and SEM

2.4.6.1 BCA Assay of Monomeric Alpha-Synuclein for Pre-Formed Fibrils

Quantification of the new α-Syn for PFF stock was performed for longitudinal aggregation studies using equimolar concentrations of α-Syn to each aptamer. The formulation of α-Syn for PFF was quantified using the BCA assay before aggregation studies began. The standard curve using BSA was generated, Figure 2.12, and the amount of α-Syn present in the stock solution was determined. Similar to the previous results of the BCA assay on the rPeptide α-Syn, the amount of α-Syn for PFF was quantified as lower than what was supplied. Two vials of 1mg α-Syn were combined and quantified, in triplicate, showing the stock contained 1830μg ±

54µg of α-Syn, or 91.5% of the expected amount. The value determined from the BCA assay was used for the aggregation assay.

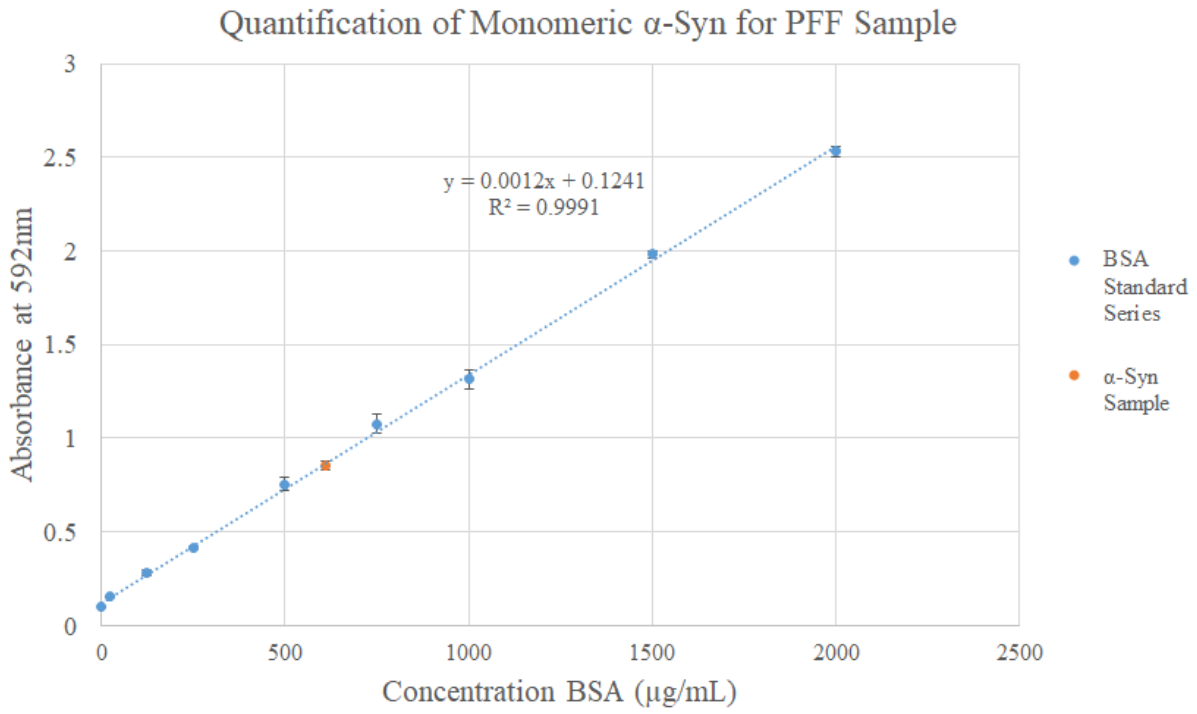

Figure 2.12: Quantification of the α-Syn for PFF stock using the BCA assay. The standard curve (blue) was created using known concentrations of BSA and the concentration of the stock α-Syn (orange) was determined using the absorbance at 562nm. Each standard and α-Syn sample was measured in triplicate.

2.4.6.2 Thioflavin T Assay and SEM Images

After a week of incubation, aggregation of the α-Syn for PFF in the presence of the aptamers was compared to aggregation observed without a-syn aptamers present. Thioflavin T, 3,6-dimethyl-2-(4-dimethylaminophenyl)-benzothiazolium cation, is a molecule that binds to amyloid fibrils and, following excitation at 440 nm, displays increased fluorescence as a result. Unbound in solution, low fluorescence of ThT is due to the free rotation between the benzylamine and benzathiole rings. However, when bound, the rotation of the rings is restricted

thus enhancing the fluorescence[98]. The mechanism of this binding is still unknown, though the current evidence suggests that ThT binds to the ß-sheet region of oligomers and amyloids to produce enhanced fluorescence[99]. Experimentally, the association of ThT to hydrophobic regions of globular proteins has also been observed; typically, the hydrophobic regions were rich in aromatic amino acids allowing for π-stacking of the ThT[98]. It has also been noted that, at high concentrations, ThT has been found to self-associate into micelles that provide increased fluorescence[100].

The fluorescence of ThT was used to monitor the aggregation of α-Syn for PFF in solution with and without the a-syn aptamers present. Fluorescence of the samples was investigated before any incubation had occurred, to observe the initial state of α-Syn in each sample, and after seven days of incubation, to observe the extent of α-Syn fibrillization in each sample, as shown in Figure 2.13. At day 7, the control solution of α-Syn showed a vast increase in fluorescence indicating the sample had undergone oligomerization. By contrast, each sample of α-Syn combined with one of the aptamers displayed far less fluorescence at day 7 than the control, thus inferring that there was little to no aggregation during the incubation. Interestingly, the absorbance of the combined α-Syn and aptamer solutions showed some fluorescence at day 0 compared to the α-Syn control. The comparatively greater fluorescence of these samples is likely due to the binding of ThT to the aptamers. ThT has been shown to bind to DNA via electrostatic interaction with the phosphate backbone[101]. Since the aptamers would not have instantly bound to α-Syn at the day 0 timepoint, it is likely that the structure of some aptamers allowed for intercalation of the ThT. The fluorescence of ThT in the presence of the aptamers without α-Syn was investigated using a single sample of each aptamer, as shown in Figure 2.14. While the fluorescence varies between sample, there is undeniably an interaction with DNA which enables

enhanced fluorescence of the thioflavin T. After seven days of incubation, the aptamers would be bound in equilibrium to the α-Syn and potentially restrict the number of binding regions for ThT to either the aptamer or the protein.

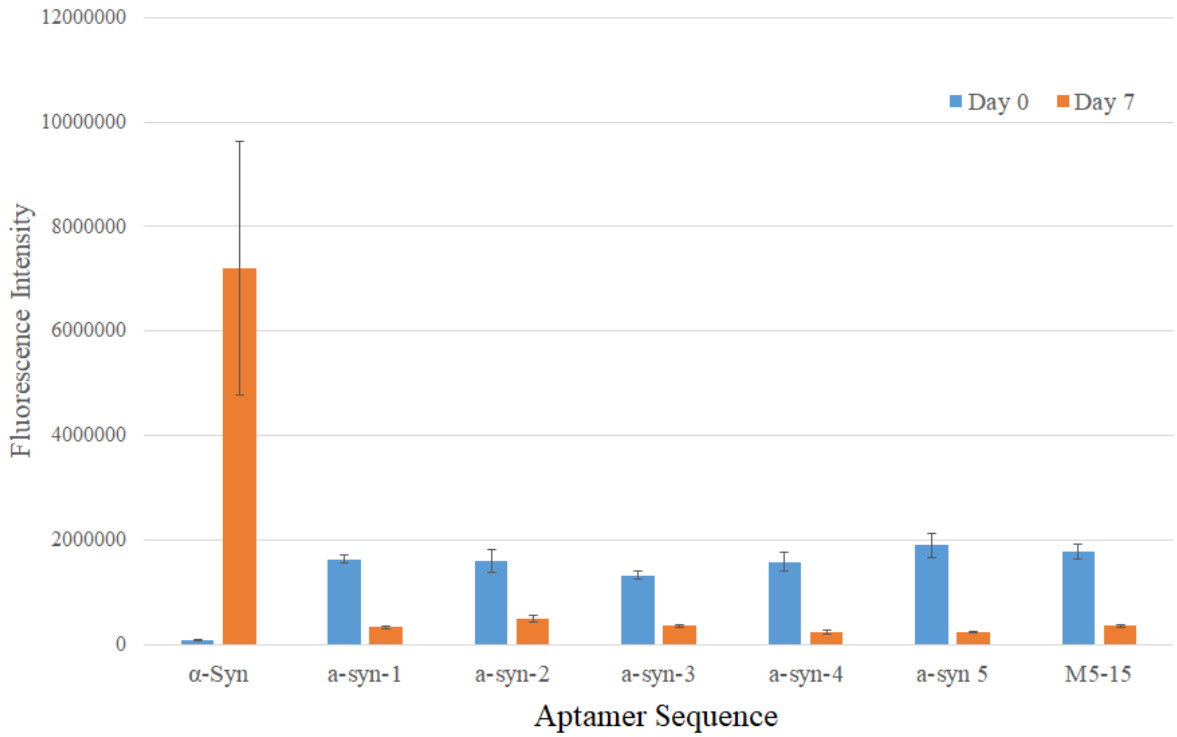

Figure 2.13: Aggregation of α-Syn for PFF monitored using thioflavin T at day 0 (blue) and day 7 (orange) of incubation of α-Syn control (α-Syn) and α-Syn mixed with each a-syn aptamer and with the M5-15 aptamer, labelled with the name of the aptamer combined with α-Syn. Each sample represents the average of triplicate fluorescence measurements and the error is one standard deviation of the fluorescence.

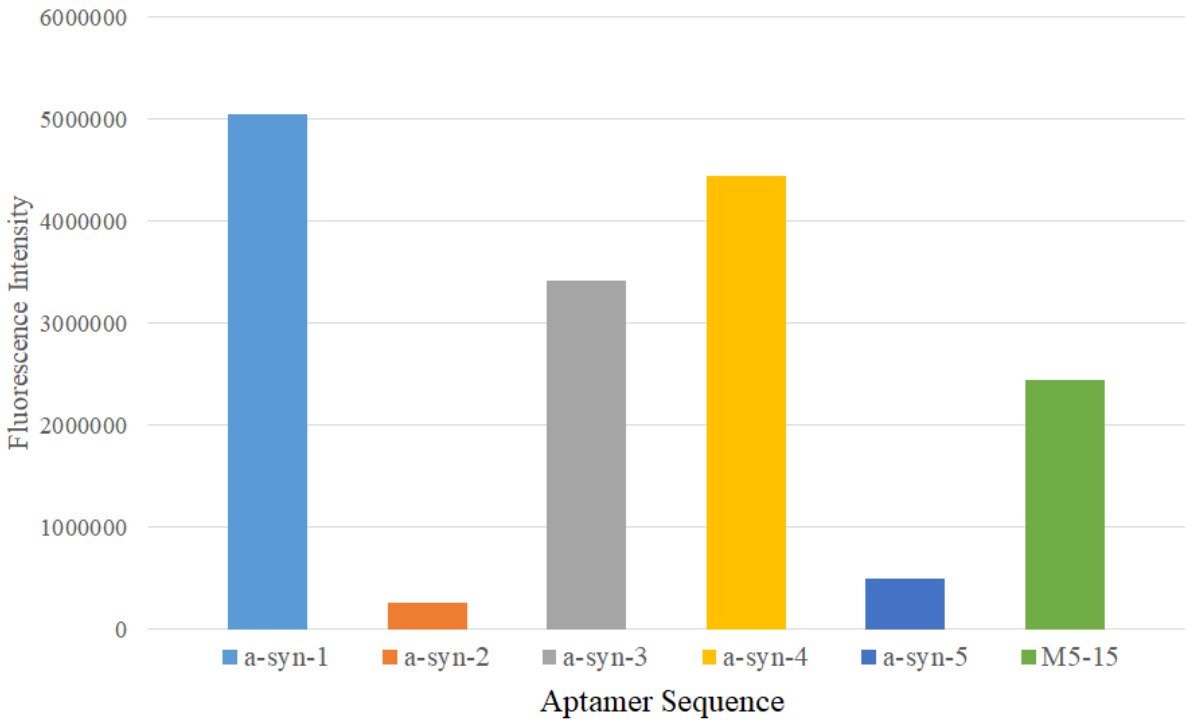

Figure 2.14: Fluorescence of thioflavin T in the presence of each aptamer without α-Syn in solution. Each data point represents a single fluorescence reading for each aptamer sequence after one hour of incubation with thioflavin T.

SEM was also utilized to monitor the aggregation of the α-Syn in solution with and without the aptamers present. Images of the α-Syn at day 0, Figure 2.15, show no fibrillization but some oligomeric morphologies. After seven days of incubation, images of the α-Syn control show that the protein underwent fibrillization Figure 2.16a. The samples of α-Syn combined with each aptamer show little to no aggregation with no fibrillization occurring in any of the samples. The a-syn-1 aptamer appeared to best inhibit the aggregation of α-Syn by SEM imaging compared to the other aptamers, shown in Figure 2.16b. The a-syn-2 aptamer also appeared to inhibit the aggregation of α-Syn greatly, shown in Figure 2.16c. The a-syn-3, a-syn-4, and a-syn-5 aptamers all show the formation of some α-Syn aggregates, but not the formation of mature

fibrils, shown in Figure 2.16d, e, f, respectively. The aggregation of the α-Syn PFF solution in the presence of the M5-15 aptamer also showed some larger aggregate formation, shown in Figure 2.16g. It is not known if these off-pathway aggregations would still exhibit the same neurotoxicity as mature fibrils.

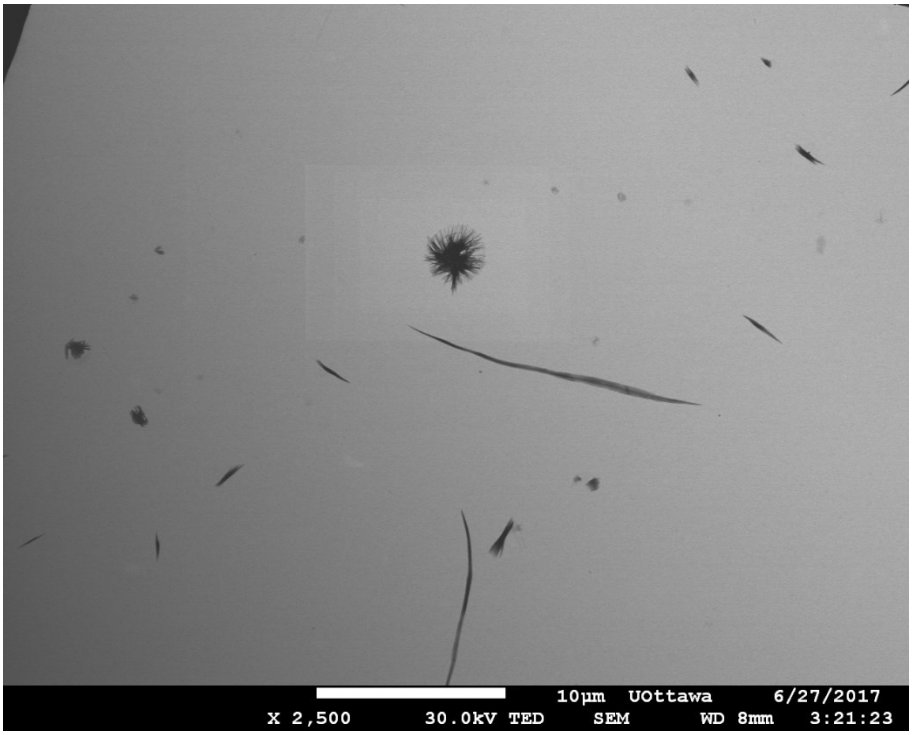

Figure 2.15: SEM image of the α-Syn for PFF solution before incubation. Large α-Syn morphologies exist in solution to seed the fibrillization of α-Syn. Image was taken at 30kV and 10µm scale.

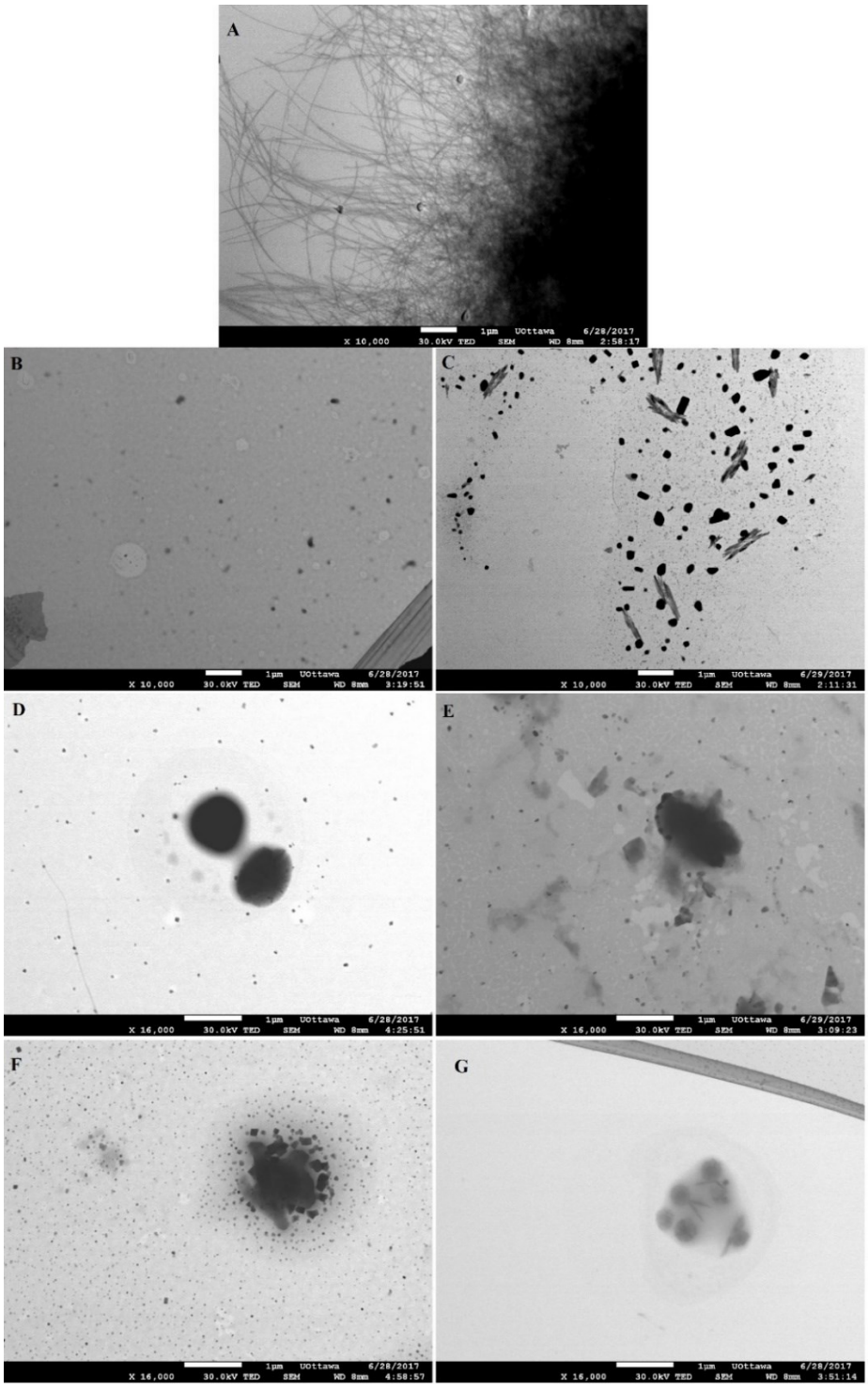

Figure 2.16: SEM images of α-Syn for PFF aggregation after seven days of incubation for the A) α-Syn control, and α-Syn incubated with B) a-syn-1 aptamer, C) a-syn-2 aptamer, D) a-syn-3 aptamer, E) a-syn-4 aptamer, F) a-syn-5 aptamer, and G) M5-15 aptamer. The α-Syn control group exhibits fibrillization of the α-Syn compared to the smaller aggregates visualized in the samples of α-Syn incubated with each aptamer. All SEM images were scaled to 1µm.

The results of the SEM imaging are in line with the results of the ThT assay; the enhanced fluorescence observed in the α-Syn control sample after seven days of incubation corresponds with the extensive fibrillization visualized by SEM. Likewise, the considerably lower fluorescence observed in the samples combining α-Syn with each aptamer agrees with the small or off-pathway aggregations visualized by SEM.

3. Packaging of a-syn-1 Aptamer into Liposomal Vector for Delivery in *in vivo* Experiments

3.1 Statement of Contribution

The procedure for the liposome synthesis was provided by Dr. Erin McConnell. Initial liposome syntheses were performed in conjunction with Dr. Erin McConnell and Josh Callahan. The preparation of liposomes loaded with the dopamine aptamer was conducted with Dr. Erin McConnell and Anna Koudrina. TEM images of the liposomes was performed by Dr. Jianqun Wang.

In vivo experiments were conducted by Katelyn Ventura and Dr. Matthew Holahan. Extraction of mouse brains, livers, and blood was performed by Katelyn Ventura. Extraction of the aptamer from the excised tissues and blood were performed in conjunction with Dr. Erin McConnell, Anna Koudrina, and Katelyn Ventura.

3.2 Introduction

3.2.1 Liposome Design and Synthesis

Typical liposome design for drug delivery involves synthesis of vesicles composed primarily with phospholipids due to their biocompatibility in living systems. Modification of the phosphate head creates different varieties of phospholipids which can alter the properties of the synthesized liposomes. Of the varieties of phospholipids, phosphatidylcholine is the most popular one used in the production of liposomes[102]. The formulation of liposomes, especially those carrying nucleic acid payloads, use cationic lipids for two primary reasons: the positive

charge of the liposome interior can encourage greater encapsulation of negatively charged drugs, and the net positive charge on the surface of the liposome is effective for fusing with negatively charged cell surfaces. During their synthesis, lipids are dried to a thin film and rehydrated resulting in large, multilamellar vesicles[103]. Production of unilamellar liposomes can be achieved by subjecting liposome solutions to freeze-thaw cycles where rapidly freezing and thawing the liposomes provides a mostly unilamellar liposome product[104,105]. Other methods of breaking multilamellar liposomes into unilamellar liposomes is via physical agitation using a sonicator or by extruding the liposomes[104]. Encapsulation of DNA into liposomes can be achieved by adding ethanol dropwise to the liposome slurry, prior to extrusion, by destabilizing the liposomes and encouraging encapsulation of the DNA[103]. Extrusion of the liposomes is performed to ensure that the liposomes are small and of similar size. This also mitigates the formation of larger vesicles due to the destabilization with the ethanol solution[103].

Clearance of liposomes from the circulation is a major concern for drug delivery, especially those with a charged surface[103]. Removal of liposomes from the bloodstream occurs due to phagocytes in the liver and spleen, known as the mononuclear phagocyte system (MPS). Liposome stability can be altered by incorporating other components into the liposome membrane. Sterols, found in naturally occurring membranes, are often used to enforce greater stability of the liposome membrane and reduce the leakage of water-soluble compounds. The integration of sterols has also been shown prevent the interaction of liposomes with proteins in the blood[102]. Modification of the liposome membrane surface with PEG has also been shown to increase the circulation time, resisting uptake of the liposomes in the MPS[106], and stability of liposomes in blood, since PEG is highly soluble in water. In addition, PEG displays biocompatibility due to its low toxicity[102,107]. PEG-modified liposomes have also been shown to

increase the uptake of drugs in cell cultures[108] and the blood brain barrier[109]. Despite these advances, multiple administrations of PEG-modified liposomes has shown some immunogenic responses in the mouse model where repeated injection have led to increasingly greater liposome clearance[110].

DNA amplification is a useful method for detecting specific sequences of DNA, either for diagnostic, forensic, or research purposes. To achieve this, a portion of the target DNA is hybridized with a complementary primer sequence and then extended the length of the target DNA using polymerases. The hybridized DNA is denatured, and the procedure repeated with primers for both strands to continue DNA replication and, thus, amplification. This cyclical process is called polymerase chain reaction, or PCR. Using qPCR (quantitative polymerase chase reaction), the quantity of DNA extracted from a sample can be determined based on the number of amplification cycles a sample experiences before a signal is detected. Signal detection is achieved using a fluorescent dye, such as SYBR-Green I, that binds to double-stranded DNA. When the fluorescence of the sample exceeds a set threshold level, termed the cycle threshold (Ct), the amount of target DNA initially in the sample can be calculated[113].

3.2.2 Chapter Objectives

The objectives of this chapter were to synthesize liposomes for encapsulating the a-syn-1 payload aptamer, modify the external surface of the liposomes with transferrin receptor aptamer (TRA), and extract the aptamer from mouse tissues following injection of the liposomes. The liposomes were also characterized for their size distribution following synthesis and their stability in buffer and human blood serum.

3.3 Materials and Methods

3.3.1 Synthesis of Aptamers for Liposome Experiments

Synthesis of the aptamers for the liposome studies follows the same general scheme presented previously. The payload aptamer used was the a-syn-1 aptamer which was conjugated with a cyanine 3.5 (Cy 3.5) modifier on the 5' end of the oligonucleotide. The dA-CE, Ac-dC-CE, dmf-dG-CE, and dT-CE phosphoramidites were dissolved in anhydrous acetonitrile to 0.1mM and connected to the synthesizer. For the a-syn-1 sequence, Cy 3.5 modifier (GlenResearch) was dissolved in anhydrous acetonitrile, to 0.1µM, and connected to the synthesizer. The TRA was 5'-modified with a C6 S-S thiol modifier (GlenResearch) dissolved in anhydrous acetonitrile, to 0.1µM concentration, and connected to the synthesizer. 1000Å 1µmol dA(Bz) CPG columns were used to provide the initial base in the a-syn-1 synthesis and 1000Å 1µmol dT CPG columns were used for the TRA synthesis. The sequences of the modified a-syn-1 aptamer and TRA are shown in Table 3.1.

Table 3.1: Sequences of the Cy 3.5-modified a-syn-1 payload aptamer and the thiol-modified TRA for conjugation to the outside of the liposome.

Sequence Name	Aptamer Sequence	Extinction Coefficient at 260nm (L mol^{-1} cm^{-1})
a-syn-1	5'-Cy 3.5-ATA GTC CCA TCA TTC ATT GTA AGG AAA CGC TAC GGG GTG GGT ACG GCA AGA TAT TAG CAA GTG TCA-3'	767000
TRA	5'-C6 S-S thiol-GAA TTC CGC GTG TGC ACA CGG TCA CAG TTA GTA TCG CTA CGT TCT TTG GTA GTC CGT TCG GGA T-3'	661400

3.3.2 Purification of Aptamers for Liposome Experiments

3.3.2.1 PAGE Purification of Cyanine 3.5-Labelled a-syn-1 Aptamer

The Cy 3.5-labelled a-syn-1 aptamer was purified using the previously described gel purification method. The oligonucleotide and ammonium hydroxide mixture was centrifuged at 5000RPM for 5 minutes and the supernatant was pipetted into a microcentrifuge tube. The supernatant was dried in the SpeedVac overnight and dissolved in deionized water.

An 18% denaturing polyacrylamide gel was created for each column of oligonucleotide that was synthesized on the DNA Synthesizer. Two gels were created by mixing 31.5g of urea with 23.5mL of 40% 19:1 acrylamide:bisacrylamide, 15mL of 5x TBE, and 14mL of deionized water. The solution was stirred until the urea fully dissolved and was then passed through filter paper 600µL of 10% APS in deionized water and 55µL of TEMED were mixed into the acrylamide solution and briefly stirred. The acrylamide solution was poured into vertical casting plates and allowed to set with a single well for sample loading. This was repeated to create a total of six gels.

An equal volume of formamide was added to the dissolved oligonucleotides and briefly vortexed. The oligonucleotide solution was pipetted onto the gels and run at 300V for 3 hours using a FB1000 Electrophoresis Power Supply. The gel was imaged using the AlphaImager. The band of full-length aptamer was cut from the gel and placed into a 50mL tube.

To extract the aptamer from the gel, the DNA band cut from the gel was shaken in water and incubated at 37°C and 130RPM overnight. After incubation, the solution was poured into a syringe with a 0.22µm pore PES filter and the oligonucleotide solution was filtered into a new

tube. Following filtration, the oligonucleotide solution was desalted using Amicon® Ultra centrifugal filter units with a 3000 molecular weight cutoff. The oligonucleotide solution was pipetted into the filter unit and centrifuged at 10000RPM for 20 minutes until the entire sample was desalted. Three washes with deionized water were also performed by centrifuging at 10000RPM for 20 minutes. After washing, the sample was collected in a new centrifuge tube and stored at -20°C until quantification.

3.3.2.2 Reverse Phase Polymer Affinity Purification of Thiol-Modified TRA

The reverse phase polymer affinity procedure for thiol-modified oligonucleotides follows the same principle steps as the aforementioned procedure. Glen-Pak DNA Purification Cartridges were connected to a vacuum manifold and conditioned with 0.5mL of acetonitrile followed by 1.0mL of 2M TEAA (GlenResearch). The vacuum was adjusted so that the flow rate of solutions through the cartridges was about one drop per second. The oligonucleotide and ammonium hydroxide mixture were centrifuged at 5000RPM for 5 minutes and the supernatant was pipetted onto the cartridges. 1.0mL of salt wash solution was placed into the centrifuge tubes containing the column supports and centrifuged at 5000RPM for 5 minutes. The salt wash supernatant was pipetted onto the purification cartridges. The cartridge was rinsed with two 1.0mL aliquots of deionized water and the aptamers were eluted with 1.0mL of 50% acetonitrile in deionized water containing 0.5% ammonium hydroxide. The collected oligonucleotides were dried on the SpeedVac. The dried oligonucleotides were dissolved in deionized water and frozen at -20°C until quantification

3.3.2.3 Quantification and Preparation of a-syn-1 Aptamer and TRA

Quantification of the Cy 3.5-labelled a-syn-1 and the TRA was performed using UV-Vis spectroscopy to find the absorbance at 260nm. Samples of the aptamer solutions were diluted in deionized water so that the absorbance measured between 0.4 and 0.8. The concentration of the aptamer stocks was determined using the Beer-Lambert law; the theoretical extinction coefficient of the aptamers and the absorbance at 260nm were used to find the concentration of the purified aptamers. 1nmol of each aptamer sequence was dried and sent to Novatia for ESI-MS.

To prepare the aptamers for the liposome synthesis, aliquots of each aptamer were pipetted into microcentrifuge tubes. 38nmol of the Cy 3.5-labelled a-syn-1 and 120nmol of thiol-modified TRA were dried on the SpeedVac for each batch of liposomes being synthesized.

3.3.3 Dual-Aptamer Liposome Synthesis with Aptamer Payload and Transferrin Receptor Aptamer Modification

3.3.3.1 Liposome Synthesis with a-syn-1 Aptamer Payload

Prior to the synthesis, all glassware used in the synthesis was washed by soaking the glassware in warm soap water for at least 15 minutes. The soap water used for soaking contained Sunlight brand dish soap to clean the glassware. The glassware was then rinsed 25 times with tap water, ten times with distilled water, and five times with deionized water. The glassware was left to dry overnight.

The POPC, DDAB, DSPE-PEG(2000), and DSPE-PEG(2000) maleimide lipids, the mini-extruder, 100nm polycarbonate filters and filter supports were all obtained from Avanti

Polar Lipids. The 50mM HEPES buffer was prepared by dissolving 11.92g of HEPES in 900mL of deionized water, correcting the pH to 7.0, and topping the solution to 1L.

To begin liposome synthesis, stock solutions of POPC, DDAB, and DSPE-PEG(2000) maleimide were created; 100mg of POPC was dissolved in 8mL of chloroform, 1.0mg of DDAB was dissolved in 1.0mL of chloroform, and 1.0mg of DSPE-PEG(2000) maleimide was dissolved in 1mL of chloroform. In a 10mL round bottom flask, 1.7mg of DSPE-PEG(2000) was added followed by 1.17mL of POPC solution, 126.3µL of DDAB solution, and 88.25µL of DSPE-PEG(2000) maleimide solution. The flask was capped with a septum and wrapped with Parafilm. The chloroform was gradually evaporated from the flask under a steady flow of argon and light shaking to create a film of lipid across the bottom of the flask. The film was hydrated using 200µL of 50mM Tris-HCl, pH=7.0, and vortexed gently for 30 minutes to form the liposomes. The sample was then stored under argon, wrapped with Parafilm, and sonicated in a water bath sonicator at room temperature for ten minutes. 38nmol of dried Cy 3.5-labelled a-syn-1 was dissolved in 200µL of 50mM Tris-HCl, pH =7.0, and added to the liposome solution. To encapsulate the aptamer, 600µL of 67% ethanol in 50mM Tris-HCl was added dropwise to the liposome solution with gentle shaking. The sample was stored under argon and underwent ten freeze/thaw cycles where the flask was placed in an ethanol/dry ice bath for five minutes followed by a 40°C water bath for two minutes. The liposome sample was drawn from the round bottom flask and extruded through a 100nm polycarbonate filter 25 times, in both directions, and stored briefly in an amber vial. The liposome sample was then placed into a Slide-A-Lyzer® Dialysis Cassette with 20000 molecular weight cutoff (ThermoFisher) and dialyzed overnight in 50mM HEPES buffer, pH=7.0. The liposome sample was removed from the dialysis and stored in an amber vial for nuclease digestion in order to remove non-specifically bound or loaded

aptamer. The liposome sample was mixed with 10µL of DNase I in 10x reaction buffer for 15 minutes with gentle, intermittent shaking. Afterwards, 5µL of stop buffer was introduced to the sample and briefly vortexed. The liposome sample was dialysed overnight in 50mM HEPES buffer, pH=7.0. After dialysis, the liposomes were conjugated with TRA containing a 5' thiol modifier. Activation of the thiol began with cleaving the disulfide bond of 120nmol of TRA in 75µL of 50mM Tris-HCl, pH=8.4, containing 100mM DTT by incubating the TRA at room temperature for 30 minutes while shaking. The TRA was purified by centrifugation at 1G for four minutes using Micro Bio-Spin Columns (Bio-Rad) and buffer exchanged into 50mM HEPES, pH=7.0, containing 7mM EDTA with four successive washes of the column at 1G for four minutes. The TRA and washes were then centrifuged in an Amicon® Ultra 3000 molecular weight cutoff centrifugal filter unit at 10G for 20 minutes until all washes were run through the column. The purified TRA was obtained by reversing the column in a fresh centrifuge tube and centrifuging the sample at 1G for four minutes. The TRA was added to the liposomes in an amber vial and allowed to react for two hours at room temperature with gentle shaking. Following the reaction, the liposome sample was dialysed in 50mM HEPES buffer, pH=7.0, for either four hours or overnight to remove the EDTA and TRA that did not react. In the scenarios where dialysis could only proceed for four hours, the buffer was changed after one hour to hasten the dialysis. The liposome preparation is outlined in Figure 3.1. Some batches of liposomes were not modified with TRA and simply underwent a third dialysis without conjugation of an aptamer. Liposomes which were modified with TRA were labelled TRA-positive and those without modification were labelled TRA-negative.

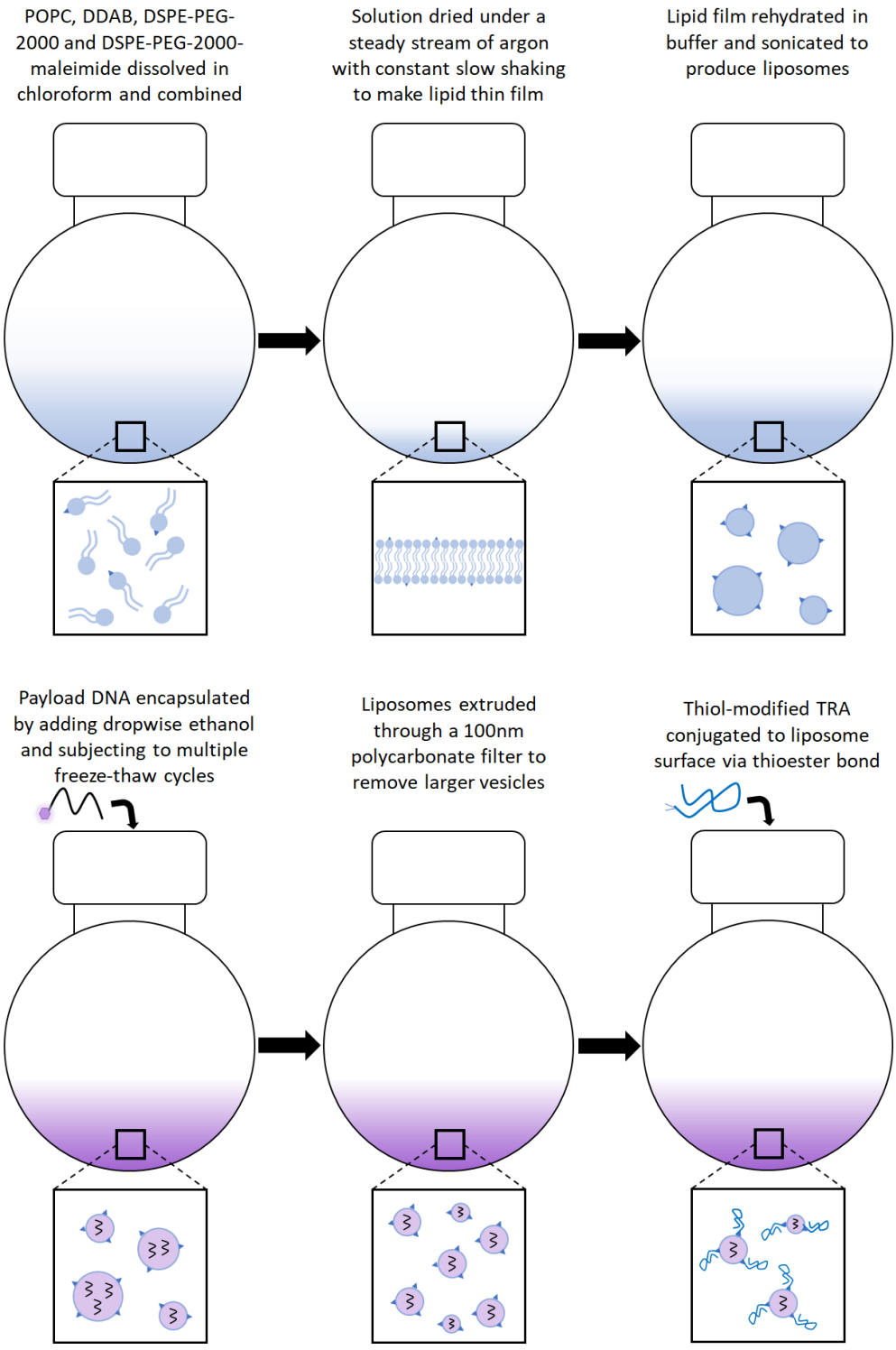

Figure 3.1: Liposome preparation schematic for the synthesis of double membrane liposomes encapsulating Cy 3.5-labelled a-syn-1 aptamer payload and externally modified with TRA to carry the liposome and payload across the BBB.

3.3.3.2 Liposome Synthesis with DBA Payload

A variation of this liposome fabrication was performed for an isolated experiment using the previously studied dopamine binding aptamer (DBA) as the payload. The DBA was not fluorescently labelled for loading, and the rhodamine-labelled lipid 1,2-dipalmitoyl-sn-glycero-3-phosphoethanolamine-N-(lissamine rhodamine B sulfonyl) (ammonium salt), or Liss Rhod PE (Avanti Polar Lipids), was used.

Stock solutions of POPC, DDAB, DSPE-PEG(2000) maleimide, and Liss Rhod PE were prepared by dissolving 100mg of POPC in 8mL of chloroform, 1.0mg of DDAB in 1mL of chloroform, 1.0mg of DSPE-PEG(2000) in 1mL of chloroform, and 1.0mg of Liss Rhod PE in 1mL of chloroform. In a 10mL round bottom flask, 1.1mg of DSPE-PEG(2000) was combined with 88.25µL of the DSPE-PEG(2000) maleimide stock, 126.3µL of the DDAB stock, 1.17mL of the POPC stock, and 250µL of the Liss Rhod PE stock. The lipids were dried under argon and gentle shaking to create a thin film and were rehydrated with 200µL of 50mM Tris-HCl, pH=7.0. The samples were vortexed gently for 30 minutes to form the liposomes and stored under argon. The liposome solutions were placed in a sonicator at room temperature for ten minutes. 38nmol of DBA, previously synthesized and dried, was dissolved in 200µL of 50mM Tris-HCl, pH=7.0, and added to each batch of liposomes. 600µL of 67% ethanol in 50mM Tris-HCl was added dropwise to the liposome solution and shaken gently. The liposomes were stored under argon and underwent ten freeze-thaw cycles with five minutes in a dry ice and ethanol bath followed by two minutes in a 40°C water bath. The liposomes were then extruded through a 100nm polycarbonate filter 25 times and dialyzed overnight in a 20000 molecular cutoff dialysis cassette in 50mM HEPES, pH=7.0. The liposome solutions underwent nuclease digestion using 10µL of DNase I in 10x reaction buffer for 15 minutes with gentle, intermittent shaking. 5µL of stop

buffer was pipetted into the liposome solution and briefly vortexed. The liposomes were dialyzed overnight in a 20000 molecular cutoff dialysis cassette in 50mM HEPES, pH=7.0. Three batches of liposomes were treated differently at this point to create three treatment options; one batch was modified with TRA, one batch with a mutant, GS24, transferrin aptamer, and one batch without an aptamer targeting the TR. 120nmol of dried TRA or dried GS24 aptamer, both 5' thiol modified, was dissolved in 75µL of 50mM Tris-HCl, pH=8.4, containing 100mM DTT and incubated for 30 minutes at room temperature while shaking. The TRA and GS24 aptamers were purified by centrifugation at 1G for four minutes using Micro Bio-Spin Columns and buffer exchanged into 50mM HEPES, pH=7.0, containing 7mM EDTA with four washes of the column at 1G for four minutes. The TRA and GS24, and their respective washes, were then centrifuged in an Amicon® Ultra 3000 molecular weight cutoff centrifugal filter unit at 10G for 20 minutes until all washes were run through the column. The TRA and GS24 were added to separate batches of liposomes and allowed to react for two hours at room temperature with gentle shaking. The TRA-modified (TRA-positive), GS24-modified, and unmodified (TRA negative) liposomes were placed into separate 20000 molecular cutoff dialysis cassettes and dialyzed overnight in 50mM HEPES, pH=7.0. Following quantification, each batch of liposomes was injected at a 1x concentration into three mice to observe whether the payload aptamer was present in brain and blood samples half an hour after intraperitoneal (i.p.) injection, injection of a sample into the stomach. DNA extraction was performed by Dr. Erin McConnell and Anna Koudrina for these samples; a total of 17 samples were sent to Syd Labs for qPCR.

3.3.4 Quantification of Liposomes for *in vivo* Applications

3.3.4.1 Quantification Method for a-syn-1 Loaded Liposomes

Following dialysis, the concentration of a-syn-1 loaded in the liposomes was determined by UV-Vis spectroscopy using a 1-in-10 dilution at 590nm, corresponding with the Cy 3.5 peak, to ensure that aptamer loading was consistent between batches. When dilutions were necessary to maintain consistency in the amount of aptamer per injection, 50mM HEPES, pH=7.0, was used to dilute the samples. The general amount of aptamer in the sample was determined using a 1-in-100 dilution at 260nm, corresponding with the absorbance of DNA, to estimate the amount of TRA present.

3.3.4.2 Quantification Method for DBA Loaded Liposomes

Quantification of the liposomes was dependent on the absorbance of the rhodamine peak at 570nm and not the payload DNA for these experiments. Dosage of the liposomes for the treatment groups followed previous experiments performed by Dr. Erin McConnell[110] where 1x treatments corresponded to an absorbance of rhodamine was approximately 0.05 for a 1-in-100 diluted sample of liposomes.

3.3.5 PAGE of Liposome Samples taken throughout Synthesis

Aliquots of the liposome samples were taken throughout the synthesis to examine the loading of a-syn-1 in the liposome and conjugation of the TRA to the liposomes using gel electrophoresis. Samples were taken before the liposomes were extruded, after they were

extruded, before DNase treatment, after DNase treatment, before TRA conjugation, and after the final product was acquired; the samples were named pre-extrusion, pre-dialysis 1, post-dialysis 1, pre-dialysis 2, post-dialysis 2, and final liposomes, respectively. A multi-well 12% non-denaturing polyacrylamide gel was prepared by combining 18mL of 40% acrylamide, 12mL of 5x TBE, and 29mL of H_2O together, followed by 60µL of TEMED and 600µL of 10% APS. The gel was poured into a vertical casting unit and a multi-well comb was used to form the wells. The gel was run at 250 V for at least 30 minutes in 1x TBE before the samples were loaded. A 40µL aliquot of each liposome sample was mixed with 40µL of 50% glycerol in deionized water, and the total volume was loaded into a well of the gel. A control lane containing pure Cy 3.5 modified a-syn-1 aptamer was run alongside the liposome samples. Wells that were not loaded with a-syn-1 or liposome samples contained an 80µL injection of 50% glycerol in deionized water to minimize smiling of samples across the gel. The PAGE was run at 250V for at least half an hour before samples were loaded into the wells, and then run at 250V for at least 2 hours after samples were loaded. The gel was then imaged using the AlphaImager.

3.3.6 Liposome Quantification using Stewart Assay and TEM

To analyze the lipid composition of the a-syn-1 loaded liposomes, lipid solutions were prepared using the stock solutions of POPC, DDAB, and DPSE-PEG(2000) maleimide from the liposome synthesis to create a standard series. 1.17mL of POPC, 126.3µL of DDAB, and 88.25µL of DSPE-PEG(2000) maleimide solutions were combined with 1.7mg of DSPE-PEG(2000) in an amber vial. The lipid solution was diluted to 0.1mg/mL using 25.12µL of the lipid stock and 2974.88µL of chloroform. A standard series was created ranging from 0 to 0.05mg/mL using chloroform to dilute all samples. The liposome solution previously synthesized

was diluted 1-in-20 in chloroform. Ferrothiocyanate reagent was made by dissolving 0.2703g of ferric chloride and 0.3040g of ammonium thiocyanate per 10mL of deionized water. Ferrothiocyanate reagent was added, in equal volume, to each sample of the standard series and the diluted liposome solutions. The samples were vortexed for approximately 20 seconds and then centrifuged at 1000RPM for ten minutes. The absorbance of each sample of the standard series was observed at 485nm by pipetting the lower layer of the samples into a cuvette. The lower layer of the liposome samples underwent an additional 1-in-10 dilution, as it was too concentrated, and the absorbance was observed at 485nm. Every sample was run in triplicate for this assay.

The size distribution of the liposomes was observed using TEM. Carbon 200 mesh TEM grids were plated with liposome solutions diluted to 1-in-10 and 1-in-100 in 50mM HEPES, pH=7.0. From the size distribution, the average liposome size was determined and used to calculate the total number of theoretical liposomes present in each batch created as well as the average number of aptamers loaded into the liposomes.

The number of liposomes in an aliquot of liposome solution was determined using a mathematical model from Montanari et. al.[113] to determine the volume of the average liposome in the solution, assuming a spherical model and uniform composition.

3.3.7 Liposome Stability in HEPES using UV-Vis Spectroscopy, Fluorimetry, and TEM

Stability of the a-syn-1 loaded liposomes was investigated through a combination of fluorometry, UV-vis spectroscopy, and TEM every day for ten days. The final liposome

solutions for TRA-positive and TRA-negative liposomes, from two batches synthesized on May 30th, 2017, were diluted 1:20 and 1:200 in 50 mM HEPES, at pH=7.0, to a total volume of 550µL per dilution for each study. All four liposome solutions were tested in 60µL aliquots using the fluorimeter, which excited the samples at 590nm and detected emission between 560 to 660nm. The absorbance of the liposome solutions was tested in 70 µL aliquots using UV-Vis spectroscopy between 800 and 200nm. All UV-Vis and fluorometric measurements were performed in triplicate and liposome solutions were left at room temperature between experiments each day.

3.3.8 Liposome Stability in Human Blood Serum using TEM

The stability of the DBA-loaded liposomes was studied in human blood serum, from human male AB plasma (Sigma Aldrich). Five different conditions were examined for liposome stability using the 1x concentration of liposomes: a 50/50 mixture of liposome solution and serum; 50/50 mixture of liposome solution and 50mM HEPES, pH=7.0; 50/50 mixture of serum and 50mM HEPES, pH=7.0; 10/90 mixture of liposome solution and serum; and a 10/90 mixture of liposome solution and 50mM HEPES. pH=7.0. The mixtures were set in the incubator at 37°C and shaken at 130RPM.

TEM grids were plated at 0 minutes, 15 minutes, 30 minutes, one hour, 12 hours, and 24 hours of incubation. 4µL of each sample was plated on Carbon 200 mesh TEM grids for ten minutes. An aliquot of each serum sample was diluted 1 in 10 with deionized water and 4µL of the diluted samples were plated on Carbon 200 mesh TEM grids for ten minutes. Excess solution was removed from the grids and disposed of. The grids were allowed to dry before being imaged.

3.3.9 Aptamer Extraction from Transgenic Mouse Brains, Livers, and Blood

Application of the Cy 3.5-labelled a-syn-1 for *in vivo* studies examined the fate of the aptamer in brain tissue following i.p. injections of a-syn-1 loaded liposomes in transgenic mice expressing human α-Syn. To quantify the amount of aptamer which made it to the mouse brain, brain tissue was extracted from the mice and frozen. Extraction protocols were then performed, see below, to purify the aptamer from the excised tissue. Liver and blood samples were also excised to determine how much of the injected aptamer was present in those tissues compared to the brain.

Two methods were followed for the extraction of the a-syn-1 aptamer from samples of mouse brain, liver and blood. Prior to any extractions were performed, the fumehood, was cleaned with concentrated bleach to remove potential DNA or DNase contaminants. The fumehood was rinsed with deionized water ten times followed by 70% ethanol in deionized water. Microcentrifuge tube trays and a tissue homogenizer were sprayed with 10% bleach in deionized water followed by 70% ethanol to remove contaminants. Pipettes and razors used throughout these processes were sprayed with 70% ethanol to remove contaminants. The fumehood surface, tube trays, falcon and microcentrifuge tubes, pipettes and tips, razors, and paper towels were subjected to UV radiation for at least 30 minutes for further decontamination.

Following extraction of the DNA from the brain, liver, and blood samples, all extracted DNA was lyophilized and sent to SydLabs for qPCR. Amplification of the aptamers was quantified by examining the Ct, the point at which the amount of aptamer amplified in a cycle exceeds a set threshold value. The lower a Ct value is, the more of the target DNA that was present initially.

3.3.9.1 Aptamer Extraction from Mouse Brain, Liver, and Blood Samples using Clarity OTX Oligo Therapeutic Extraction Kit

Following liposome injections, transgenic mice expressing the human α-Syn were live decapitated. Brains and livers were excised from the mice, and blood was drawn from the hearts of the mice. The tissue samples were frozen and delivered to the DeRosa lab where they were stored in -80°C until they were used for aptamer extraction. Tissue extraction and handling was performed by Katelyn Ventura. In this experiment, seven mice were injected with 100µL of either saline solution (mouse 1), TRA-negative liposomes with a-syn-1 aptamer payload (mice 2-4), and TRA-positive liposomes with a-syn-1 aptamer payload (mice 5-7).

The Clarity OTX kit (Phenomenex) is used for extracting oligonucleotide therapeutics and came equipped with 100mg/3mL solid-phase extraction (SPE) cartridges, Lysis-Loading buffer, Equilibration buffer, Wash buffer, and Elution buffer. The formulations of the buffers, except for the lysis-loading buffer, were supplied. Modified Equilibration buffer was created for the extraction of oligonucleotides from tissues by combining 100µL of 0.5% Triton X-100 to 20mL of Equilibration buffer.

3.3.9.1.1 Tissue Sample Preparation by Homogenization Method

Half brains from transgenic mice were placed into a sterilized petri dish and minced with a razor before being transferred to a microcentrifuge tube. Lysis-Loading buffer was added to the brain sample using thrice as much lysis-loading buffer as the approximate brain volume. The tissue was homogenized in the lysis buffer using a mechanical homogenizer. Samples were centrifuged at 10G for approximately 15 seconds to pellet the tissue out of solution and set aside

for SPE. Samples which did not homogenize effectively were mixed with three times the volume of acetonitrile to crash out proteins and substituents of the cell lysates.

3.3.9.1.2 Tissue Sample Preparation by Proteinase K Digestion Method

A 100mL stock solution of digestion buffer was prepared by dissolving 1.21g Tris in deionized water and adjusting the pH to 8.0. 0.55g of $CaCl_2$ was added to the Tris buffer to complete the digestion buffer.

To digest the brain and liver samples, 40µL of Proteinase K (Qiagen) and 890µL of digestion buffer were mixed together in a microcentrifuge tube and the tissue was added afterwards. The samples were incubated at 50°C for three hours. After incubation, the samples were centrifuged at 16G for 30 minutes. The supernatant solution was transferred to a new microcentrifuge tube, mixed with 900µL of lysis buffer, and vortexed for approximately 15 seconds. The samples were centrifuged for approximately 15 seconds at 10G and set aside for SPE.

3.3.9.1.3 Preparation of Blood Samples

Lysis-Loading buffer was added to thawed blood samples using an equal volume of buffer to blood. The samples were vortexed for approximately 15 seconds and then centrifuged at 16G for 5 minutes to pellet coagulated blood. The samples were set aside for SPE.

3.3.9.1.4 Solid-Phase Extraction of Oligonucleotides from Brain and Liver Samples using Clarity OTX Columns

The Clarity OTX SPE cartridges were connected to a vacuum manifold and underwent pretreatment using 1mL of methanol followed by 1mL of Modified Equilibration buffer with an applied vacuum of 3" Hg.

The samples of brain and liver in lysis buffer were applied to the cartridges at 3" Hg vacuum. For the obstinate samples moving slowly through the cartridges, the vacuum was increased gradually up to 20" Hg, depending on flow rate, to pull the solution through. The cartridges were rinsed with 1mL of Modified Equilibration buffer followed by two washes with 2mL of Wash Buffer and two rinses with 2mL of Equilibration buffer. The cartridges were subjected to 10-20" Hg vacuum to evacuate all of the solution. The collection tubes beneath the cartridges were changed and 1.5mL of Elution buffer was applied to the cartridge to elute the collected oligonucleotide. The eluted samples were frozen in liquid nitrogen for two minutes and lyophilized overnight.

3.3.9.1.5 Solid-Phase Extraction of Oligonucleotides from Blood Samples using Clarity OTX Columns

The Clarity OTX SPE cartridges were connected to a vacuum manifold and underwent pretreatment using 1mL of methanol and 1mL of Equilibration buffer with an applied vacuum of 3" Hg.

The supernatant of the blood samples in lysis buffer were loaded onto the cartridges with an applied vacuum of 3" Hg. Samples which moved slowly through the columns experienced

increased vacuum pressure, up to 20” Hg, to pull the solution through. The cartridges were washed with 4mL of Wash buffer followed by 2mL of Equilibration buffer at 3” Hg vacuum followed by applied vacuum of 15-20” Hg to pull the entire solution through the cartridge. The collection tubes were changed and 1.5mL of Elution buffer was applied to the cartridge to elute the collected oligonucleotides. The eluted samples were frozen in liquid nitrogen for two minutes and lyophilized overnight.

3.3.9.1.6 Troubleshooting of Solid-Phase Extraction Protocols

Throughout the SPE procedure, some blood, brain, and liver samples did not move through the SPE cartridges at the flow rate the protocol determined they would. In some instances, the solutions would progress slowly through the columns. For brain samples 3 and 4, this observation, from previous samples, prompted the addition of acetonitrile to the brain samples in the microcentrifuge tubes, in three times the volume of the brain sample, to crash out any proteins and interfering tissue. The samples were vortexed for 30 seconds, then centrifuged at 16G for 45 minutes. The supernatant was collected and lyophilized.

3.3.9.2 Aptamer Extraction from Mouse Tissue using Tri-Reagent Extraction Method and PureLink™ RNA Micro Kit

Quarter brains from transgenic mice were collected in microcentrifuge tubes and frozen at -80°C until ready to use. The PureLink™ RNA Micro Kit supplied PureLink™ RNA Micro Kit Columns, Wash Buffer I and Wash Buffer II, RNase-free water, and Lysis Buffer.

While the tissues were frozen, 500µL of TRI-reagent was added to the samples. The samples were homogenized using a mechanical homogenizer. The samples were incubated at room temperature for five minutes and then placed on ice until the extraction process.

To extract the aptamer from the tissues, 100µL of chloroform was added to the samples. The samples were vortexed for approximately 15 seconds and set at room temperature for two minutes. The samples were centrifuged at 12000RPM for 15 minutes at room temperature. A 250µL portion of the supernatant was collected and mixed with 250µL of 70% ethanol in deionized water. The sample was vortexed for approximately 15 seconds before being pipetted onto a PureLink™ RNA Micro Column and centrifuged for one minute at 12000RPM. The samples were then washed by pipetting 500µL of Wash Buffer II onto the column and centrifuging at 12000RPM for 15 seconds. The samples were centrifuged for an additional minute at 12000RPM to remove excess solution from the samples. The columns were moved to new collection tubes and 30µL of RNase-free water was pipetted directly onto the membrane of the column. The samples were incubated for one minute at room temperature and then centrifuged at 12000RPM for two minutes. The collected eluate was frozen in liquid nitrogen and lyophilized overnight.

3.4 Results and Discussion

3.4.1 Synthesis and Purification of Cyanine 3.5-Labelled a-syn-1 and TRA

Synthesis of the Cy 3.5-labelled a-syn-1 aptamer was performed on the MerMade 6 DNA Synthesizer. Purification of the a-syn-1 for use as a liposome payload in *in vivo* applications was achieved using the PAGE method of purification since the structure of the Cy 3.5 modifier does

not allow for reverse phase polymer affinity purification. Images of the gels were taken using the epi UV and 302nm fluorescent settings to visualize the DNA and the Cy 3.5 label. A single band of fluorescently-labelled DNA was imaged and removed from the gel; since the fluorescent modifier is added last to the synthesis, only full-length sequences will have been modified. Images in Appendix 6.1a and b show the epi UV and fluorescent images of the gel for purification of the a-syn-1, respectively. The mass spectrometry results are shown in Appendix 6.2.

Stocks of TRA were purified using the reverse phase polymer affinity method for thiol-modified oligonucleotides; however, the procedure provided was stopped before the disulfide bond was to be reduced. The TRA was eluted, dried down, and dissolved in deionized water for quantification. Reduction of the disulfide to provide a thiol for conjugation to the liposomes was performed hours before the reaction of the TRA to the maleimide group present as part of the liposomes.

3.4.2 Liposome Analysis

3.4.2.1 Liposome Synthesis and Loading of Aptamer Payload

The liposomes synthesized in this study utilized PEG modified lipids, specifically 1,2-distearoyl-sn-glycerol-3-phosphoethanolamine-N-[amino(polyethylene glycol)-2000], due to its biocompatibility, biodegradability, and efficiency for encapsulating drugs[114] and POPC for its cationic properties and enhanced encapsulation of DNA.

The PAGE analysis of the liposome preparation was performed using samples of the liposome solutions at stages throughout the synthesis to visualize the encapsulation of the a-syn-

1 aptamer and the introduction of the TRA to the external surface of the liposomes. The steps of the synthesis used for this investigation were the liposomes pre-extrusion, pre-dialysis 1, post-dialysis 1, pre-dialysis 2, post-dialysis 2, and the final liposome product. These appear on the gel, shown in Figure 3.2a and b, as bands in lanes 4, 5, 6, 7, 8, and 9, respectively. A control lane of a-syn-1 aptamer was run in lane 2. To confirm that the liposomes contained the payload aptamer, the final liposome product was dried and mixed with a lysis buffer to release encapsulated a-syn-1. The lysed liposomes were run on a gel compared to the final liposome sample, Figure 3.2c. The liposome sample had been at room temperature for one month and underwent an additional dialysis to remove any aptamer which had leached from the liposomes in that time; the original and dialyzed liposome solutions were run on the gel in lanes 6 and 8, respectively. The lysed liposomes appear in lane 10 and the a-syn-1 control in lane 3.

TEM imaging was also used to confirm the formation of the liposomes, as shown in Figure 3.3. The size distribution of the liposomes was also determined using multiple TEM images, see Figure 3.3. The average size of the liposomes, based on a sample size of n=8, was 29nm in diameter with a standard deviation of 13nm.

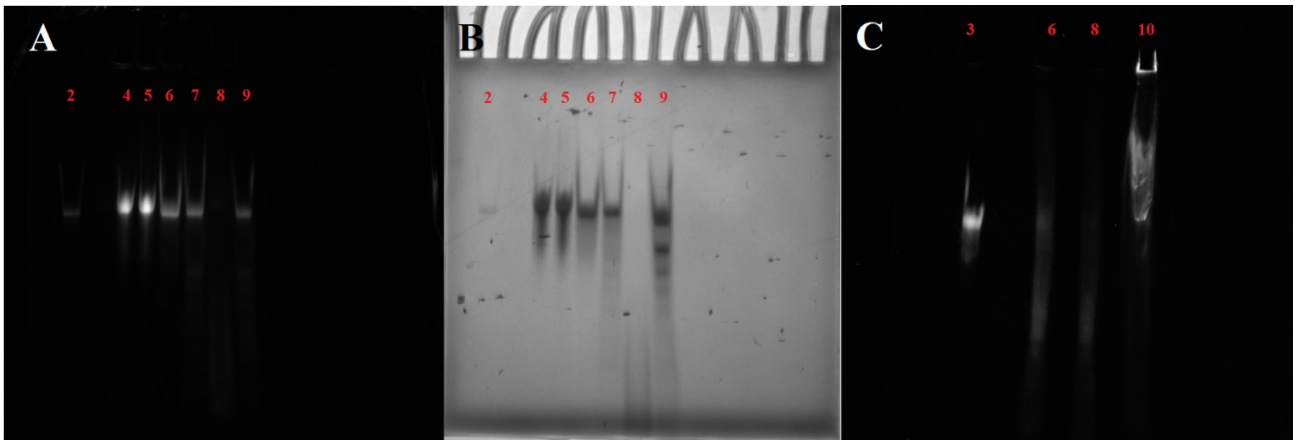

Figure 3.2: Synthesis of liposomes and encapsulation of Cy 3.5-labelled a-syn-1 confirmed using non-denaturing PAGE analysis at various points of liposome synthesis. Lanes in A), the fluorescent gel image, and B), the epi UV gel image, contain a-syn-1 (lane 2), pre-extrusion liposomes (lane 4), pre-dialysis 1 liposomes (lane 5), post-dialysis 1 (lane 6), pre-dialysis 2 (lane 7), post-dialysis 2 (lane 8), and final liposome product (lane 9). Lanes in C) contain a-syn-1 (lane 3), loaded liposomes (lane 6), liposomes after dialysis (lane 8), and lysed liposomes (lane 10) to confirm the encapsulation of a-syn-1.

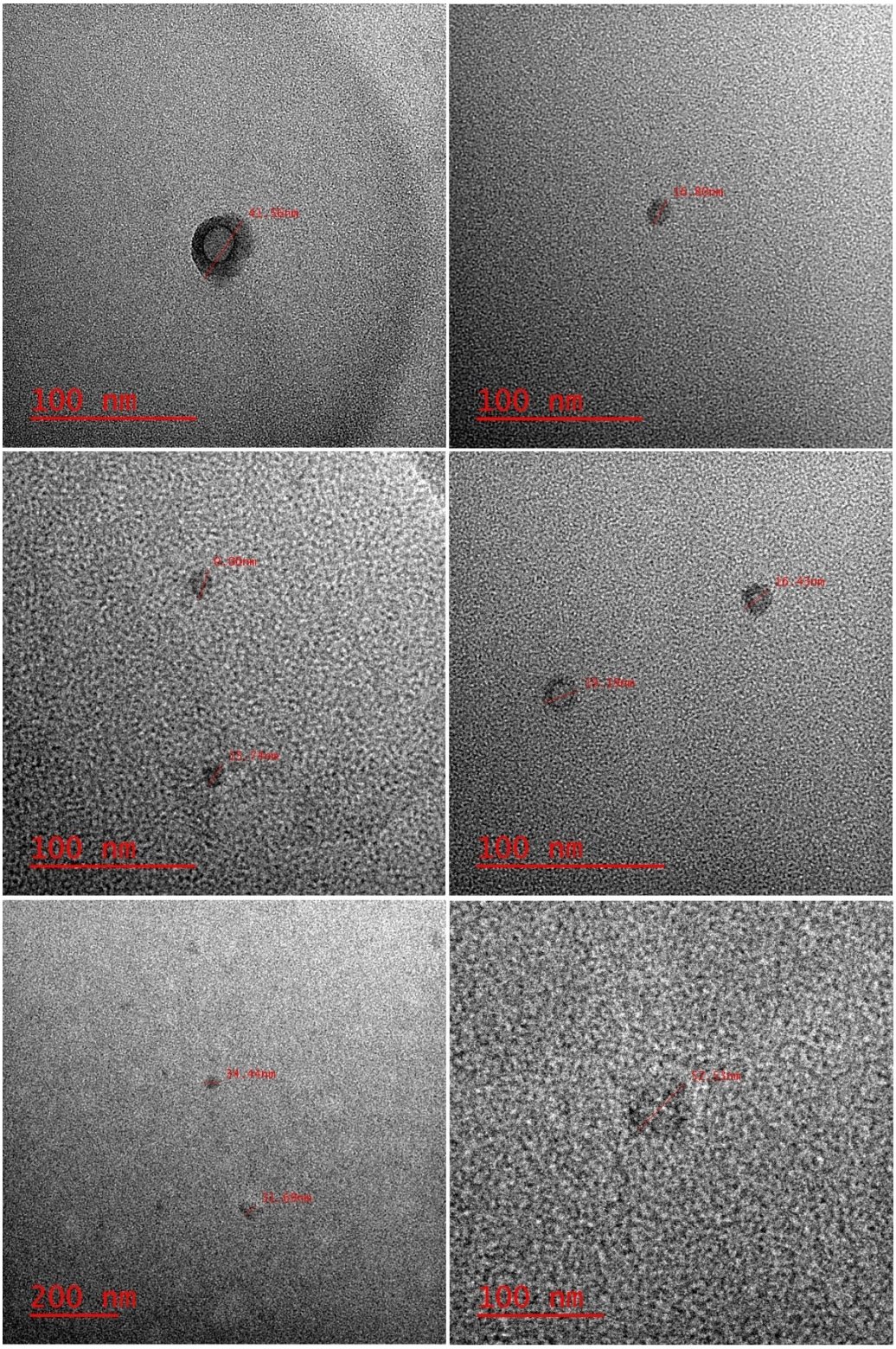

Figure 3.3: Size-distribution of the synthesized liposomes was performed using TEM. The TEM images also show the liposome synthesis produced unilamellar liposomes. Images were taken at the 100nm and 200nm scale and at 120kV.

The a-syn-1 aptamer was packed into the liposomes, but the efficiency of the loading was low, see Table 3.4 in Section 3.3.2.3. The pre-extrusion and pre-dialysis 1 lanes display a band for the aptamer in both the fluorescent and UV images of the gel. This shows that the a-syn-1 aptamer did not completely load into the liposomes in the initial steps of the synthesis. During the freeze-thaw cycles, a-syn-1 which was part of any multi-walled liposomes would have been released into solution and may not have been recaptured when the liposomes reassembled. The extrusion of the liposomes could have also resulted in loss of packaged a-syn-1 as the larger liposomes are broken into smaller liposomes. Any aptamer that was not encapsulated in the liposomes would remain in solution or be bound non-specifically to the liposome surface. The post-dialysis 1 lane also shows the existence of the non-encapsulated a-syn-1 that was not removed from the first dialysis and would then undergo nuclease digestion. The laddering observed in the pre-dialysis 2 lane results from the nuclease digestion of the a-syn-1 aptamer, which could then be removed by dialysis. However, the laddering observed in the post-dialysis 2 lane indicates that there was still non-encapsulated a-syn-1, and the digested portions, still in the liposome solution. The final liposome solution still produced a fluorescent band on the gel for the full-length a-syn-1 aptamer; there was still some a-syn-1 bound non-specifically to the outside of the liposome. Additionally, the enhanced band seen in then UV image of the gel resulted from the addition of the TRA; the TRA is 64 bases long whereas the a-syn-1 aptamer is 66 bases long. The reappearance of the fluorescent a-syn-1 band in the lysis lane of the gel confirms that the liposomes were loaded with the payload aptamer. The fins observed by the migration of the lysis sample may be due to the interaction of the Cy 3.5 with the lipids or surfactants in solution. Several fluorescent dyes have exhibited the ability to associate with lipid membranes, including cyanine 3 and cyanine 5[115], which are similarly structured to Cy 3.5.

3.4.2.2 Efficiency of Liposome Synthesis

The efficiency of liposome synthesis was determined using the Stewart assay to find the amount of lipids in the final liposome product compared to the initial amount of lipids used. Three different batches of liposomes were studied using the Stewart assay, batches four, six and seven. Importantly, since batches six and seven were diluted with HEPES buffer, the dilution factor is accounted for in the calculation of the final lipid concentration. The results of the Stewart assay show that the production of liposomes varied in each batch, shown in Table 3.2. The average concentration of the lipids in the liposome solutions is 7.0mg/mL ± 2.3mg/mL. The lipid concentration for batches six and seven account for the dilution of the samples so that the payload aptamer concentration of each batch was comparable to batch four, shown in Section 3.3.2.3. The percent yield of the liposome production is determined by comparing the calculated concentration of the lipids in the final liposome solution to the starting mass of lipids, 11.9mg, used in the synthesis. The average percent yield of liposomes is 59% ± 19%.

Table 3.2: Concentration of the lipids in the final liposome solutions of batches four, six, and seven as determined using the Stewart assay. Variance in the efficiency of liposome production is observed between batches of liposomes as the concentration varies. The efficiency of liposome production is a comparison of the concentration of lipids in the liposome solution to the starting mass of lipids.

Liposome Batch	Concentration of Lipids (mg/mL)	% Yield
4	6.08 ± 0.01	51%
6	4.39 ± 0.24	40%
7	10.2 ± 1.1	86%

The efficiency of liposome production varied greatly per batch, though loss of lipid is expected in the synthesis of liposomes. Incomplete transfer of the liposomes to extrusion and

loss of lipids in the polycarbonate extrusion filters will have resulted in lower yields of liposomes from the synthesis.

Furthermore, the estimated number of liposomes per 100µL injection was calculated. A mathematical model from Montanari et. al.[113] was used to find the estimated number of liposomes in solution based on the average size of the liposomes and the assumption the solution contains monodisperse and perfectly spherical unilamellar, double membrane liposomes. As determined from the TEM images of the liposomes, the average observed size of the liposomes was approximately 29nm ± 13nm. The average concentration of the liposome solutions, based on the results of the Stewart assay, used for the calculation is 7.03mg/mL. The calculation for the number of liposomes per injection assumes that the size and physical properties of the liposomes are made entirely of POPC. For the calculation of the molar weight of the phospholipids, the molar mass used is the sum of the ratiometric amount of mass from each lipid, with POPC contributing 95% of the molar mass to the liposome synthesis. The calculations also assume 100% conversion of the lipids in solution to liposomes. The steps in the calculation of the number of liposomes is outlined in Table 3.3. The average number of liposomes per 100µL injection in mice is determined to be approximately 1.5×10^{13} liposomes.

Table 3.3: Equations supplied by Montanari et. al.[113] and steps taken to calculate the average number of liposomes per 100µL injections used in *in vivo* trials. *Liposome radius determined as half of the average diameter determined from TEM images. **Average mass of lipids in solution determined using the average of the three trials of Stewart assay. ***Lipid head surface area was assumed using the value of the phosphatidylcholine used in the calculations by Montanari et. al.[113]. ****Molar weight of the phospholipid was determined as a ratiometric contribution of molar mass from each phospholipid in the synthesis.

Variable		Equation	Value
Liposome radius	r_L	*	14.5nm
Average lipid mass in solution	m_{PL}	**	7.03mg/mL
Liposome surface area	S_L	$=4\pi(r_L)$	$2570nm^2$
Lipid head surface area	S_{PL}	***	$0.6nm^2$
Lipid head radius	r_{PL}	$=(S_{PL}/4\pi)^{(1/2)}$	0.219nm
Area of single lipid in liposome	S_{APL}	$=(2\times r_{PL})^2$	$0.191nm^2$
Number of lipids in inner layer	$N_{PL/C}$	$=S_L/S_{APL}$	13455
Number of lipids in liposome	$N_{PL/L}$	$=2.5\times N_{PL/C}$	33637
Molar weight of phospholipid	MW_{PL}	****	820.83g/mol
Total number of phospholipids	N_{PL}	$=(m_{PL}\times(6.022\times10^{23}) / MW_{PL})$	5.15×10^{18} molecules/mL
Number of liposomes per 100µL injection	N_L	$=(N_{PL}/N_{PL/L})/10$	1.5×10^{13} per 100µL

3.4.2.3 Quantification of Payload Aptamer and Payload Loading Efficiency

Quantification of the payload aptamer in the liposomes was performed to determine the overall loading efficiency of each batch of liposomes and to observe consistency between syntheses. To find the amount of Cy 3.5 labelled a-syn-1 in the liposome solution, UV-Vis spectroscopy was used to find the absorbance of the Cy 3.5 at 590nm. The concentration was

then determined using the Beer-Lambert law and extinction coefficient of Cy 3.5 at 591nm, 116000Lmol^{-1}cm^{-1}, and accounting for the 1-in-10 dilution of the sample. Quantification of the a-syn-1 aptamer was assumed to be unaffected by potential light scattering in the liposome sample. The concentration of a-syn-1 in each batch of liposomes is shown in Table 3.4 as the amount of aptamer per 100µL of liposome solution. The concentration was determined in this fashion since the injection volumes of the liposomes for *in vivo* studies were performed in 100µL aliquots. The loading of the a-syn-1 aptamer in each batch of liposomes varied; the efficiency of liposome loading was determined by comparing the amount of a-syn-1 aptamer in the final liposome solution compared to the initial 38nmol used for each synthesis, as shown in Table 3.4. The average loading efficiency of the Cy 3.5-labelled a-syn-1 was 14.8% ± 5.3%, corresponding to 0.42nmol/100µL ± 0.17nmol/100µL. Liposome batch number five is omitted from the table due to a mis-quantification of a cyanine 5-labelled a-syn-1 payload at the beginning of the liposome synthesis.

For the set of *in vivo* experiments utilizing batches four to eight, maintaining a similar amount of aptamer delivered was kept constant. In order to achieve this, liposome batches that were enriched with the a-syn-1 aptamer were diluted with HEPES so that the absorbance of the of each batch was similar to batch four. The concentrations of the diluted samples are also reflected in Table 3.4.

Table 3.4: Loading efficiency of Cy 3.5-labelled a-syn-1 payload aptamer in each batch of liposomes. The amount of a-syn-1 encapsulated in each liposome is determined using the previously calculated number of liposomes per 100µL of liposome solution and the amount of aptamer in 100µL of liposome solution. The loading efficiency of the a-syn-1 in each batch of liposomes is calculated by determining the total aptamer present in the liposome solution compared to the initial 38nmol used for each batch of the synthesis.

Liposome Batch	Amount of a-syn-1 per 100µL Liposomes	Amount of a-syn-1 per Liposome	Diluted Amount of a-syn-1 per 100µL Liposomes	Loading Efficiency
1	1.12×10^{14}	7.5	N/A	6.87%
2	1.45×10^{14}	9.6	N/A	9.48%
3	2.01×10^{14}	13.4	N/A	13.2%
4	2.36×10^{14}	15.8	N/A	13.4%
6	3.92×10^{14}	26.1	2.18×10^{14}	22.2%
7	2.90×10^{14}	19.3	2.39×10^{14}	16.5%
8	2.31×10^{14}	15.4	N/A	13.1%
9	4.10×10^{14}	27.3	N/A	23.3%

Conjugation of the TRA to the maleimide group of the liposomes was estimated using UV-Vis spectroscopy at 260nm and accounting for the 1-in-100 dilution of the sample. While there would be some interference of the absorbance at 260nm from the a-syn-1 aptamer loaded within the liposomes, the interference was considered negligible. Liposomes were loaded with a-syn-1 aptamer and left unmodified by TRA to determine the relative contribution of the loaded aptamer to the absorbance at 260nm.

3.4.3 Liposome Stability

The stability of the liposomes was examined using UV-Vis spectroscopy and fluorescence for a week to monitor differences in the liposome samples. TEM imaging was employed to visualize the liposome solution mixed with either HEPES buffer or in human blood serum to determine of the liposomes will remain stable in solution.

3.4.3.1 Liposome Stability in HEPES

The stability of the a-syn-1 loaded aptamers was tested by examining the absorbance and fluorescence of the Cy 3.5 fluorophore for one week to observe potential leeching of the payload aptamer from the liposome. Both TRA-positive and TRA-negative liposomes were examined for a-syn-1 leeching. The absorbance and fluorescence of the liposome samples are shown in Figure 3.4a and b, respectively.

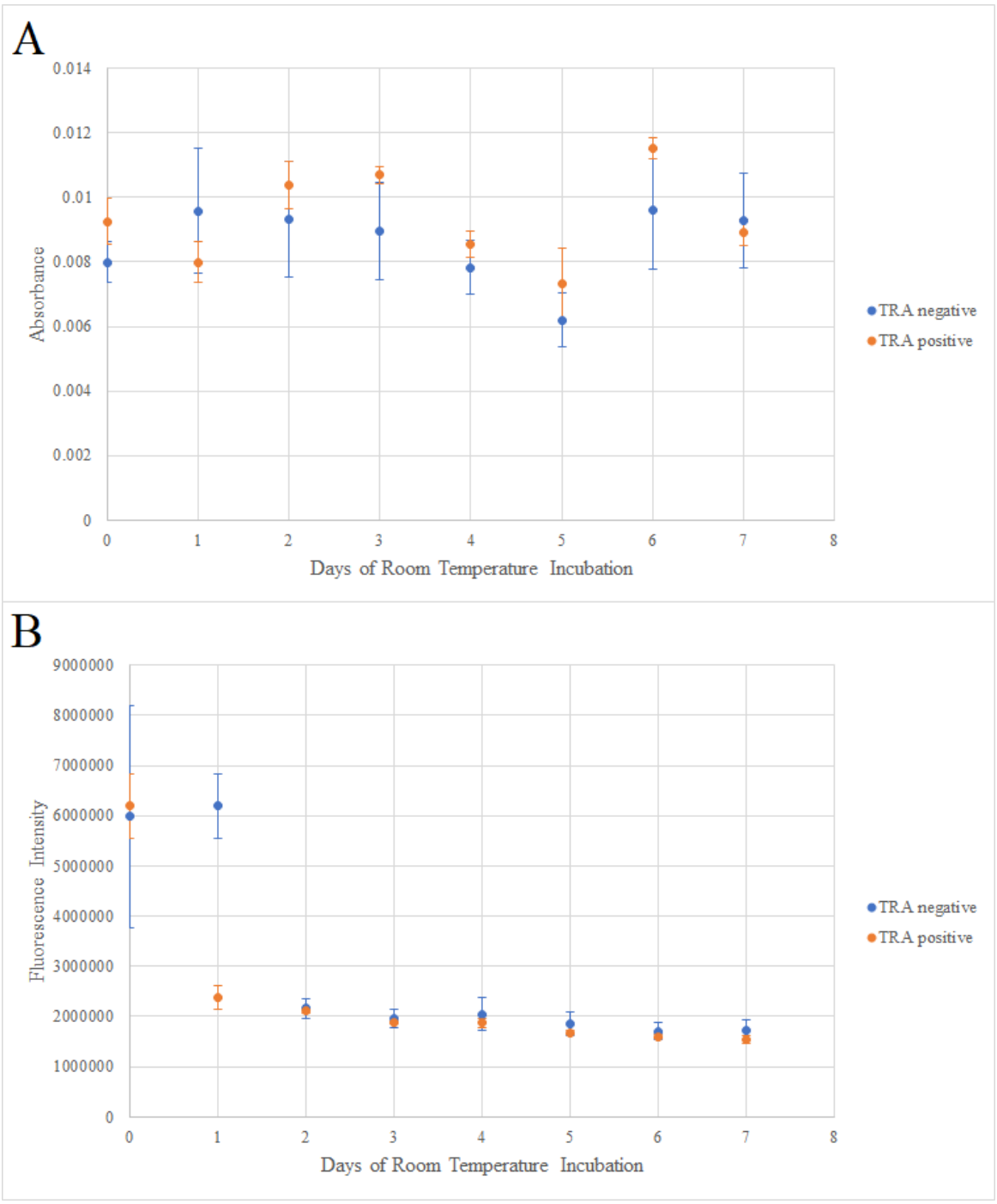

Figure 3.4: A) Absorbance, at 590nm, of the Cy 3.5-labelled a-syn-1 aptamer encapsulated in TRA-negative (blue) and TRA-positive (orange) liposomes over seven days of incubation. B) Fluorescence of Cy 3.5-labelled a-syn-1 aptamer encapsulated in TRA-negative (blue) and TRA-positive (orange) over seven days of incubation. Absorbance and fluorescence of the payload aptamer, at 1-in-20 dilution, were measured to observe potential leeching of the a-syn-1 aptamer. All measurements were performed in triplicate.

The absorbance of the TRA-positive and TRA-negative liposomes remained consistent over the course of a week. Since no change in absorbance was observed, it was assumed that any potential leakage of the a-syn-1 aptamer from the liposomes was either non-existent or minimal and unobservable through UV-Vis spectroscopy. The basis of the assumption is that any light passing through the sample will scatter due to the liposomes, thus altering the absorbance of the Cy 3.5 fluorophore, and any leeching of the aptamer would result in increased absorbance of the light. However, there is no observable trend to imply that the a-syn-1 aptamer was evacuating the liposome from either the TRA-positive or TRA-negative liposomes, and fluctuations in readings is likely due to pipetting error each day.

The fluorescence of the liposome samples initially gave a large relative fluorescence and suddenly dropped in intensity after one day of incubation and then remained relatively steady. One potential occurrence is the change in the microenvironment of the liposomes making it more favourable for the Cy 3.5 fluorophore to undergo self-quenching[116]. This is possible when considering the Stokes shift of Cy 3.5; max excitation is observed at 591nm and max emission is observed at 604nm. Since the variance in the fluorescence intensity do not change greatly after one day, the liposomes do not appear to be leeching the aptamer into solution and variance in the measurements may be due to pipetting error each day. As the gel results of Figure 3.2 illustrate, the liposomes still contained aptamer payload after one month at room temperature.

TEM images of the liposomes in HEPES were acquired using the liposomes manufactured with the Liss Rhod PE lipid and DBA-payload aptamer. Stability in HEPES was visualized using a 50/50 mixture and a 10/90 mixture of liposome solution and HEPES buffer to investigate the longevity of the liposomes after incubation at 37°C for 12 hours. Figure 3.5a and b show the liposomes in the 10/90 combination of liposome solution and HEPES after 0 and 12

hours of incubation, respectively. The 50/50 combination was not imaged since the film on the TEM grid was unable to be imaged effectively. Even with the 10/90 ratio of liposome solution in HEPES, the TEM grids were often hard to image. Liposomes were located after 0 hours of incubation and after 12 hours, though the images obtain for the 12-hour sample displayed fewer liposomes in the sample. This could have been due to dilution of the sample or due to liposome amalgamation and/or lysis. Despite that, the gels in Figure 3.2 show little leeching of aptamer from the liposomes after one month, so the fewer liposomes in Figure 3.5b than a may be due simply to plating the sample on the grid.

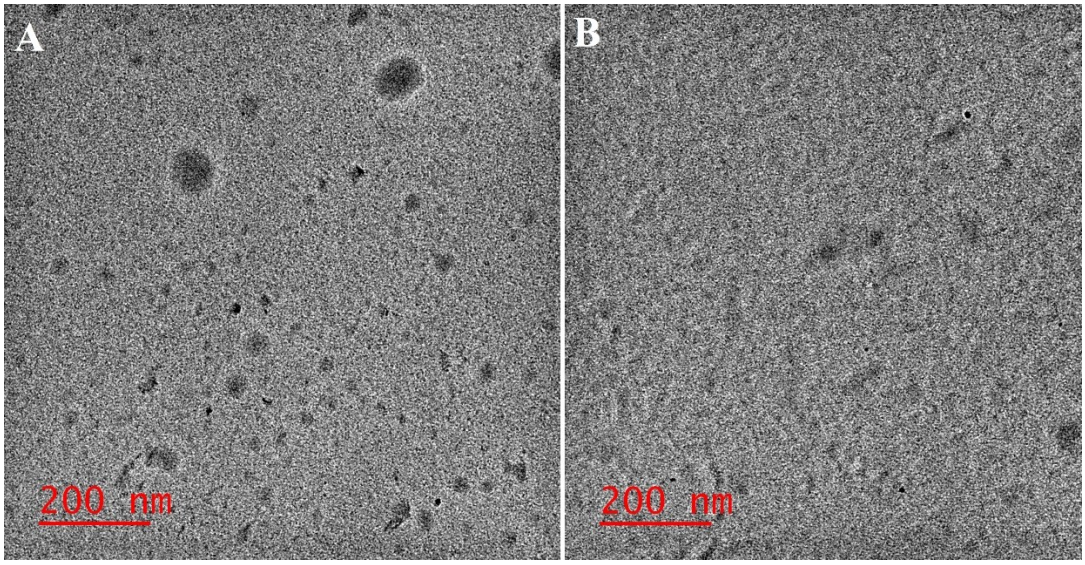

Figure 3.5: Stability of liposomes in HEPES buffer, pH=7.0, was monitored using TEM imaging after A) 0 hours and B) 12 hours of incubation at 37°C. The liposomes at time 0 show a variety of sizes and after 12 hours showed some vesicles with similar sizes. Images were taken at 200nm scale and 120kV.

3.4.3.2 Liposome Stability in Human Blood Serum

Liposome stability was also tested in human serum to determine if the liposomes undergo degradation in an environment similar to the circulatory system. The liposomes were incubated in serum for 24 hours; previous *in vivo* studies showed a prompt delivery of the aptamer across the brain following treatment[112] and *in vivo* applications of the a-syn-1 aptamer, covered in section 3.3.4, have shown the aptamer to persist at detectable levels in the blood for at least two hours. For this study, the batch of liposomes manufactured with the Liss Rhod PE lipid and DBA-payload were examined.

TEM images of the liposomes in blood serum were difficult to acquire. Constituents of the blood serum made locating and imaging liposomes difficult at many timepoints. However, liposomes were visualized in the blood serum after 12 hours of incubation at the 10/90 ratio of liposome solution to blood serum. Figure 3.6a and b show the liposomes in serum after 0 and 12 hours of incubation, respectively. Size and morphology of the liposomes does not appear to have changed significantly during the 12 hours of incubation. No images were obtained for the 50/50 combination of liposome solution and HEPES buffer since the film created was unable to be imaged with the TEM.

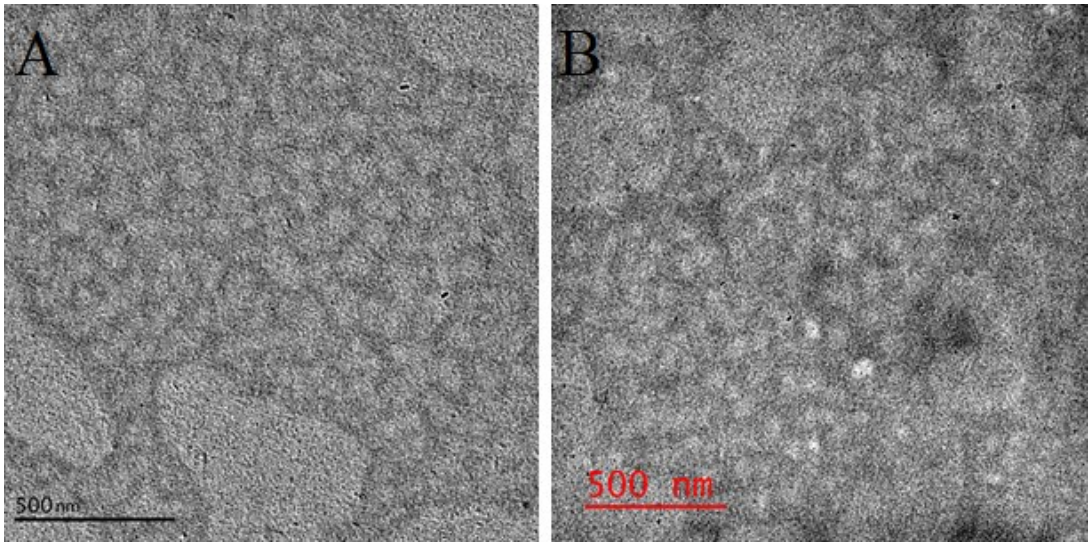

Figure 3.6: Stability of liposomes in human blood serum was monitored using TEM imaging after A) 0 hours and B) 12 hours of incubation at 37°C. The liposomes have persisted in the blood serum for 12 hours and evidence of liposomes in each sample was observed. Images were taken at 500nm scale and 120kV.

3.4.4 Extraction of Aptamers from Transgenic Mouse Brains, Liver, and Blood

After injection of a-syn-1 loaded liposomes into transgenic mice expressing human α-Syn, the biodistribution of the aptamer was investigated by extracting the aptamer from brain, liver and blood of the mice. Extractions from the mouse tissues were performed using two different extraction methods since inconsistencies in qPCR results led to troubleshooting aptamer extraction. The first method used the Clarity OTX kit cartridges and extraction methods. Initially, brain and liver samples were homogenized in lysis buffer using a mechanical homogenizer and the supernatant run on the cartridges. Blood samples were also treated with the lysis buffer, showed rapid coagulation of the whole blood, and the supernatant was run on the cartridges.

The first batch of tissue samples to undergo oligonucleotide extraction used seven mice; one injected with saline solution, three with TRA-positive liposomes, and three with TRA-

negative liposomes; mouse 1 received the saline injection, mice 2-4 received the TRA-negative liposomes, and mice 5-7 received the TRA-positive liposomes. The mice had been sacrificed 30 minutes after a 100μL injection of the respective solution. The Clarity OTX kit was used for all extractions. Brain tissue from mice 3 and 4 underwent mechanical homogenization and a large amount of debris was observed in the lysis buffer. To ensure the debris did not clog the cartridges, acetonitrile was added to the lysis buffer to crash out protein and cellular material. Brain tissue from mouse 2 was treated with proteinase K to circumvent the issues of the mechanical homogenization process. The brain tissues from mice 1, 5, 6, and 7 were all treated using the proteinase K procedure. Extraction from liver samples were performed using the proteinase K method since the mechanical homogenization of liver tissues was noted to be less effective.

The expectation from the qPCR of the mice injected with TRA-positive liposomes was the expression of a-syn-1 in the blood, brain, and liver. Since the liposomes would be circulating in the bloodstream, some of the a-syn-1 should have been present in the brain. By comparison, a heightened amount of a-syn-1 should have been present in the blood and liver; the blood since it is the carrier of the liposomal delivery vector, and the liver since it also expresses TRA and is responsible for the first pass of the liposomes in the blood. However, the qPCR on the samples extracted from the mice, shown in Table 3.5, did not yield consistent results. The saline samples, as expected, show no Ct value of the aptamer after 40 cycles of amplification. The blood from mice injected with either TRA-negative or TRA-positive liposomes showed amplification of the a-syn-1 aptamer, except for one of the mice injected with TRA-negative liposomes. Concerningly, very little amplification was observed in the livers of the mice injected with the

TRA-positive liposomes. Worse yet, the only amplification from samples extracted from the brain was noted in mice which were injected with TRA-negative liposomes.

Table 3.5: qPCR results of aptamer extractions from brain, liver, and blood of transgenic mice 30 minutes after i.p. injection of either saline (mouse 1), TRA-negative liposomes (mice 2-4), and TRA-positive liposomes (mice 5-7). DNA was extracted from the tissues and blood using the Clarity OTX cartridges. Extractions sent to Syd Labs for qPCR were tested in triplicate. Average Ct values are displayed for each tissue. *Amplification was observed in only one of the replicates performed.

Animal	Tissue Sample	Average Ct Value
1 (saline)	Brain	No Ct
	Liver	No Ct
	Blood	No Ct
2 (TRA-negative)	Brain	No Ct
	Liver	No Ct
	Blood	No Ct
3 (TRA-negative)	Brain	24.29
	Liver	No Ct
	Blood	26.38
4 (TRA-negative)	Brain	26.92
	Liver	No Ct
	Blood	20.38
5 (TRA-positive)	Brain	No Ct
	Liver	No Ct *
	Blood	30.81
6 (TRA-positive)	Brain	No Ct
	Liver	No Ct *
	Blood	17.44
7 (TRA-positive)	Brain	No Ct
	Liver	No Ct
	Blood	36.42

With the samples that were mechanically homogenized, there are a couple of factors which could influence the results of the qPCR. Firstly, the incomplete perfusion of some brain and liver samples will provide inaccurate results for the amount of aptamer contained within the

tissue due to blood contamination. Incomplete homogenization of the tissue and, thus, incomplete extraction of a-syn-1 from tissue samples would decrease the amount of aptamer initially placed onto the cartridges.

The brain tissues which were provided had evidence of blood remaining due to incomplete perfusion of the sample, and any amplification signal detected would be due, at least partially, to the presence of the aptamer in the blood. Brains from mice 2 and 3, injected with TRA-negative, liposomes were still bloody following perfusion and showed amplification during the qPCR procedure. The livers of mice 2, 3 and 4 were noted to be quite bloody, and the livers of mice 5, 6 and 7 were comparatively less bloody. Despite the presence of blood in the liver samples, amplification was not observed for any oligonucleotide extraction from the livers.

Additionally, the protocol from SydLabs states that approximately $1/20^{th}$ of the lyophilized sample was used per amplification experiment, with each sample amplified in triplicate. Since the liposome and payload aptamer must first pass through the liver, the potential amount of aptamer reaching the brain would be comparatively small. Further to that point, following release of the payload aptamer in either the liver or the brain or degradation of liposomes in the blood, endogenous DNase will have time to interact with and begin degradation of the aptamer payload. Despite the sensitivity of qPCR, the amount of aptamer present in the brain tissue may reside under the threshold for amplification to be observed. For instance, the aptamer present in the blood sample of mouse C3 had been quantified using the average Ct of the sample, 36.42 cycles of amplification, compared to a standard amplification curve which calculated to approximately 3800 aptamers present in the aliquot studied. From the standard curve produced at SydLabs for this experiment, amplification of pure aptamer could be quantified within 40 cycles of amplification provided there was at least 300 copies of the

aptamer present initially in the sample. One potential reason for the inconsistent signal produced from the qPCR could be from extraction of the a-syn-1 aptamer, possibly from inefficient adherence to the columns provided. The columns are supposed to exhibit efficient extraction of oligomers that are 50 bases or shorter. That the a-syn-1 aptamer is composed of 66 bases may influence the ability for the aptamer to bind to the column and be collected for qPCR. The blood samples should have presented the most facile extraction process. However, rapid blood coagulation was observed with the addition of lysis buffer, and it is possible that a portion of the aptamer was trapped and retained within the coagulated blood.

To supplement the extractions of the a-syn-1 aptamer from the mouse tissues, brain slices had been imaged using fluorescence microscopy to probe the location and fate of the aptamer in the brain. Colocalization of the aptamer with α-Syn had been visualized in brain slices of mice sacrificed 30 minutes after injection. Ongoing longitudinal studies are investigating the lifetime of the aptamers in the brain using PCR and sacrificing the mice at certain time intervals. The imaging of the aptamer in the mouse brain is shown in Appendix 6.5.

An additional extraction was performed on brain, liver, and blood from a transgenic mouse injected with TRA-positive liposomes and sacrificed 30 minutes after i.p. injection. The brain and liver tissues were extracted using the TRI-reagent method to see if increased extraction and, thus, increased qPCR amplification could be observed. The results of the qPCR are shown in Table 3.6.

Table 3.6: qPCR results of aptamer extractions from brain, liver, and blood of a transgenic mouse 30 minutes after i.p. injection. DNA was extracted from the tissues using the TRA-reagent procedure; DNA extraction from the blood sample performed using the Clarity OTX cartridges. Extractions sent to Syd Labs for qPCR were tested in triplicate. Only the extraction from the liver showed amplification of the a-syn-1 aptamer.

Tissue	Replicate	Ct Value
Brain	1	No Ct
	2	No Ct
	3	No Ct
Liver	1	26.4
	2	25.86
	3	25.84
Blood	1	No Ct
	2	No Ct
	3	No Ct

Only the extraction from the liver sample provided a Ct for the a-syn-1 aptamer; no aptamer signal was found in the brain samples using the same extraction method. Since i.p. injections are subject to first pass through the liver, a relatively high amount of payload being released in the liver is a potential fate of the liposomal delivery system. The brain showed no amplification during qPCR after this method of extraction; either the amount of aptamer present in the brain was again too low to be detected by this method of qPCR or the TRI-reagent was insufficient for the extraction of the aptamer from the brain. Theoretically, the extraction of the aptamer from the brain and liver samples should have been consistent; the guanidinium thiocyanate present in TRI-reagent protects DNA and RNA whilst also denaturing proteins and cells during homogenization, the chloroform and ethanol purify the RNA and DNA, and the PureLink™ RNA Micro Columns have a silica-based membrane upon which RNA has been shown to bind. It was noted that TRIzol, the same formulation as TRI-reagent, and the RNA columns had been used previously for the purification of aptamers for PCR purposes. One difference between the protocol used for the extraction of a-syn-1 and the supplied protocol is

the use of a refrigerated centrifuge. The brain and liver samples were not able to be centrifuged at 4°C after homogenization in TRI-reagent due to technical limitations. Instead, the samples were homogenized in TRI-reagent while frozen, centrifuged at room temperature, and kept on ice when possible to keep the samples cold but not frozen. However, the liver and brain samples were extracted following the same procedure, so discrepancies in the PCR signal arise due to sheer amount of aptamer present in the tissue and potentially unavoidable error in the extraction method.

Further experiments to determine the fate of the aptamer at different timepoints after injection are ongoing using two different injection volumes, deemed 1x and 2x for 100µL and 200µL injections, respectively.

4 Conclusion and Contributions to Knowledge and Future Work

The presence of the aptamers selected against monomeric α-Syn has been shown to stall the aggregation of α-Syn *in vitro*, as confirmed by the thioflavin T assay and SEM imaging. The potential for aptamers to target proteins critical to the pathology of neurodegenerative diseases is groundbreaking for the potential application of aptamers as therapeutics for diseases afflicting the central nervous system. The a-syn-1 aptamer has displayed the greatest propensity for inhibiting the aggregation of α-Syn, as visualized by SEM, and was utilized for *in vivo* experiments.

Liposomes were successfully prepared and loaded with the cyanine 3.5-labelled a-syn-1 aptamer. The liposomes were successfully modified with transferrin receptor aptamer making the liposomes an effective delivery vessel for *in vivo* applications to carry a-syn-1 across the blood brain barrier. Extraction and quantification of the a-syn-1 aptamer from the brain, liver, and blood

Determining the dissociation constant of the a-syn aptamers to monomeric α-Syn continues to be the priority for this research project. While the ability to measure the dissociation constant has remained elusive through gel-based assays, such as EMSA and DNase assays, and even microscale thermophoresis for some aptamers, more research efforts are ongoing using electrochemical impedance spectroscopy to find the dissociation constant of the aptamers to monomeric α-Syn.

The *in vivo* applications of the a-syn-1 aptamer continue to be examined for long-term effects of the aptamer on a living system and evaluating potential downsides or toxicity of the aptamer as a result of binding to α-Syn. Long term studies in the *in vivo* system also wish to

examine the ability for the aptamers to stall the aggregation of human α-Syn in the mouse model. The visualization of a-syn-1 binding to and inhibiting the aggregation of α-Syn is currently being studied in cell cultures of cells expressing human α-Syn.

5 References

(1) Siddiqui, I. J., Pervaiz, N., Abbasi, A. A. The Parkinson Disease gene SNCA: Evolutionary and Structural Insights with Pathological Implication. *Scientific Reports*. **2016,** 6, 24475.

(2) Lykkebo, S. and Jensen, P. H. Alpha-Synuclein and Presynaptic Function. *Neuromolecular Med.* **2002,** 2, 115-129.

(3) Polymerpoulos, M. H., Lavedan, C., Leroy, E., Ide, S. E., Dehejia, A., Dutra, A., Pike, B., Root, H., Rubenstein, J., Boyer, R., Stenroos, E. S., Chandrasekharappa, S., Athanassiadou, ., Papapetropoulos, T., Johnson, W. G., Lazzarini, A. M., Duvoisin, R. C., Di Iorio, G., Golbe, L. I., Nussbaum, R. L. Mutation in the α-Synuclein Gene Identified in Families with Parkinson's Disease. *Science.* **1997,** 276 (5321), 2045-2047.

(4) Qu, J., Yu, S., Zheng, Y., Zheng, Y., Yang, H., Zhang, J. Aptamer and Its Applications in Neurodegenerative Diseases. *Cell. Mol. Life. Sci.* **2017,** 74, 683-695.

(5) Statistics Canada. Parkinson's Disease: Prevalence. Diagnosis and Impact. **2014,** Statistics Canada Catalogue no. 82-003-X.

(6) Riederer, P. and Müller, T. Monoamine Oxidase-B Inhibitors in the Treatment of Parkinson's Disease: Clinical-Pharmacological Aspects. *J. Neur. Transm.* **2018,** 1-7.

(7) Poewe, W., Seppi, K., Tanner, C. M., Halliday, G. M., Brundin, P., Volkmann, J., Schrag, A. E., Lang, A. E. Parkinson Disease. *Nat. Rev. Dis. Primer.* **2017,** 3, 17013.

(8) Krüger, R., Kuhn, W., Müller, T., Woitalla, D., Graeber, M., Kösel, S., Przuntek, H., Epplen, J. T., Schöls, L., Riess, O. Ala30Pro Mutation in the Gene Encoding α-Synuclein in Parkinson's Disease. *Nat. Genet.* **1998,** 18 (2), 106-108.

(9) Weinren, P. H., Zhen, W., Poon, A. W., Conway, K. A., Lansbury, P. T. NACP, A Protein Implicated in Alzheimer's Disease and Learning, Is Natively Unfolded. *Biochem.* **1996,** 35 (43), 13709-13715.

(10) Breydo, L., Wu, J. W., Uversky, V. N. α-Synuclein Misfolding and Parkinson's Disease. *Biochim. Biophys. Acta.* **2012,** 1822 (2), 261-285.

(11) Lashuel, H. A., Overk, C. R., Oueslati, A., Masliah, E. The Many Faces of α-Synuclein: From Structure and Toxicity to Therapeutic Target. *Nat. Rev. Neurosci.* **2013,** 14 (1), 38-48.

(12) Goedert, M. Alpha-Synuclein and Neurodegenerative Diseases. *Nat. Rev.* **2001,** 2 (7), 492-501.

(13) Burré, J. The Synaptic Function of α-Synuclein. *J. Parkinsons Dis.* **2015,** 5, 699-713.

(14) Kim, T. D., Paik, S. R., Yang, C. H. Structural and Functional Implications of C-Terminal Regions of α-Synuclein. *Biochemistry.* **2002,** 41, 13782-13790.

(15) Zhu, M., Li, J., Fink, A. L. The Association of α-Synuclein with Membranes Affects Bilayer Structure, Stability, and Fibril Formation. *J. Biol. Chem.* **2002,** 278 (41), 40186-40197.

(16) Burré, J., Sharma, M., Südhof, T. C. α-Synuclein Assembles into Higher-Order Multimers Upon Membrane Binding to Promote SNARE Complex Formation. *Proc. Natl. Acad. Sci.* **2014,** 111 (40), e4274-e4283.

(17) Scott, D. and Roy, S. α-Synuclein Inhibits Intersynaptic Vesicle Mobility and Maintains Recycling-Pool Homeostasis. *J. Neurosci.* **2012,** 32 (30), 10129-10135.

(18) Spillantini, M. G., Schmidt, M. L., Lee, V. M. Y., Trojanowskim J. Q., Jakes, R., Goedert, M. α-Synuclein in Lewy Bodies. *Nature.* **1997,** 388, 839-840.

(19) Baba, M., Nakajo, S., Tu, P., Tomita, T., Nakaya, K., Lee, V. M., Trojanowski, J. Q., Iwatsubo, T. Aggregation of α-Synuclein in Lewy Bodies of Sporadic Parkinson's Disease and Dementia with Lewy Bodies. *Am. J. Pathol.* **1998,** 152, 879-884.

(20) PH, T. *et al.* Glial Cytoplasmic Inclusions in White Matter Oligodendrocytes of Multiple System Atrophy Brains Contain Insoluble Alpha-Synuclein. *Ann Neurol.* **1998,** 44 (3), 415-422.

(21) Crowther, R. A., Jakes, R., Spillantini, M. G., Goedert, M. Synthetic Filaments Assembled from C-terminally Truncated α-Synuclein. *FEBS Lett.* **1998,** 436 (3), 309-312.

(22) Gai, W. P., Power. H. T., Blumbergs, P. C., Culvenor, J. G., Jensen, P. H. α-Synuclein Immunoisolation of Glial Inclusion from Multiple System Atrophy Brain Tissue Reveals Mutliprotein Components. *J. Neurochem.* **1999,** 73 (5), 2093-2100.

(23) Kabiraj, P., Marin, J. E., Varela-Ramirez, A., Narayan, M. An 11-mer Amyloid Beta Peptide Fragment Provokes Chemical Mutations and Parkinsonian Biomarker Aggregation in Dopaminergic Cells: A Novel Road Map for "Transfected" Parkinson's. *Chem. Neurosci.* **2016,** 7, 1519-1530.

(24) Szargel, R., Rott, R., Engelender, S. Synphilin-1 Isoforms in Parkinson's Disease: Regulation by Phosphorylation and Ubiquitylation. *Cell. Mol. Life Sci.* **2008,** 65, 80-88.

(25) Mann, Brown, Owen, Baba, Iwatsubo. Amyloid β Protein (Aβ) Deposition in Dementia with Lewy Bodies: Predominance of $A\beta_{42(43)}$ and Paucity of $A\beta_{40}$ Compared with Sporadic Alzheimer's Disease. *Neuropathol. Appl. Neurobiol.* **2002,** 24 (3), 187-194.

(26) Pasanen, P., Myllykangas, L., Siitonen, M., Raunio, A., Kaakkola, S., Lyytinen, J., Tienari, P. J., Pöyhönen, M., Paetau, A. A Novel α-Synuclein Mutation A53E Associated with Atypical Multiple System Atrophy and Parkinson's Disease-Type Pathology. *Neurobiology of Aging.* **2014,** 35, 2180e1-2180e5.

(27) Giasson, B. I., Murray, I. V. J., Trojanowski, J. Q., Lee, V. M. Y. A Hydrophobic Stretch of 12 Amino Acid Residues in the Middle of α-Synuclein is Essential for Filament Assembly. *J. Biol. Chem.* **2001,** 276 (4), 2380-2386.

(28) Hashimoto, M., Hsu, L. J., Sisk, A., Xia, Y., Takeda, A., Sundsmo, M., Masliah, E. Human Recombinant NACP/α-Synuclein is Aggregated and Fibrillated *in vitro*: Relevance for Lewy Body Disease. *Brain Res.* **1998,** 799, 301-306.

(29) Sidhu, A., Segers-Nolten, I., Raussens, V., Claessens, M., Subramaniam, V. Distinct Mechanisms Determine A-syn Fibril Morphology during Growth and Maturation. *Chem. Neurosci.* **2017,** 8 (3), 538-547.

(30) Paik, S. R., Shin, H. J., Lee, J. H. Metal-Catalyzed Oxidation of α-Synuclein in the Presence of Copper(II) and Hydrogen Peroxide. *Arch. Biochem, Biophys.* **2000,** 378, 269-277.

(31) Miotto, M. C., Rodriguez, E. E., Valiente-Gabioud, A. A., Torres-Monserrat, V., Binolfi, A., Quintanar, L., Zweckstetter, M., Griesinger, C., Fernández, C. O. Site-Specific Copper-Catalyzed Oxidation of α-Synuclein: Tightening the Link between Metal Binding and Protein Oxidative Damage in Parkinson's Disease. *Inorg. Chem.* **2014,** 53 (9), 4350-4358.

(32) Fujiwara, H., Hasegawa, M., Dohmae, N., Kawashima, A., Masliah, E., Goldberg, M. S., Shen, J., Takio, K., Iwatsubo, T. α-Synuclein is Phosphorylated in Synucleinopathy Lesions. *Nat. Cell. Biol.* **2002,** 4, 160-164.

(33) Souza, J. M., Gaisson, B. I., Chen, Q., Lee, V. M. Y., Ischiropoulos, H. Dityrosine Cross-Linking Promotes Formation of Stable α-Synuclein Polymers. *J. Biol. Chem.* **2000,** 275 (24), 18344-18349.

(34) Danielson, S. R., Held, J. M., Schilling, B., Oo, M., Gibson, B. W., Andersen, J. K. Preferentially Increased Nitration of α-Synuclein at Tyrosine-39 in a Cellular Oxidative Model of Parkinson's Disease. *Anal. Chem.* **2009,** 81 (18), 7823-7828.

(35) Hodara, R., Norris, E. H., Gaisson, B. I., Mishizen-Eberz, A. J., Lynch, D. R., Lee, V. M. Y., Ischiropoulos, H. Functional Consequences of α-Synuclein Tyrosine Nitration. *J. Biol. Chem.* **2004.** 279 (46), 47746-47753.

(36) Waxman, E. A., and Giasson, B. I. Molecular Mechanisms of α-Synuclein Neurodegeneration. *Biochim. Biophys. Acta.* **2009,** 1792 (7), 616-624.

(37) Cheng, H., Wang, L., Wang, C. Domain *a*' of Protein Disulfide Isomerase Plays Key Role in Inhibiting α-Synuclein Fibril Formation. *Cell Stress Chaperones.* **2010,** 15, 415-421.

(38) Paillusson, S., Gomez-Sauga, P., Stolca, R., Little, D., Gissen, P., Devine, M. J., Noble, W., Hanger, D. P., Miller, C. C. J. α-Synuclein Binds to the ER-Mitochondria Tethering Protein VAPB to Disrupt Ca^{2+} Homeostasis and Mitochondrial ATP Production. *Acta. Neuropathol.* **2017,** 134, 129-149.

(39) Cookson, M. R. and Brug, M. v. d. Cell Systems and the Toxic Mechanisms of α-Synuclein. *Exp. Neurol.* **2008,** 209, 5-11.

(40) Peng, X. M., Tehranian, R., Dietrich, P., Stefanis, L., Perez, R. G. α-Synuclein Activation of Protein Phosphatase 2A Reduces Tyrosine Hydroxylase Phosphorylation in Dopaminergic Cells. *J. Cell. Sci.* **2005,** 118, 3523-3530.

(41) Grassi, D., Howard, S., Zhou, M, Diaz-Perez, N., Urban, N. T., Guerrero-Given, D., Kamasawa, N., Volpicelli—Daley, L. A., LoGrasso, P., Lasmézas, C. I. Identification of a Higly Neurotoxic α-Synuclein Species inducing Mitochondrial Damage and Mitophagy in Parkinson's Disease. *Proc. Natl. Acad. Sci.* **2018,** 115 (11), E2634-E2643.

(42) Wille, H. and Requena, J. R. The Structure of PrP^{Sc} Prions. *Pathogens.* **2018,** 7 (1), 20.

(43) Sanghera, N., Wall, M., Vénien-Bryan, C., Pinheiro, T. J. T. Globular and Pre-Fibrillar Prion Aggregates are Toxic to Neuronal Cells and Perturb Their Electrophysiology. *Biochim. Biophys. Acta.* **2008,** 1784, 873-881.

(44) Pruisner, S. B., Woerman, A. L., Mordes, D. A., Watts, J. C., Rampersaud, R., Berry, D. B., Patel, S., Oehler, A., Lowe, J. K., Kravitz, S. N., Geschwind, D. H., Glidden, D. V., Halliday, G. M., Middleton, L. T., Gentlemen, S. M., Grinberg, L. T., Giles, K. Evidence for α-Synuclein Prions Causing Multiple System Atrophy in Humans with Parkinsonism. *Proc. Natl. Acad. Sci.* **2015,** 112 (38), E5308-E5317.

(45) Djamshidian, A. and Poewe, W. Apomorphine and Levodopa in Parkinson's Disease: Two Revolutionary Drugs from the 1950's. *Parkinsonism Relat. Disord.* **2016,** 33, S9-S12.

(46) Aquilonius, S.-M. and Nyholm, D. Development of New Levodopa Treatment Strategies in Parkinson's Disease – From Bedside to Bench to Bedside. *Ups. J. Med. Sci.* **2017,** 122 (2), 71-77.

(47) Hinz, M., Stein, A., Cole, T. Parkinson's Disease: Carbidopa, Nausea, and Dyskinesia. *Clin. Pharmacol.* **2014,** 9, 189-194.

(48) Connolly, B. S. and Lang, A. E. Pharmacological Treatment of Parkinson Disease. A Review. *JAMA.* **2017,** 311 (16), 1670-1683.

(49) Binde, C. D., Tvete, I. F., Gåsemyr, J., Natvig, B., Klemp, M. A Multiple Treatment Comparison Meta-Analysis of Monoamine Oxidase Type B Inhibitors for Parkinson's Disease. *Br. J. Clin. Pharmacol.* **2018,** 84, 1917-1927.

(50) Fernandez, H. H. and Chen, J. J. Monoamine Oxidase-B Inhibition in the Treatment of Parkinson's Disease. *Pharmacotherapy.* **2007,** 27 (12 Pt. 2), 174S-185S.

(51) Rascol, O., Brooks, D. J., Korczyn, A. D., De Deyn, P. P., Clarke, C. E., Lang, A. E. A Five Year Study of the Incidence of Dyskinesia in Patients with Early Parkinson's Disease Who Were Treated with Ropinirole or Levodopa. *N. Eng. J. Med.* **2000,** 342 (20), 1484-1491.

(52) Riederer, P., and Laux, G. MAO-inhibitors in Parkinson's Disease. *Exp. Neurobio.* **2011,** 20, 1-17.

(53) Lees, A. J., Ferreira, J., Rascol, O., Poewe, W., Rocha, J.F., McCrory, M, Soares-da-Silva, P. Opicapone as Adjunct to Levodopa Therapy in Patients with Parkinson Disease and Motor Fluctuations. A Randomized Clinical Trial. *JAMA Neurol.* **2017,** 74 (2), 197-206.

(54) Groiss, S. J., Wojtecki, L., Südmeyer, M., Schnitzler, A. Deep Brain Stimulation in Parkinson's Disease. *Ther. Adv. Neurol. Disord.* **2009,** 2 (6), 379-391.

(55) Perni, M., Galvagnion, C., Maltsev, A., Meisl, G., Müller, M. B. D., Challa, P. K., Kirkegaard, J. B., Flagmeier, P., Cohen, S. I. A., Cascella, R., Chen, S. W., Limbocker, R., Sormanni, P., Heller, G. T., Aprile, F. A., Cremades, N., Cecchi, C., Chiti, F., Nollen, E. A. A., Knowles, T. P. J., Vendruscolo, M., Bax, A., Zasloff, M., Dobson, C. M. A Natural Product Inhibits the Initiation of α-Synuclein Aggregation and Suppresses its Toxicity. *Proc. Natl. Acad. Sci.* **2017,** E1009-E1017.

(56) Perni, M., Flagmeier, P., Limbocker, R., Cascella, R., Aprile, F. A., Galvagnion, C., Heller, G. T., Meisl, G., Chen, S. W., Kumita, J. R., Challa. P. K., Kirkegaard, J. B., Cohen, S. I. A., Mannini, B., Barbut, D., Nollen, E. A. A., Cecchi, C., Cremades, N., Knowles, T. P. J., Chiti, F., Zasloff, M., Vendruscolo, M., Dobson, C. M. Multistep Inhibition of α-Synuclein Aggregation and Toxicity *in Vitro* and *in Vivo* by Trodusquemine. *ACS Chem. Biol.* **2018,** (in press).

(57) Gao, L., Yang, R.-Y., Lian, W.-W., Fang, J.-S., Pang, X.-C., Qin, X.-M., Liu, A.-L., Du, G.-H. Ameliorative Effects of Baicalein in MPTP-Induced Mouse Model of Parkinson's Disease: A Microstudy Array. *Pharmacol. Biochem. Behav.* **2015,** 133, 155-163.

(58) Bunka, D. H. J., Platonova, O., Stockley, P. G. Development of Aptamer Therapeutics. *Curr. Opin. Pharmacol.* **2010.** 10, 557-562.

(59) Ellington, A. D. and Szostak, J. W. *In vitro* Selection of RNA Molecules that Bind Specific Ligands. *Nature.* **1990,** 346, 818-822.

(60) Tuerk, C. and Gold, L. Systematic Evolution of Ligands of Exponential Enrichment: RNA Ligands to Bacteriophage T4 DNA Polymerase. *Science.* **1990,** 249 (4968), 505-510.

(61) Cheng, C., Chen, Y. H., Lennox, K. A., Behlke, M. K., Davidson, B. L. *In vivo* SELEX for Identification of Brain-Penetrating Aptamers. *Mol. Ther. Nucleic Acids.* **2013,** 2, e67.

(62) Keefe, A. D., Pai, S., Ellington, A. Aptamers as Therapeutics. *Nat. Rev. Drug Discov.* **2010,** 9, 537-550.

(63) Lakhin, A. V., Taranful, V. Z., Gening, L. V. Aptamers: Problems, Solutions and Prospects. *Acta Naturae.* **2013,** 5 (4), 34-43.

(64) Weiss, S., Proske, D., Neumann, M. RNA Aptamers Specifically Interact with the Prion Protein PrP. *J. Virol.* **1997,** 71, 8790-8797.

(65) Tsukakoshi, K., Harada, R., Sode, K., Ikebuhuro, K. Screening of DNA Aptamer which Binds to α-Synuclein. *Biotechnol. Lett.* **2010.** 32, 643-648.

(66) Zheng, Y., Qu, J., Xue, F., Zheng, Y., Yang, B., Chang, Y., Yang, H., Zhang, J. Novel DNA Aptamers for Parkinson's Disease Treatment Inhibit α-Synuclein Aggregation and Facilitate its Degradation. *Mol. Ther. Nucleic Acids.* **2018,** 11, 228-242.

(67) Callahan, J. (2017) The Selection of DNA Aptamers for the Prevention of Alpha-Synuclein Aggregation as a Therapeutic Tool in Parkinson's Disease. Carleton University, Ottawa, Canada.

(68) Qian, Z. M., To, Y., Tang, P. L., Feng, Y. M. Transferrin Receptors on the Plasma Membrane of Cultured Rat Astrocytes. *Exp. Brain Res.* **1999,** 129, 473-476.

(69) Pardridge, W. M. Blood-Brain Barrier Biology and Methodology. *J. Neurovirol.* **1999,** 5, 556-569.

(70) Pardridge, W.M. Blood-Brain Barrier Delivery of Protein and Non-Viral Gene Therapeutics with Molecular Trojan Horses. *J. Control Release.* **2007,** 122, 345-348.

(71) Deane, R., Zheng, W., Zlokovic, B. V. Brain Capillary Endothelium and Choroid Plexus Epithelium Regulate Transport of Transferrin-Bound and Free Iron into the Rat Brain. *J. Neurochem*. **2004,** 88 (4), 813-820.

(72) Kandel, E. R., Schwartz, J. H., Jessell, T. M., Siegelbaum, T. M., Hudspeth, A. J. *Principles of Neural Science*, 5th ed. McGraw Hill Professional: 2013.

(73) Zheng, Y, Schlachetzki, F., Pardridge, W. M. Global Non-Viral Gene Transfer to the Primate Brain Following Intravenous Administration. *Mol. Ther.* **2003,** 7 (1), 11-18.

(74) Partridge, W. M. Molecular Trojan Horses for Blood-Brain Barrier Drug Delivery. *Curr. Opin. Pharmacol.* **2006,** 6, 494-500.

(75) Lange, E. C. M. The Physiological Characteristics and Transcytosis Mechanisms of the Blood-Brain Barrier (BBB). *Curr. Pharm. Biotechnol.* **2012,** 13, 2319-2327.

(76) Chen, C. B., Dellamaggiore, K. R., Quellette, C. P., Sedano, C. D., Lizadjohry, M., Chernis, G. A., Gonzales, M., Baltasar, F. E., Fan, A L., Myerowitz, R., Neufeld, E. F. Aptamer-Based Endocytosis of a Lysosomal Enzyme. *Proc. Natl. Acad. Sci.* **2008,** 105 (41), 15908-15913.

(77) Peng, Y., Zhoa, Y., Chen, Y., Yang, Z., Zhang, L., Xiao, W., Yang, J., Guo, L., Wu, Y. Dual-Targeting for Brain-Specific Liposomes Drug Delivery System: Synthesis and Preliminary Evaluation. *Bioorg. Med. Chem.* **2018** (in press).

(78) Rentzeperis, D., Alessi, K., Marky, L. A. Thermodynamics of DNA Hairpins: Contribution of Loop Size to Hairpin Stability and Ethidium Binding. *Nucleic Acids Res.* **1993,** 21 (11), 2683-2689.

(79) Bonnet, G., Tyagi, S., Libchaber, A., Kramer, F. R. Thermodynamic Basis for the Enhanced Specificity of Structured DNA Probes. *Proc. Natl. Acad. Sci.* **1999,** 96, 6171-6176.

(80) Gellert, M., Lipsett, M. N., Davies, D. R. Helix Formation by Guanylic Acid. *Proc. Natl. Acad. Sci.* **1962,** 48, 2013-2018.

(81) Liu, W., Zhu, H., Zheng, B., Cheng, S., Fu, Y., Li, W., Lau, T.-C., Liang, H. Kinetics and Mechanism of G-Quadruplex Formation and Conformational Switch in a G-Quadruplex of PS2.M Induced by Pb^{2+}. *Nucleic Acids Res.* **2012,** 40 (9), 4339-4236.

(82) Pollard, T. D. A Guide to Simple and Informative Binding Assays. *Mol. Biol. Cell.* **2010,** 21, 4061-4067.

(83) Hellman, L. M. and Fried, M. G. Electrophoretic Mobility Shift Assay (EMSA) for Detecting Protein- Nucleic Acid Interactions. *Nat. Protoc.* **2007,** 2 (8), 1849-1861.

(84) Lane, D., Prentki, P., Chandler, M. Use of Gel Retardation to Analyze Protein-Nucleic Acid Interactions. *Microbiol. Rev.* **1992,** 56 (4), 509-528.

(85) Galas, D. J. and Schmitz, A. DNase Footprinting: A Simple Method for the Detection of Protein-DNA Binding Specificity. *Nucleic Acids Res.* **1978,** 5 (9), 3157-3170.

(86) Brenowitz, M., Senear, D. F., Shea, M. A., Ackers, G. K. Quantitative DNase Footprint Titration: A Method for Studying Protein-DNA Interactions. *Methods Enzymol.* **1986,** 130, 132-181.

(87) Connaghan-Jones, K. D., Moody, A. D., Bain, D. L. Quantitative DNase Footprint Titration: A Tool for Analyzing the Energetics of Protein-DNA Interactions. *Nat. Protoc.* **2008,** 3 (5), 900-914.

(88) Shevchenko, Y., Francis, T. J., Blair, D. A. D., Walsh, R., DeRosa, M. C., Albert, J. In Situ Biosensing with a Surface Plasmon Resonance Fiber Grating Aptasensor. *Anal. Chem.* **2011,** 83, 7027-7034.

(89) Fetter, L., Richards, J., Daniel, J., Roon, L., Rowland, T. J., Bonham, A. J. Electrochemical Aptamer Scaffold Biosensors for Detection of Botulism and Ricin Toxins. *Chem. Commun.* **2015,** 51, 15137-15140.

(90) Reuter, J. S. and Mathews, D. H. RNAstructure: Software for RNA Secondary Structure Prediction and Analysis. *BMC Bioinformatics.* **2010,** 11, 129.

(91) Moussa, C. E., Wersinger, C., Rusnak, M., Tomita, Y., Sidhu, A. Abnormal Migration of Human Wild-Type Alpha-Synuclein upon Gel Electrophoresis. *Neurosci. Lett.* **2004,** 371 (2-3), 239-243.

(92) Jerabek-Willemsen, M., André, T., Wanner, R., Roth, H. M., Duhr, S., Baaske, P., Breitsprecher, D. MicroScale Thermophoresis: Interaction Analysis and Beyond. *J. Mol. Struct.* **2014,** 1077, 101-113.

(93) Smith, P. K., Krohn, R. I., Hermanson, G. T., Mallia, A. K. Gartner, F. H., Provenzano, M. D., Fujimoto, E. K., Goeke, N. M., Olson, B. J., Klenk, D. C. Measurement of Protein using Bicinchoninic Acid. *Anal. Biochem.* **1985**, 150, 76-85.

(94) Huang, T., Long, M., Huo, B. Competitive binding to Cuprous Ions of Protein and BCA in the Bicinchoninic Acid Protein Assay. *Open Biomed Eng. J.* **2010,** 4, 271-278.

(95) Wiechelman, K. J., Braun, R. D., Fitzpatrick, J. D. Investigation of the Bicinchoninic Acid Protein Assay: Identification of the Groups Responsible for Color Formation. *Anal. Biochem.* **1988**, 175 (1), 231-237.

(96) Clark, K., Karsch,-Mizrachi, I., Lipman, D. J., Ostell, J., Sayers, E. W. GenBank. *Nucleic Acids Res.* **2016**, 44 (CAA76847), D67-D72.

(97) Pieri, L., Madiona, K., Melki, R. Structural and Functional Properties of Prefibrillar α-Synuclein Oligomers. *Sci. Rep*. **2016**, 6:24526.

(98) Biancalana, M., and Koide, S. Molecular Mechanism of Thioflavin-T Binding to Amyloid Fibrils. *Biochim. Biophys. Acta.* **2010,** 1804 (7), 1405-1412.

(99) Krebs, M. R. H., Bromley, E. H. C., Donald, A. M. The Binding of Thioflavin-T to Amyloid Fibrils: Localisation and Implications. *J. Struct. Biol.* **2005,** 149 (1), 30-37.

(100) Khurana, R., Coleman, C., Ionescu-Zanetti, C., Carter, S. A., Krishna, V., Grover, R. K., Roy, R., Singh, S. Mechanism of Thioflavin T Binding to Amyloid Fibrils. *J. Struct. Biol.* **2005,** 151 (3), 229-238.

(101) Ilanchelian, M., and Ramaraj, R. Emission of Thioflavin T and its Control in the Presence of DNA. *J. Photochem. Photobiol.* **2004,** 162 (1), 129-137.

(102) Nogueira, E., Gomes, A. C., Preto, A., Cavaco-Paulo, A. Design of Liposomal Formulation of Cell Targeting. *Colloids Surf. B. Biointerfaces.* **2015,** 136, 514-526.

(103) Crooke, S. T. *Antisense Drug Technology Principles, Strategies and Applications*, 2nd ed. CRC Press: 2007.

(104) Akbarzadeh, A., Rezaei-Sadabady, R., Davaran, S., Joo, S. W., Zarghami, N., Hanifehpour, Y., Samiei, M., Kouhi, M., Nejati-Koshki, K. Liposome: Classification, Preparation, and Applications. *Nano. Res. Lett.* **2013,** 8 (102).

(105) Pick, U. Liposomes with a Large Trapping Capacity Prepared by Freezing and Thawing of Sonicated Phospholipid Mixtures. *Arch. Biochem. Biophys.* **1981,** 212, 186-194.

(106) Li, S. D. and Huang, L. Stealth Nanoparticles: High Density but Sheddable PEG is a Key for Tumor Targeting. *J. Control. Release.* **2010,** 145 (3), 178-181.

(107) Nakamura, K., Yamashita, K., Itoh, Y., Yoshino, K., Nozawa, S., Kasukawa, H. Comparative Studies of Polyethylene Glycol-Modified Liposomes Prepared using Different PEG-Modification Methods. *Biochem. Biophys. Acta.* **2012,** 1818, 2801-2807.

(108) Giansanti, L., Bozzuto, G., Fracassi, A., Bombelli, C., Stringaro, A., Molinari, A., Piozzi, A., Sennato, S., Mancini, G. Effect of Preparation Protocol on Physiochemical Features and Biointeractions of Pegylated Liposomes. *Colloids Surf. A.* **2017,** 532, 444-450.

(109) Vieira, D. B. and Gamarra, L. F. Getting into the Brain: Liposome-Based Strategies for Effective Drug Delivery Across the Blood-Brain Barrier. *Int. J. Nanomedicine.* **2016,** 11, 5381-5414.

(110) Semple, S. C., Harasym, T. O., Clow, K. A., Ansell, S. M., Klimuk, S. K., Hope, M. J. Immunogenicity and Rapid Blood Clearance of Liposomes Containing Polyethylene Glycol-Lipid Conjugates and Nucleic Acid. *J. Pharmacol. Exp. Ther.* **2004,** 312 (3), 1020-1026.

(111) Ponchel, F., Toomes, C., Bransfield, K., Leong, F. T., Douglas, S. H., Field, S. L., Bell, S. M., Combaret, V., Puisieux, A., Mighell, A. J., Robinson, P. A., Inglehearn, C. F., Isaacs, J. D., Markham, A. F. Real-Time PCR Based on SYBR-Green I Fluorescence: An Alternative to the TaqMan Assay for a Relative Quantification of Gene Rearrangements, Gene Amplifications, and Micro Gene Deletions. *BMC Biotechnology.* **2003,** 3 (18).

(112) McConnell, E. M. (2016) Selection and Use of DNA Aptamers for Applications within the Central Nervous System. Carleton University, Ottawa, Canada.

(113) Montanari, J. A. M., Bucci, P. L., Alonso, S. d. Y. A Model Based in the Radius of Vesicles to Predict the Number of Unilamellar Liposomes. *Int. J. Res. Pharm. Chem.* **2014**, 4 (2), 484-489.

(114) Che, J., Okeke, C. I., Hu, Z.-B., Xu, J. DSPE-PEG: A Distinctive Component in Drug Delivery System. *Curr. Pharm. Des.* **2015,** 21 (12), 1598-1605.

(115) Hughes, L. D., Rawle, R. J., Boxer, S. G. Choose Your Label Wisely: Water-Soluble Fluorophores Often Interact with Lipid Bilayers. *PLOS One*. **2014,** 9 (2), e87649.

(116) Gaigalas, A. K., Li, L., Henderson, O., Vogt, R., Barr, J., Marti, G., Weaver, J., Schwartz, A. The Development of Fluorescence Intensity Standards. *J. Res. Natl. Stand Technol.* **2001**, 106, 381-389.

6 Appendix

Appendix 6.1 PAGE Purification of Fluorescently Labelled DNA

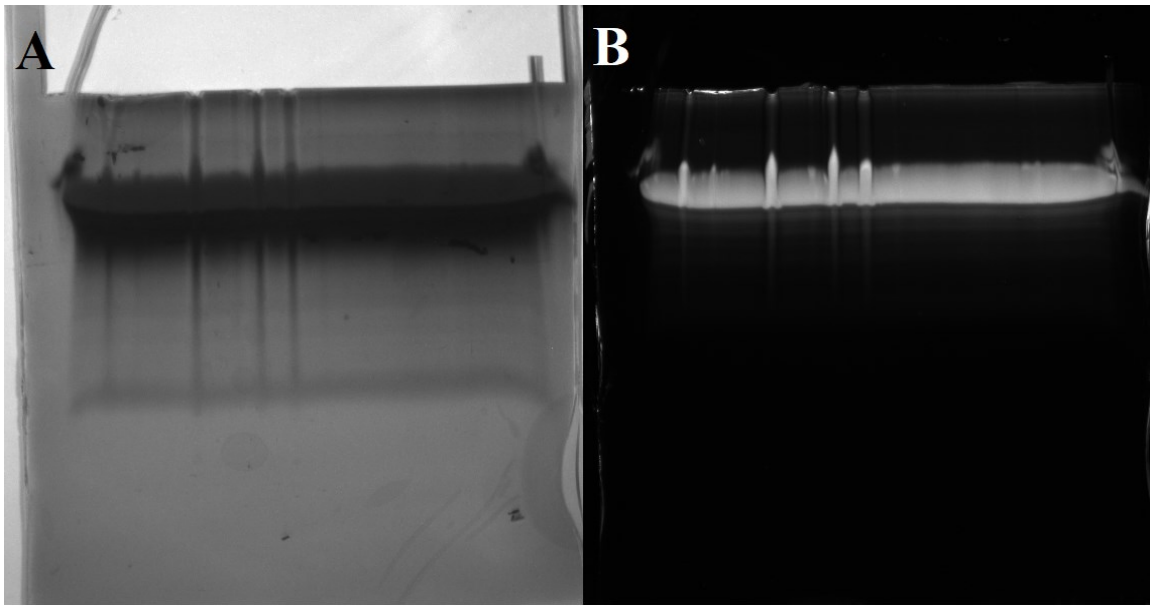

Gel purification of Cy 3.5-labelled a-syn-1 aptamer imaged using A) epi UV imaging and B) fluorescent imaging. The fluorescent band was cut from the gel to extract the synthesized aptamer.

Appendix 6.2: Mass Spectrometry Results

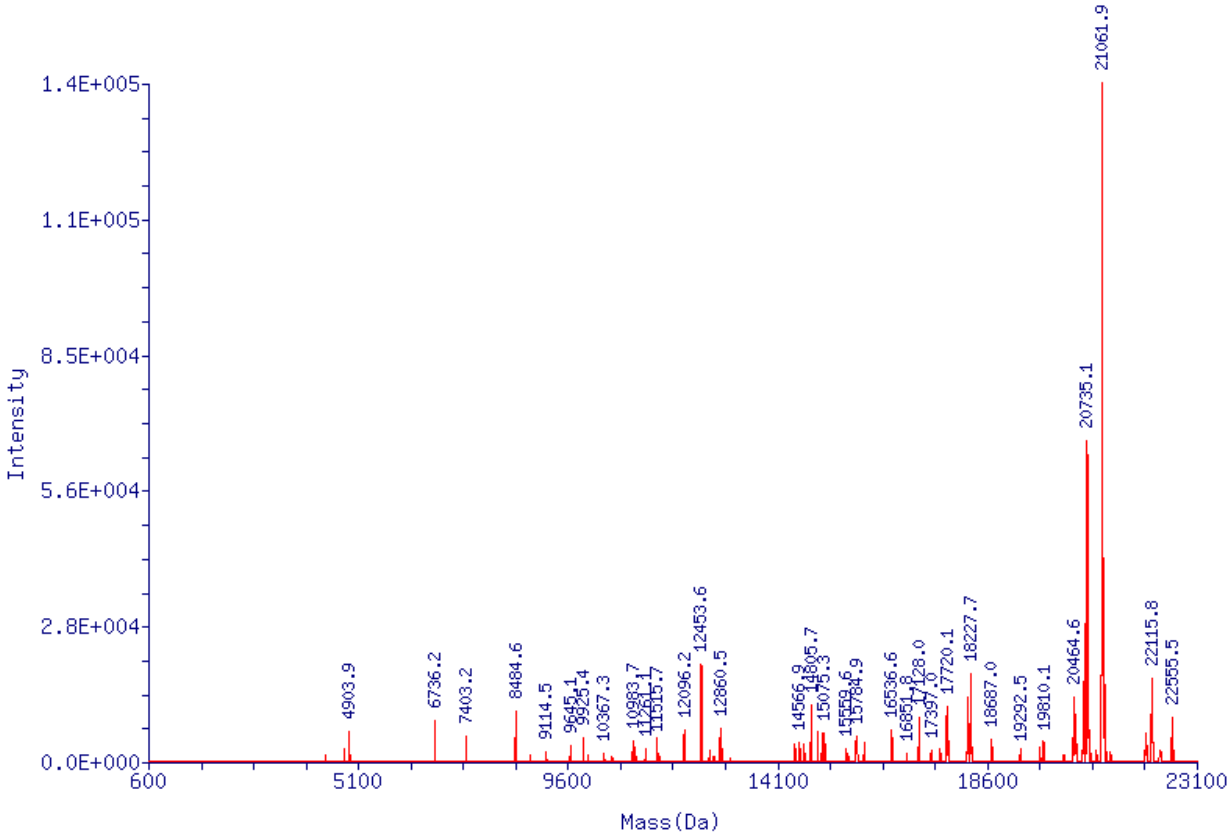

Mass spectrometry results for the a-syn-1 aptamer modified with a 5' fluorescein phosphoramidite. The target mass of the aptamer is 21062Da. A peak appears in the deconvoluted mass spectrum for the aptamer, but the purity from this batch was low (28.5% pure) with interference from impurities due to incomplete aptamer synthesis. This batch underwent additional purification, using PAGE, to obtain a purer sample.

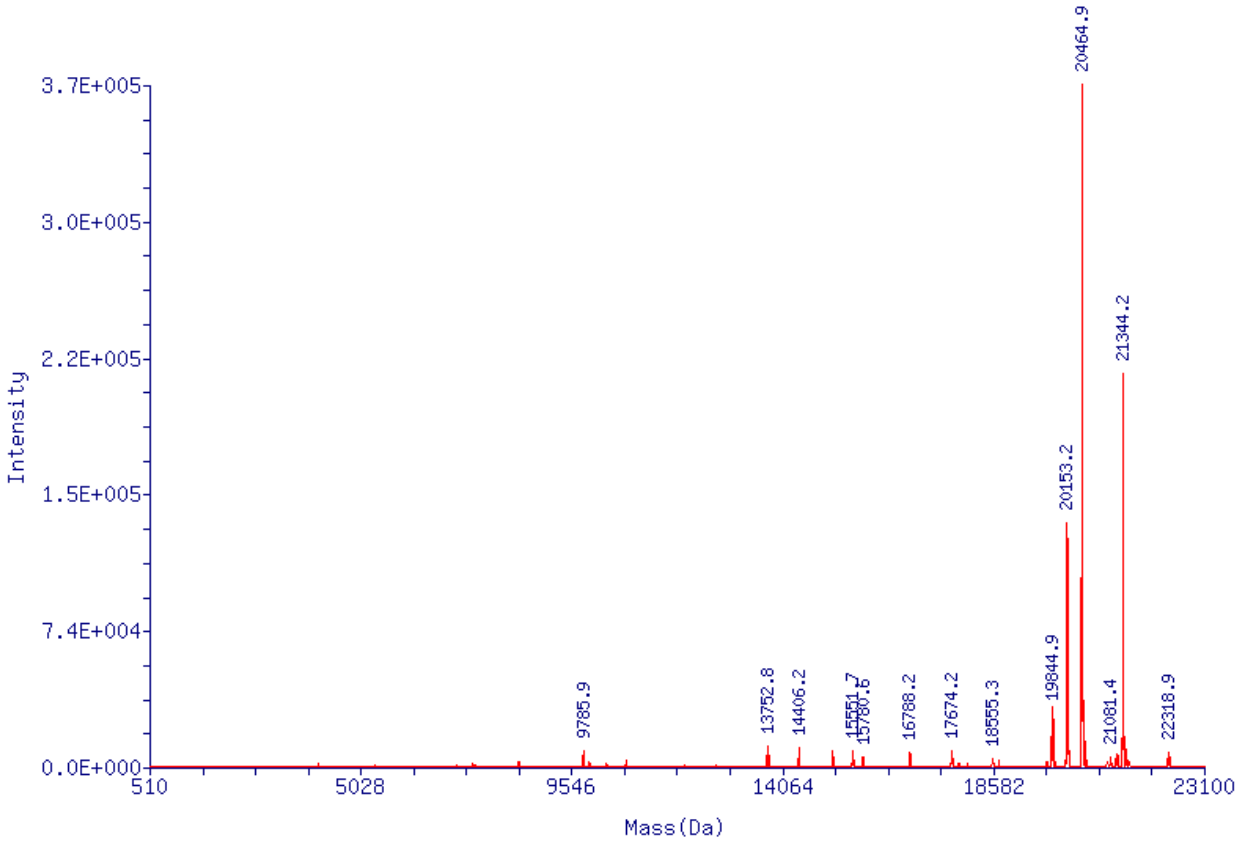

Mass spectrometry results for the a-syn-1 aptamer modified with a Cy 3.5 modifier. The target mass of the aptamer is 21073Da. A peak appears in the deconvoluted mass spectrum for the aptamer sequence without the modifier (20464Da). However, the gel purification, in Appendix 6.1, shows a band for the fluorescently-modified full-length sequence. The dye may have become removed when the sample was analyzed during mass spectrometry.

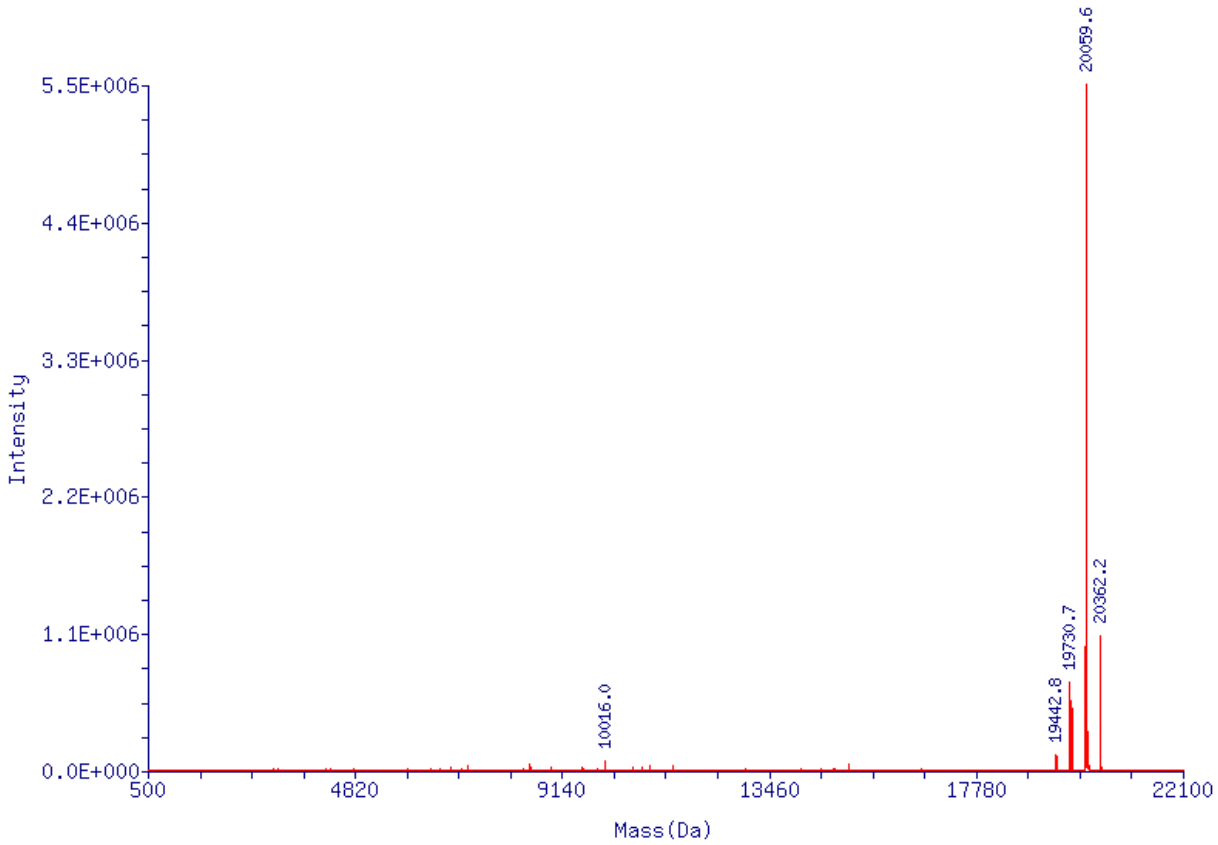

Mass spectrometry results for the 5'-thiol-modified TRA. The target mass of the aptamer was 20058Da and the majority of the peak from the deconvoluted mass spectrum appears at 20059Da. The purity of this batch was 67.3%.

Appendix 6.3: EMSA gels

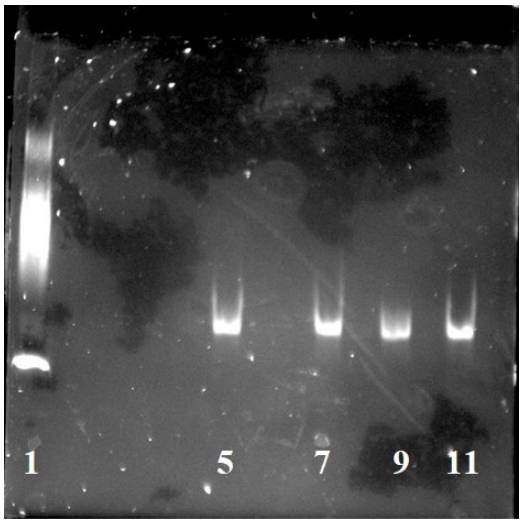

Attempted EMSA using a fresh vial of α-Syn monomer. A triplicate of 30μM α-Syn and 30μM a-syn-1 were combined and incubated and run using an 8% non-denaturing PAGE. No shift on a-syn-1 fluorescence was observed. Lane 1 is the protein ladder, lane 5 is the aptamer control with no α-Syn, and lanes 7, 9, and 11 are the combination of α-Syn and a-syn-1.

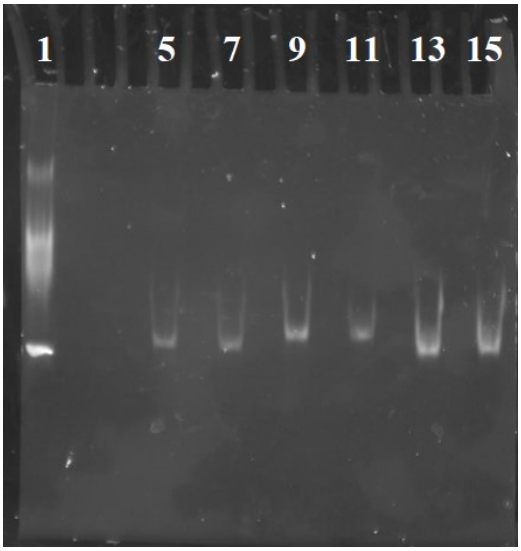

Attempted EMSA using the A30P mutant variant of α-Syn. Lane 1 is the protein ladder, lane 5 is the a-syn-1 aptamer control with no α-Syn, lane 7 is the combination of 0.5μM α-Syn and 30μM a-syn-1, lane 9 is the a-syn-2 control with no α-Syn, lane 11 is the combination of 0.5μM α-Syn with 30μM a-syn-2, lane 13 is the a-syn-3 control with no α-Syn, and lane 15 is the combination of 0.5μM α-Syn and 30μM a-syn-3. No shift was observed between the aptamer controls and aptamers incubated with α-Syn.

Appendix 6.4: DNase gels

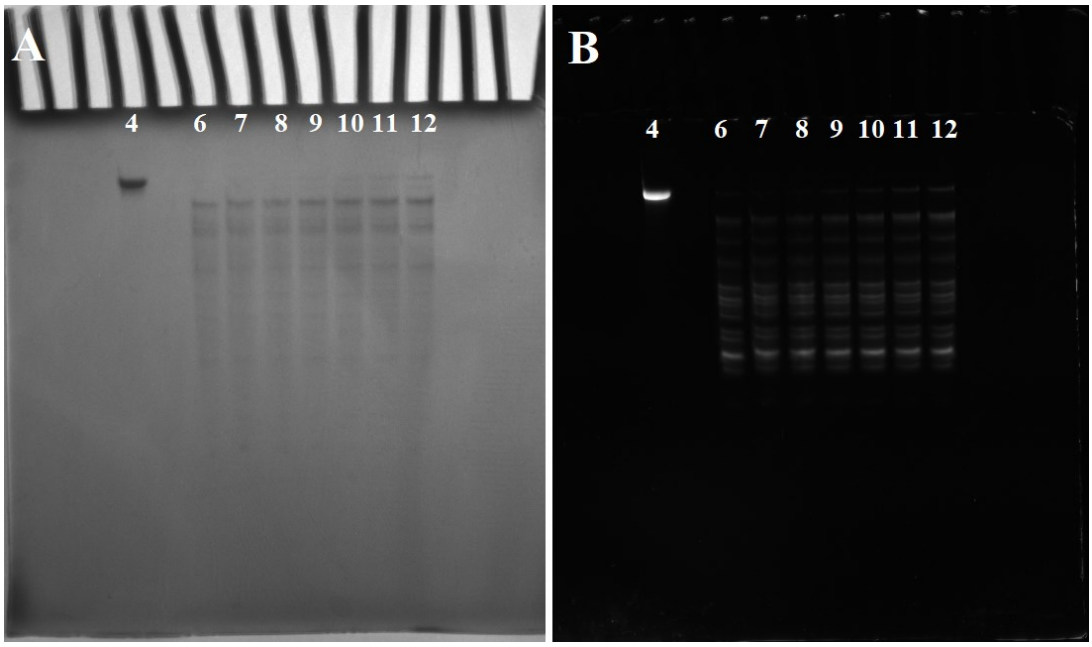

The a-syn-1 aptamer was tested using DNase assay several times with a concentration gradient of α-Syn concentrations from 15μM to 0.0024μM using 19% denaturing PAGE. Lane 4 is the full-length a-syn-1 aptamer, lane 6 is the digestion of the aptamer without α-Syn, and lanes 7-12 are 15μM, 1.5μM, 0.3μM, 0.06μM, 0.012μM, and 0.0024μM α-Syn, respectively. No observable trend was observed with the digestion bands. The full-length aptamer, in fact, shows no fluorescence in the control digestion lane (6) and in the highest concentration of α-Syn (7), but is observed at every other concentration of α-Syn. Similar issues with inconsistent fluorescent bands were observed in the DNase assays of the other a-syn aptamers.

6.5: Co-Localization of a-syn-1 Aptamer and Anti-Alpha-Synuclein Antibody in Mouse Brain

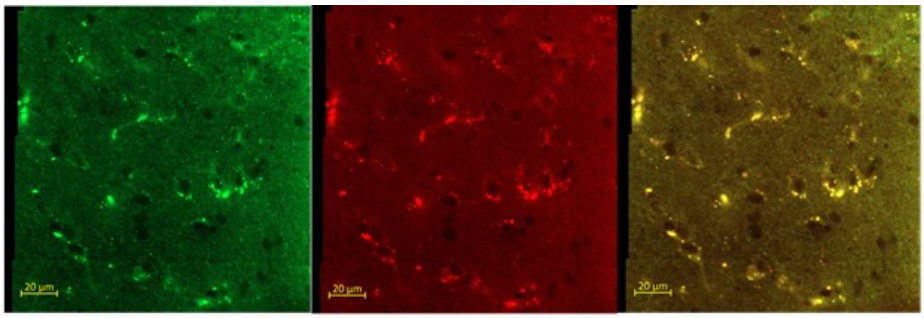

Anti-Alpha-synuclein (phosphoS129) antibody (ab59264)

Cy 3.5-labelled aptamer

The following *in* vivo work was performed by Katelyn Ventura and Matthew Holahan.

Transgenic mice expressing the human α-Syn were live decapitated 30 minutes after injection of liposomes, modified to cross the BBB, containing Cy 3.5-labelled a-syn-1 aptamer. Brain slices were stained with an anti-alpha-synuclein antibody and imaged under fluorescence microscopy. The left panel is the visualization of the anti-alpha-synuclein antibody location in the brain slice binding to the α-Syn, where the brighter green regions correspond with greater amounts of α-Syn; the central panel is the visualization of the a-syn-1 aptamer in the brain slice, where the brighter red regions represent the location of fluorescent aptamer; and the right panel is an overlay of the antibody and aptamer fluorescence images to view co-localization of the antibody and aptamer as yellow. The bright yellow marks provide clear evidence that the fate of the aptamer and anti-alpha-synuclein antibody are the same; the co-localization greatly implies that the aptamer is binding to α-Syn in the brain.